Improving the Fatigue and Control Performance of Loader Cranes

Pedersen, Mikkel Melters

Department of Mechanical and Manufacturing Engineering
Aalborg University, Denmark.
Special Report No. 71

Improving the Fatigue and Control Performance of Loader Cranes

Ph.D. Thesis

by

Mikkel M. Pedersen

Department of Mechanical and Manufacturing Engineering, Aalborg University
Pontoppidanstræde 101, DK-9220 Aalborg East, Denmark
e-mail: mmp@m-tech.aau.dk

Typeset in LaTeX and printed in Aalborg, 2011.

ISBN 87-91464-25-0

Preface

This dissertation has been submitted to the Faculty of Engineering, Science and Medicine in partial fulfillment of the requirements for the degree of Doctor of Philosophy in Mechanical Engineering.

The work has been carried out at the Department of Mechanical and Manufacturing Engineering, Aalborg University and at Højbjerg Maskinfabrik A/S (HMF) as an Industrial PhD project in the period from August 2007 to January 2011.

The work has been partially funded by the Danish Ministry of Science, Technology and Innovation, under the Industrial PhD initiative as project no. 07-017594.

I would like to thank my supervisors Prof. Michael R. Hansen at University of Agder and Assoc. Prof. Ole Ø. Mouritsen from Aalborg University. Also my colleagues and supervisors from HMF are thanked; Morten Ballebye, Jes G. Andersen, Jimmi Wenderby and Gudmund Braendgaard. Last but not least, I thank my family and especially my girlfriend, Mie, for patiently listening to a lot of talk about cranes.

Mikkel Melters Pedersen
Højbjerg, January 2011.

Abstract

This industrial Ph.D. project concerns methods for development of loader cranes with higher performance than currently possible. It covers two topics which are highly related when considering a fatigue prone welded structure subjected to significant dynamic loading due to the control of the hydraulic actuation, i.e.:

- *Fatigue of welded joints*, and
- *Control of mobile hydraulics*

While these topics may seem quite distinct, it should be considered, that the first governs the fatigue resistance and the second governs the fatigue loading. It is therefore expedient to take a holistic approach and consider both topics within the same project.

In regards to fatigue of welded joints, this project establishes methods for improving the fatigue performance of welded joints by post weld treatment and design optimization using the notch stress approach. Existing methods are investigated and adapted to the specific conditions of loader cranes. These include, very high strength steel, thin sections, complex geometry, high stress ranges and low-to-medium cycle fatigue lives. Furthermore, a proposal is made for extending the notch stress approach to consider post weld treatment in the fatigue assessment. The fatigue resistance of the critical welded joints can thus be optimized in the design stage.

In order to limit the dynamic peak loading during operation of the crane, especially at increased speeds, it is expedient to use more advanced control principles than the current direct control of the individual actuators. Therefore, a tool point control scheme is investigated and further developed, considering application related issues, such as joint limit avoidance, deflection compensation and configuration control. A practical approach for control development is established using interactive, real-time dynamic simulation in order to included the effects of an active operator in the control loop. Additionally, in order to verify correct implementation of such tool point control in the current controller, a hardware-in-the-loop simulator is developed to satisfy future testing needs.

Based on the contributions of this work, it will be possible to develop high performance, lightweight and durable loader cranes and the addition of tool point control should pave the way for improved productivity.

Resume

Dette ErhvervsPhD projekt omhandler metoder til udvikling af lastbilkraner med højere ydeevne, end muligt for nuværende. Det omhandler to emner, som er særdeles relaterede, når man betragter udmattelsesfølsomme svejste strukturer udsat for dynamiske belastninger pga. styringen af den hydrauliske aktuering, nemlig:

- *Udmattelse af svejste samlinger*, og
- *Styring af mobilhydraulik*

Umiddelbart kan disse emner virke fjernt beslægtede, men for lastbilkraner er udmattelsesstyrken styret af de svejste samlinger og udmattelseslasten bestemmes af styringen af den hydrauliske aktuering. Det er derfor hensigtsmæssigt, ud fra en holistisk tilgangsvinkel, at bearbejde begge emner i det samme projekt.

Indenfor udmattelse af svejste samlinger etableres der i dette projekt metoder til at forbedre udmattelsesstyrken ved efterbehandling og designoptimering vha. notch metoden. Eksisterende metoder undersøges og tilpasses til de specifikke forhold der gælder for lastbilkraner. Dette inkluderer højstyrkestål, tynde tværsnit, komplekse geometrier, høje spændingsvidder og korte levetider. Desuden gives et forslag til udvidelse af notch metoden til at inkludere efterbehandling i levetidsvurderingen. Udmattelsesstyrken af de kritiske samlinger i en kran kan derved optimeres på designstadiet.

For at begrænse de dynamiske spidsbelastninger kranen udsættes for, specielt ved forhøjede hastigheder, er det hensigtsmæssigt at anvende mere avancerede styreprincipper, end det nuværende med direkte styring af de individuelle aktuatorer. Derfor undersøges og videreudvikles et tool point styreprincip, under hensyntagen til applikationen, f.eks. udbøjningskompensation og arbejdsstillingskontrol. Der anvendes en praktisk tilgangsvinkel til udvikling af det nye styreprincip, som gør brug af interaktiv, dynamisk simulering i realtid for at inkludere effekten af en aktiv bruger i kontrolløkken.

På baggrund af dette arbejde vil det være muligt at udvikle højtydende og holdbare lette lastbilkraner og samtidig brug af tool point styring skulle muliggøre højere produktivitet i kranarbejdet.

Appended papers

This thesis is based on the following papers. All papers are reproduced as-published, only adapted to fit this printing format.

Papers A and *B* have also been presented in the IIW as documents XIII-2272-09 and XIII-WG3-10-09, respectively. *Paper D* has also been presented at the 2010 NODE seminar, Grimstad, Norway.

Publications in refereed journals

- *Paper A*: MM Pedersen, OØ Mouritsen, MR Hansen, JG Andersen, J Wenderby
  Comparison of Post Weld Treatment of High Strength Steel Welded Joints in Medium Cycle Fatigue. *Welding in the World*, **54**(7/8), pp. 208–217 (2010).
- *Paper B*: MM Pedersen, OØ Mouritsen, MR Hansen, JG Andersen, J Wenderby
  Re-analysis of fatigue data for welded joints using the notch stress approach. *International Journal of Fatigue*, **32**, pp. 1620–1626 (2010).
- *Paper D*: MM Pedersen, MR Hansen, M Ballebye
  Developing a Tool Point Control Scheme for a Hydraulic Crane Using Interactive Real-time Dynamic Simulation. *Journal of Modelling, Identification and Control*, **31**(4), pp. 133–143 (2010).

Publications in proceedings

- *Paper C*: MM Pedersen, OØ Mouritsen, MR Hansen, JG Andersen
  Experience with the Notch Stress Approach for Fatigue Assessment of Welded Joints. In: *Proceedings of the Swedish Conference on Light Weight Optimized Welded Structures*, (ed. Z. Barsoum and J. Samuelsson), March 24–25, 2010, Borlänge, Sweden, pp. 122–133.
- *Paper E*: MM Pedersen, MR Hansen, M Ballebye
  A Cost-Effective Approach to Hardware-In-The-Loop Simulation. *Submitted to the 9th International Conference: Mechatronics 2011, September 21–24, Warsaw, Poland, 2011.*

Division of work between the authors

For all papers M.M. Pedersen did the main work, and the co-authors contributed with valuable discussion and helpful comments.

Nomenclature

$\Delta\sigma$	Stress range
σ_n	Nominal stress
σ_{hs}	Hotspot structural stress
σ_k	Notch stress
$\sigma_{k,PS}$	Notch stress, principal stresses
σ_c	Characteristic fatigue strength at $2 \cdot 10^6$ cycles
σ_y	Yield strength
N_f	Fatigue life, cycles to failure
k_m	Stress magnification factor considering misalignment
R	Radius or Stress ratio
R_{ref}	Reference radius
P_S	Probability of survival
P_F	Probability of failure
K_t	Geometric stress concentration factor
K_f	Fatigue notch factor
K_w	Notch factor (σ_k/σ_{hs})
f_R	Factor considering stress ratio
j_σ	Factor considering probability of survival
m	Inverse negative slope coefficient of SN curve
n	Number of specimens
$\dot{\mathbf{r}}_{TP}$	Tool point velocity vector
$\boldsymbol{\theta}$	Joint coordinates vector
$\mathbf{J}$	Jacobian matrix
$\mathbf{J}^+$	Moore-Penrose pseudo inverse of the Jacobian matrix
$\mathbf{z}$	Arbitrary vector in joint space
$\mathbf{F}_c$	Cylinder forces vector
$\mathbf{u}$	Control signals vector

Abbreviations

DOF	Degrees of freedom
HMF	Højbjerg Maskinfabrik
HIL	Hardware-in-the-loop
AW	As-welded
BG	Burr grinding
TIG	Tungsten inert gas
UIT	Ultrasonic impact treatment
UP	Ultrasonic peening
HiFIT	High frequency impact treatment
HFP	High frequency peening, common for UIT, UP and HiFIT etc.
IO	Input/output
OCV	Over-center valve
CAN	Controller area network
LAN	Local area network

Contents

1

Introduction

This thesis concerns improvement of the fatigue and control performance of truck mounted loader cranes. The project is initiated by Højbjerg Maskinfabrik A/S and therefore takes its basis in the loader cranes produced by them.

1.1 Højbjerg Maskinfabrik

Højbjerg Maskinfabrik A/S (HMF) is a Danish manufacturer of hydraulic loader cranes for truck mounting. HMF is a middle sized company with production in Denmark and sales in most of the world, however, main markets are Europe and the USA. Over some 60 years, HMF has grown out of a bicycle repair shop to become one of the largest manufacturers of loader cranes in the world, HMF (2010).

The loader crane market is dominated by few, relatively large companies. Palfinger is the market leader, followed by Hiab, and then Fassi, Effer, HMF and others in varying order depending of the parameter used for ranking.

HMF is currently implementing a new business strategy and is focusing activity on development and production of high-end loader cranes. Especially considering welded high strength steel components, which is one of the core competences of the company. This project was therefore initiated to help secure the position of HMF as a leading brand and increase the competitiveness of their products.

1.2 Loader Cranes

Truck mounted loader cranes, as shown in 1.1, are primarily used for loading and unloading building material, machinery, sand, scrap, etc. to/from trucks. Today these cranes are complex welded structures made from ultra high strength steel (in the range S700-S1300) in order to limit their self weight and maximize the lifting capacity. Mobile cranes in general represent the leading edge in what can be accomplished within the field of lightweight welded structures. Newly developed

ultra high strength weldable steel grades are even sometimes referred to as *crane steels* by steel manufacturers.

Figure 1.1: Two examples of HMF loader cranes.

Due to increased safety demands, e.g. EN12999 (2010), a typical loader crane now includes an advanced controller and a large number of sensors. A loader crane thus represents a so-called mechatronic system with highly interacting mechanic-, hydraulic- and electronic systems. The control system is very important, since it governs the end-user's daily experience of working with the crane.

Whereas loader cranes have reached a dominant design mechanically speaking, i.e. most manufacturers apply almost identical principles, the control systems are still evolving quite diversely. There is a tendency - both regarding cranes, but also components - to convert mechanical/hydraulic features into electronic features. This facilitates late product configuration, larger volumes, less stock, etc.

1.3 Background and Motivation

The business segment of truck mounted loader cranes represents a highly competitive field, where a continuous increase in product performance is required. The two most significant measures of performance are the *ratio of lifting capacity to self-weight* and the *operational speed*.

A high lifting capacity is desired for obvious reasons, but the low self-weight is motivated by several factors. Firstly, at longer reaches, most of the lifting capacity is consumed by the self-weight moment of the crane. Furthermore, the self-weight of the crane limits the load-carrying capacity of the truck and increases its fuel

consumption. The challenge is therefore to achieve the highest lifting capacity while at the same time minimizing the self-weight. This is achieved using very high strength steel.

The attainable operational speed, on the other hand, is directly proportional to the amount of work the end-user can perform and thus his/her achievable profit. However, increased speed often leads to premature fatigue failures, since the dynamic loads on the crane increases. Therefore, when adjusting the operational speed, it's essential to consider and maintain the fatigue performance.

Using high strength steel in welded structures poses several challenges. The reason for using higher strength steel is obviously that it allows higher loads to be transferred using less material, i.e. higher stresses in reduced plate thickness. Unfortunately, the fatigue strength of welded joints do not follow the static strength of the base material. The difference between the fatigue strength and static strength of a welded structure in high strength steel thus increase with the base material strength. It therefore becomes difficult to fully utilize the high static strength of the new steels, since the fatigue strength remains relatively low for welded joints irregardless of the base material strength. This problem is one of the main barriers preventing further use of ultra high strength steels in development of durable, high strength, lightweight welded structures.

On the other hand, if the fatigue strength of the welded joints can be increased, further utilization of the high strength steel can be achieved. Fatigue strength improvement of welded joints is thus one of the keys to achieve higher performance of loader cranes.

A significant implication of high strength steel design with reduced plate thickness, is increased structural flexibility. Loader cranes with an operating range of up to 40m operate under considerable deflection (several meters) and reducing the plate thickness will only increase this deflection. It is thus expedient to introduce more sophisticated control principles such as tool point control, both in order to ensure safe high speed maneuverability and limit dynamic peak loading, in order to maintain a high fatigue performance.

Put shortly, the fatigue resistance of the crane is governed by the critical welded joints and the fatigue loading is governed by the hydraulic control system. Therefore, when considering a dynamically loaded, fatigue prone welded structure as a loader crane, the fatigue- and control aspects are interconnected.

1.4 Research Objectives

Since this is an industrial Ph.D. project, the objectives are twofold; in addition to generating scientific progress, it must also consider the applicability in industry. The research presented here will therefore be very application-minded and will

address the main challenges in loader crane development, as discussed above. The research objective is therefore defined as follows:

The project shall establish a set of methods enabling development of loader cranes with higher fatigue- and control performance than currently possible, i.e.

1. *Determine how the fatigue strength can be improved by post weld treatment, and how this improvement can be included in the fatigue assessment of the complex welded parts comprised by a loader crane?*
2. *Determine how more sophisticated control principles, i.e. tool point control, can be implemented in loader cranes considering development, implementation and testing?*

1.5 Research Approach

Different approaches will be taken within the two sub-topics as explained in the following.

Fatigue of welded joints

This work will focus on post weld treatment and local fatigue assessment. Existing methods will be investigated and adapted to the specific conditions of loader cranes after careful analysis. The following aspects characterize the conditions that needs to be taken into account when considering loader cranes:

- Ultra high strength steels, e.g. S700, S900 and S1100
- Complex geometries and relatively thin sections
- Medium cycle fatigue life (20.000 to 500.000 cycles)
- Very high stress ranges, $\Delta\sigma_n > 500MPa$

Firstly, different post weld treatments will be subjected to experimental investigation in order to compare them against each other under the above mentioned conditions. The treatments will also be analyzed qualitatively in order to determine the most suitable treatment, considering practical implementation in mass production of loader cranes.

The commonly used nominal stress approach is not well-suited for fatigue assessment of the complex geometries that characterize loader cranes. The effective notch stress approach appears more suitable, however, the amount of published experimental evidence of the reliability of this approach is very limited. A systematic re-analysis of fatigue data in the notch stress system will therefore be carried out.

Lastly, in order to account for post weld treatment during development and fatigue assessment of loader cranes, a proposal is made for extension of the notch stress approach to include effects of TIG dressing, burr grinding and high frequency peening in a practical manner.

Control of mobile hydraulics

Current loader cranes are typically controlled by electro-hydraulic actuation via remote control. One axis on the remote controls one hydraulic cylinder. In order to move the tool point (hook) in a controlled way, it is normally necessary to use several DOF of the crane simultaneously. This is often a highly nonlinear task, which only experienced operators can do fast, safe and accurate. Hence, there is a potential for increased operational speed and productivity by implementing semi-automatic, intuitive tool point control.

Practical implementation of tool point control in loader cranes will therefore be addressed, based on existing methods from robotics. Control of mobile hydraulic machinery is very different from that of robotics. Among others, the following conditions complicate the control of mobile hydraulics:

- Reference input assigned continuously by operator
- Significant structural flexibility (up to several meters)
- Highly varying and unknown loading
- Complex interconnected dynamics of the mechanical and hydraulic systems
- Multiple saturation phenomena in the hydraulic actuation

The current simple control scheme where each axis of the crane is controlled directly and individually from the remote control, is not suited for optimizing the operational speed. It is assumed that using tool point control instead, it will be possible to increase the operational speed and reduce the effort and skill needed to safely operate the crane, while maintaining fatigue performance. Such tool point control scheme will therefore be investigated and further developed.

Implementing a new control principle in the existing controller requires thorough testing before releasing the software. Current testing facilities were developed for simple control principles and are not adequate for the more complex controller software required for tool point control. A hardware-in-the-loop simulator will therefore be developed to satisfy future controller software testing needs.

1.6 Outline of Thesis

Following this Introduction, two technical chapters presents the state of the art and summarizes the work carried out within the project.

Chapter 2 concerns fatigue of welded joints and focus on post weld treatment and local fatigue assessment using the notch stress approach.

Chapter 3 is on control of mobile hydraulics, considering tool point control of loader cranes and controller software testing using Hardware-in-the-loop simulation.

The conclusion in Chapter 4 reviews the main contributions from the present work and gives suggestions for future work.

2

Fatigue of Welded Joints

2.1 Introduction

It is a well known fact that welded joints have a low fatigue strength compared to the base material. This is mainly caused by local stress concentrations due to the presence of notches and high tensile residual stresses due to contraction of the weld metal during cooling and solidification. It is one of the dominating causes of failure in welded structures and has thus received much scientific attention, Maddox (1991, 2003).

The fatigue strength of welded joints proves to be practically independent of the base material strength, Fig. 2.1. Hence, when applying higher strength steels, the gap between the static strength and fatigue strength increases. It is therefore expedient to improve the fatigue strength of the welded joints, in order to fully utilize higher strength steel when designing lightweight structures.

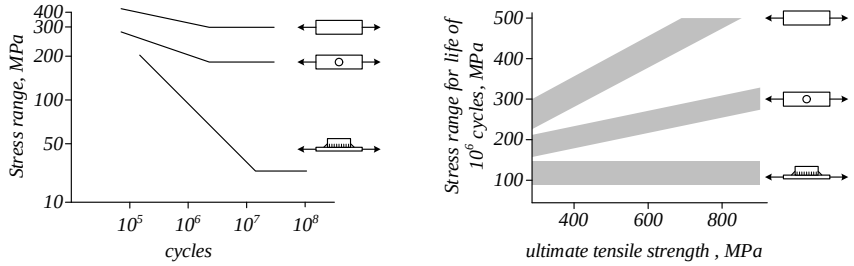

Figure 2.1: the low fatigue strength of welded joints is independent from the base material strength, after Haagensen (1985).

Increasing the fatigue strength of welded joints can be achieved in several ways. This work mainly concerns improvement by design through local fatigue assessment and the application of post weld treatment. This chapter presents the state of the art and summarizes the contributions of this work within these areas. For details, see the appended *Papers A, B* and *C*.

2.2 Post Weld Treatment

Post weld treatment has typically been applied in repair or life extension of existing welded structures, but it is getting more and more interesting for application to new high strength steel structures.

Due to high tensile residual stresses and abrupt geometry changes in the weld toe, the weld will experience an increased and elevated stress range in the as-welded condition, as shown in Fig. 2.2(a). The stress ratio of the applied loading is to a large extend insignificant to the local stress ratio, due to the high tensile residual stresses.

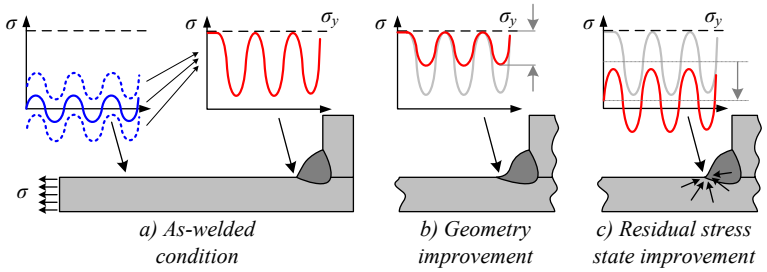

Figure 2.2: Local effects of post weld treatment.

Improving the geometry of the weld toe leads to a reduction of the stress concentration here. The weld will therefore experience a reduced stress range, as shown in Fig. 2.2(b). Geometry improvement considers both reduction of the macroscopic stress concentration due to the section change of the joint, but also reduction or removal of stress concentrations on the microscopic level due to weld defects.

By improving the residual stress state, the local stress ratio is reduced, so that all or part of the local stress range becomes compressive, Fig. 2.2(c). Local compressive loading significantly reduces the crack growth rate.

Generally, geometry improvement can be considered more robust than residual stress state improvement, in the low cycle/high stress area, since the latter improvement can be destroyed by overloading. On the other hand, residual stress state improvement tends to be more effective under the right conditions, i.e. high cycle/low stress range and low stress ratio.

Improvement of the fatigue strength of welded joints by application of post weld treatment has received much attention, especially in connection with high strength steel. Gurney (1979) mentions a variety of post-weld improvement methods. Since then, several major reviews of different post weld treatment methods have been published, e.g. Booth (1983), Haagensen (1985), Kirkhope et al. (1999) and Haagensen (2007). The IIW provides recommendations for post weld treatment considering grinding, TIG dressing and hammer/needle peening, Haagensen and Maddox (2008).

Most recent research on post-weld treatment includes a relatively new method – high frequency peening, e.g. ultrasonic impact treatment (UIT), because of very impressive

results. A number of Ph.D. theses have also been written on the subject, including Roy (2006), Lihavainen (2006), Dürr (2007) and Weich (2008).

A large European research project, Lagerqvist et al. (2007) investigated improvement of welded joints in S700, S960 and S1100, considering burr grinding and TIG dressing. Samuelsson (2007) reports on a Nordic research project, which investigates fatigue improvement of S355, S700, S900 and S1100, including UIT, LTT electrodes and grinding. Results show a tendency, that the effectiveness of post weld treatment increases with increased base material strength, however not fully consistent.

This work investigates three post weld treatments in the medium cycle area, under very high stress ranges. The treatments will be subjected to both experimental investigation and qualitative analysis, to determine the most effective and suitable treatment for mass production of loader cranes.

2.2.1 Post Weld Treatment Techniques

A selection of the most widely applied post weld treatment techniques is illustrated in Fig. 2.3, divided according to their working principle. A large number of techniques exist, both generic, such as grinding, and proprietary, e.g. ultrasonic impact treatment (UIT). Most peening techniques also provide some degree of geometry improvement, but their primary improvement is related to residual stress state improvement.

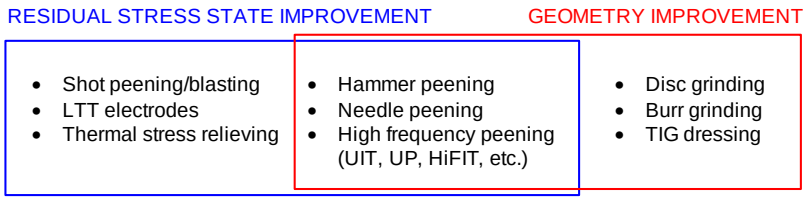

Figure 2.3: Selected improvement techniques.

In this project, three of the most common techniques are investigated; burr grinding, TIG dressing and ultrasonic impact treatment. The main objective is to determine the most suitable treatment for loader crane components, considering both its effectiveness and implementation issues. Fig. 2.4 shows the resulting weld toe profiles due to the three improvement techniques.

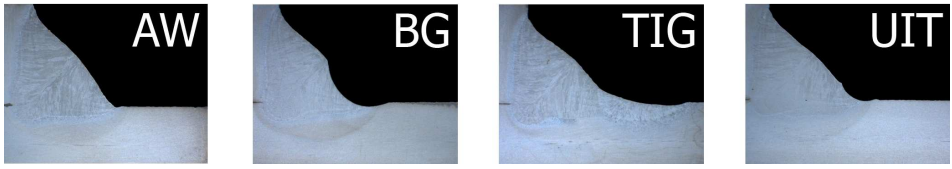

Figure 2.4: Micrographs of weld toes obtained by post-weld treatment, *Paper A*.

The level of improvement due to the investigated techniques will be discussed in the next section using the notch stress approach. This allows for comparing more data, since the effect of different joint geometries can be disregarded to some extend. *Paper A* gives the details of the current experimental work and *Paper C* presents a re-analysis of published fatigue data from investigations of post weld treatment.

Its is clear from the presented data, that the geometry improvement techniques, burr grinding and TIG dressing supports parallel shifting of the SN curve upwards. How much can always be debated, but here conservative suggestions are given, i.e. an approximate 30% increase in fatigue strength.

For high frequency peening treatment, the data supports rotating the SN curve, in addition to parallel shifting it upwards. This technique thus appears to be much more effective in the high cycle range, as opposed to the low/medium cycle area. Still Wiedner et al. (2010), and the author (*Paper A*) found the UIT treatment to give significant improvements in the low/medium cycle area, at least under bending loading.

2.2.2 Implementation of Post Weld Treatment

Post weld treatment is sometimes considered an expensive solution, but in many cases, only a very small part of a component is stressed to such extent, that post weld treatment is necessary. Thus, applying post weld treatment locally - where needed - can actually be the cheaper solution, as opposed to increasing the plate thickness in order to reduce stresses.

As an example, Fig. 2.5 shows a welded crane component, the main part of which consists of a hexagonal beam-like profile made from high strength steel. During service, it is subjected to very high cyclic loading, and in order to ensure the required fatigue life, the designers have two options; 1) post weld treatment of the highly stressed area or 2) increasing the plate thickness of the beam-like part.

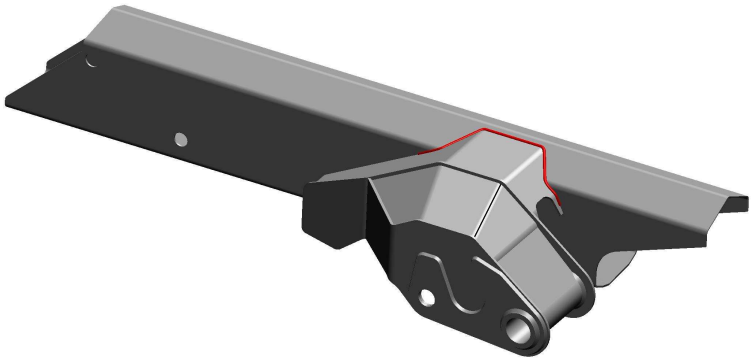

Figure 2.5: Welded crane component locally subjected to TIG dressing.

The designated weld seam (red) is subjected to TIG dressing, in order to increase its fatigue strength to a level closer to the remainder of the component. In this case, TIG

dressing of approximately 500mm of weld seam is clearly both the cheaper and better solution, since it will allow a much lighter and thus more competitive product.

However, implementing e.g. TIG dressing in production takes time and effort. Instructions were prepared and a short course was given for the operators and quality control personnel. A new weld quality class was adopted for specification of post weld treatment in technical drawings, similar to VB in the new Volvo CE weld quality system, described by Jonsson and Samuelsson (2008). Fig. 2.6 (left) shows the initial TIG dressing quality achieved, which featured both deep undercuts and slag inclusions. After further instructions and more practice, however, a consistent high quality TIG dressing were achieved, Fig. 2.6 (right).

Figure 2.6: Initial quality problems (left) and final quality TIG dressing (right), *Paper A*.

2.3 Fatigue Assessment

Many approaches exist for fatigue assessment of welded joints. They are typically categorized into nominal stress, structural stress, notch stress, notch strain and fracture mechanical approaches, Radaj et al. (2006). The IIW continuously monitors the state of the art and derives recommendations accordingly, Hobbacher (2008).

Traditionally, the nominal stress approach has been applied for fatigue assessment, but more sophisticated approaches are now more widely used due to the increase in available computational power. These so-called local approaches correlate local stresses in the vicinity of the weld toe (or root), typically obtained using finite element analysis (FEA), with the fatigue life, Fricke (2003), Nykänen et al. (2007) and Radaj et al. (2009).

The fatigue performance of a welded detail can then be improved during the design stage by optimizing the joint geometry, including the weld shape, using local approaches.

In this work, the notch stress approach has been chosen for further investigation and development, since it is found to be the most suitable approach for assessing the welded components of loader cranes. This is in regard to the size and complexity of the components, and it fits well into the current design approach using FEA.

2.3.1 Notch Stress Approach

The notch stress approach has become increasingly attractive due to the available computational power and the need for assessing more complex geometries, see e.g. Barsoum (2008), Fricke and Feltz (2009) and Fukuoka and Mochizuki (2010). In this work, the notch stress approach is investigated regarding the reliability of the claimed fatigue resistance, with special attention to mild notch joints. Furthermore, a proposal for extending the notch stress approach to post weld treated details is presented.

The notch stress approach have evolved over some 40 years, as described by Radaj et al. (2006) and different sub-approaches exist. In this work, we consider the notch stress approach according to the IIW, Fricke (2008). The approach is based on the early work by Radaj (1990), considering Neuber's fictitious notch rounding concept, but modified as described by Olivier et al. (1989, 1994). The reference radius of $R1$ is determined as a mean value of measurements and the fatigue strength (FAT225) is derived from experimental data.

The basic work flow of the notch stress approach is shown in Fig. 2.7. The weld is included in a finite element model and rounded in the toe or root by a reference radius R1 (the notch). Here, a very fine mesh is applied in order to ensure convergence of the local stresses. Then, the 1st principal stress range (or other stress components) is determined in the notch and assessed against a SN curve.

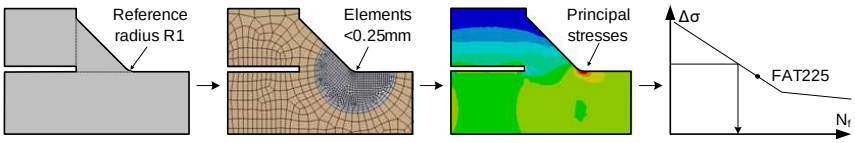

Figure 2.7: Work flow of the notch stress approach, *Paper C*.

2.3.2 Fatigue Resistance in the Notch Stress System

The IIW recommends the use of FAT225 when considering the fatigue strength of welded steel joints using the notch stress approach and the principal stress hypothesis. This value was derived from the results of a large experimental investigation of different T- and Y-joints Olivier et al. (1994) and further re-analysis of the data assembled by Olivier and Ritter (1979), as shown in Fig. 2.8.

Kranz and Sonsino (2009) explain the assumptions that led to the derivation of the FAT225 fatigue class in the IIW recommendations: The average mean local stress range ($R = 0, P_S = 50\%$) in Fig. 2.8 (347MPa) is used as a starting point and recalculated to fit the IIW system. This means dividing by $f_R = 1.10$ to account for high tensile residual stresses ($R = 0.5$) and dividing by $j_\sigma = 1.37$ to account for a probability of survival of $P_S = 97.7\%$, which leads to a value of FAT231. IIW uses a fixed spacing of 12.5% between FAT classes, so the value is rounded down to FAT225 to fit the IIW numerical system.

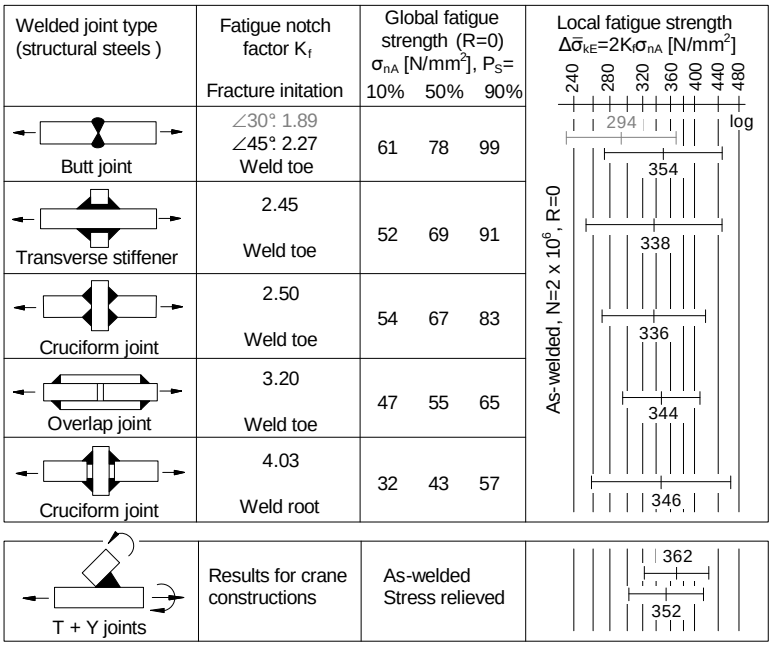

Figure 2.8: Fatigue strength in the notch stress system, after Olivier et al. (1994).

The global fatigue strength in Fig. 2.8 is derived from a very extensive database fatigue test results, containing several thousand individual results and must therefore be considered very reliable.

The fatigue notch factors for each joint type in Fig. 2.8 is determined in general for a thickness of $10mm$ and a flank angle of 45°, see Olivier et al. (1994). The fatigue notch factor of the butt joints was initially determined for a flank angle of 30°, but then increased by assuming 45° in order to account for generally larger flank angles. However, the IIW recommendations suggest the use of a flank angle of 30°, Hobbacher (2008).

This approach of applying a single general fatigue notch factor for each joint type can be problematic since the fatigue notch factor varies significantly with the dimensions of the joint, especially the thickness, as shown in Fig. 2.10.

In *Paper B*, a systematic re-analysis of fatigue data is carried out with more accurate determination of the fatigue notch factor for the individual specimens. Fig. 2.9 shows some of the results, i.e. the same fatigue data for transverse stiffeners in the nominal and notch stress systems, respectively.

When comparing the data in the two systems, it is seen, that a larger portion of the data in the notch stress system lies below the recommended SN curve. It is thus found

that the notch stress approach can be slightly less conservative than the nominal stress approach.

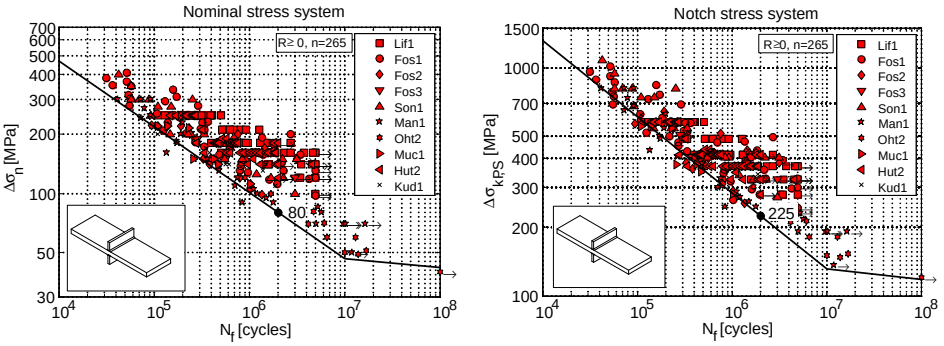

Figure 2.9: Fatigue data in the nominal and notch stress system, *Paper B*.

2.3.3 Mild Notch Joints

It is a known issue, that the notch stress approach can lead to non-conservative assessments in connection with mild notch joints, and Fricke (2008) therefore proposes a minimum notch factor of $K_w = 1.6$ as a preliminary approach. This solution is not verified and hence there is a need for better understanding of the issue.

Paper B illustrates the problem of non-conservative assessment of butt joints - especially thinner ones - when using the geometry idealization proposed by the IIW. Here, a remedial action was proposed, i.e. requiring a minimum notch factor of $K_w = 2.0$ instead of the current 1.6.

An alternative could be to model the weld with a flank angle of 45° instead of the 30° suggested in the IIW recommendations. Using 2D finite element analysis, the fatigue notch factor of a butt joints can easily be determined for different thicknesses as shown in Fig. 2.10. It's clear that using a 45° flank angle would be a much more conservative approach.

Fig. 2.10 furthermore shows a line indicating full correspondence between the nominal and notch stress approaches, i.e. the notch factor, that will force the notch stress approach to give the same result as the nominal stress approach. Since the nominal stress approach does not include any thickness effects in this range, the line is horizontal. This notch factor is determined from the characteristic fatigue strength at $2 \cdot 10^6$ cycles for the two systems, including a stress magnification factor k_m to account for misalignment in the notch stress system.

$$K_f = \frac{\Delta\sigma_{c,k}}{\Delta\sigma_{c,n} \cdot k_m} = \frac{225MPa}{90MPa \cdot 1.1} = 2.27 \tag{2.1}$$

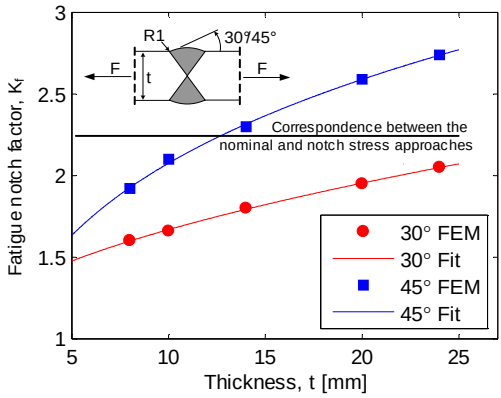

Figure 2.10: Notch factor of butt joints with different flank angles.

Using the notch stress approach, the estimated fatigue strength is proportional to the fatigue notch factor and the approach will clearly lead to quite different results than the nominal stress approach, depending on the thickness.

In *Paper B*, the thickness effect of butt joints is briefly investigated, and it is found that experimental data suggests in favor of the nominal stress approach, i.e. not assuming any thickness dependency in this range (5-25mm). Ohta et al. (1990) also found the thickness effect of butt joints to be insignificant in this range. It thus appears, that the implicit thickness effect of the notch stress approach is too sensitive to the thickness variation in this range, regardless of the chosen flank angle.

In *Paper C*, a welded crane detail is investigated using the notch stress approach, especially considering the flank angle. Using the measured flank angle of approximately 15° yields non-conservative results. If applying an idealized flank angle of 45°, instead of the measured one, much safer results are obtained. The experimental investigation of the crane detail was carried by Rasmussen (2008) in corporation with the author.

Sonsino et al. (2009) also report problems with fatigue assessment using the notch stress approach considering thin/flexible welded joints. They observed shallower slopes of the SN curves for these particular joints and therefore suggest the use of $m = 5.0$, while maintaining the FAT225 value. This solution seems to solve the problem, but it appears much too conservative in the low-to-medium cycle area, and the compatibility between the nominal and notch stress approaches will be lost.

2.3.4 Extension to Post Weld Treatment

Applying the notch stress approach to post weld treated joints is a subject still under debate. According to the IIW guideline, Fricke (2008), it is suggested to use the *actual* weld toe radius, i.e. in the treated condition, increased by 1mm and evaluate the principal stress range here against the FAT200 SN curve. However, it is also stated, that this

approach is only valid for relatively sharp notches ($R1 - R3mm$) and that it has not yet been verified.

A problem in this approach is, that it is difficult to determine the *actual* weld toe radius in a design situation. As shown in Fig. 2.11, the toe radius varies significantly from test series to test series and is assumed to follow a normal distribution within each test series. An unanswered question therefore remains; how to define the *actual* radius? Should it be the mean or minimum or something else?

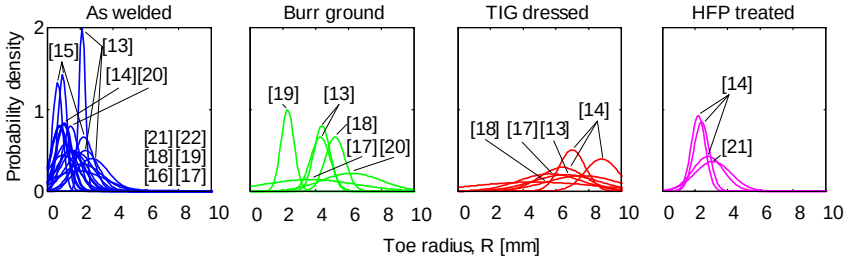

Figure 2.11: Measurements of weld toe radii, *Paper C*.

With the design situation in mind, a new proposal for fatigue assessment of post weld treated details using the notch stress approach is presented in *Paper C*. Instead of altering the idealized notch geometry (radius), it is proposed to use different SN curves for different post weld treatments, and thus maintain the reference geometry ($R1mm$). Then, a design engineer can use the same FE model to assess the fatigue performance - both in the as-welded and post weld treated states.

In order to establish SN curves for post weld treated details in the notch stress system, a large amount of fatigue data is collected and transformed into the notch stress system. The transformation is carried out by scaling the nominal stress range with the fatigue notch factor determined for each specimen using the standard idealized geometry, i.e. identical to the as-welded case.

Fig. 2.12 shows the collection of fatigue data for TIG dressed welded details in the notch stress system. Statistical analysis of these data collections is avoided, and a conservative SN curve is suggested, e.g. FAT300 for TIG dressed joints. *Paper C* furthermore presents suggested SN curves for burr ground and high frequency peened joints. For both burr grinding and TIG dressing, FAT300 and $m = 3.0$ is suggested, whereas for high frequency peening, FAT360 and $m = 5.0$ fits the data collection well.

This approach to some extend ignores the original intention of the notch stress approach, that the stress range should be determined from the real (idealized) local geometry. However, it is very practical and it allows the nominal, structural and notch stress approaches to be compatible regarding post weld treated details, as is the case for as-welded details in the IIW recommendations.

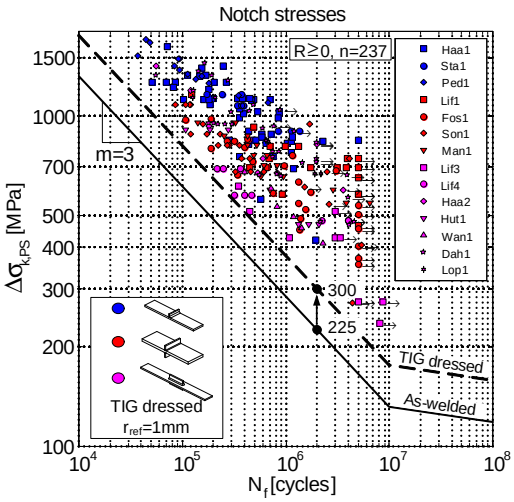

Figure 2.12: Fatigue data for TIG dressing in the notch stress system, *Paper C*.

2.4 Summary

This chapter have presented the work carried out in regards to fatigue of welded joints with the aim to provide methods for the development of durable, high strength, lightweight loader cranes. The following topics are covered:

- Evaluation of the three post weld treatments; burr grinding, TIG dressing and UIT treatment by experimental investigation and qualitative analysis.
- Investigation of the fatigue resistance used in the notch stress approach based on re-analysis of a large amount of published fatigue data.
- Investigation of the problems involved when applying the notch stress approach for fatigue assessment of mild notch joints.
- Established a proposal for extension of the notch stress approach regarding fatigue assessment of post weld treated details.

3

Control of Mobile Hydraulics

3.1 Introduction

Earlier loader cranes had purely mechanical/hydraulic safety and control systems. Typically, the operator controlled the flow to the cylinders directly by mechanical handles linked to the hydraulic directional control valves and the lifting capacity was limited by hydraulic devices.

Today however, advanced loader cranes are typically operated by a wireless remote control which sends a flow reference to an onboard controller, which then evaluates the input and, if acceptable, forwards the flow command to electro-hydraulic actuated directional control valves.

From the control signal is generated in the operator interface, i.e. the remote control, until it arrives in the valve, it passes several electronic modules, each with increasingly advanced programmable micro-controllers. Additionally, much communication in vehicle systems nowadays are transmitted by digital networks, mainly CANbus and the use of analogue components are declining in favor of network attached components.

Using such complex systems allows for advanced control features, such as selective stopping of movements and smart speed reduction depending on operating conditions. And with the increased amount of sensors mounted and digitally controlled valves, it is possible to implement very advanced control principles.

But when complexity increases, so does the risk of errors, and finding these errors becomes more and more difficult, since the IO interface of the controller now includes network busses, and not only A/D voltage signals. It is thus difficult to provide the stimuli to test controller software without connecting it to the real machine.

In general, working with control of loader cranes using the real machine, it is neither safe nor efficient. Model based development is therefore preferred and will be used extensively in this work.

Within control of mobile hydraulics, this work concerns two topics; tool point control and hardware-in-the-loop simulation, see the appended *Papers D* and *E*, respectively.

3.2 Tool Point Control

In this work, tool point control refers to a semi-automatic control scheme, assisting the operator in smooth, efficient and intuitive operation of the crane. The operator controls the speed and direction of the tool point (hook) of the crane directly, instead of the individual actuators, as is currently the case, Fig. 3.1. The main advantages of tool point control is the reduced skill level required and increased productivity.

Tool point control of mobile hydraulic manipulators has been subjected to research for several years. Krus and Palmberg (1992) presented a simple vector control strategy for a 2 DOF hydraulic crane in the early nineties. Mattila and Virvalo (2000) describe a more advanced control scheme for a similar crane; where an online model is used to reduce the pressure levels and thus the energy consumption. Beiner (1997) solves the redundancy in a 3 DOF hydraulic crane using the minimum norm of the actuator forces. Recently, Yuan et al. (2009) presented a motion control for a 4 DOF aerial lift. An interactive real time simulation was achieved by Esqué et al. (2003) for a simplified 2 DOF crane. Tool point control of mobile hydraulic manipulators has been a key area of research at Aalborg University for several years, see Pedersen and Nielsen (2002), Münzer (2003), Hansen and Andersen (2005), Ebbesen (2007) and Kabus and Haastrup (2008).

The typical control scheme is based on open-loop velocity control of the crane, where the operator 'closes the loop', i.e. he/she compensates for deviations in the tool point trajectory using visual feedback. However, this concept needs to be verified, especially considering the operator perception of e.g. saturation handling or joint limit avoidance. In order to secure the usefulness and commercial value of a tool-point control scheme it is important to have some kind of user-interaction at the initial stages. This work therefore presents an approach to tool point control development for loader cranes, using interactive real-time dynamic simulation.

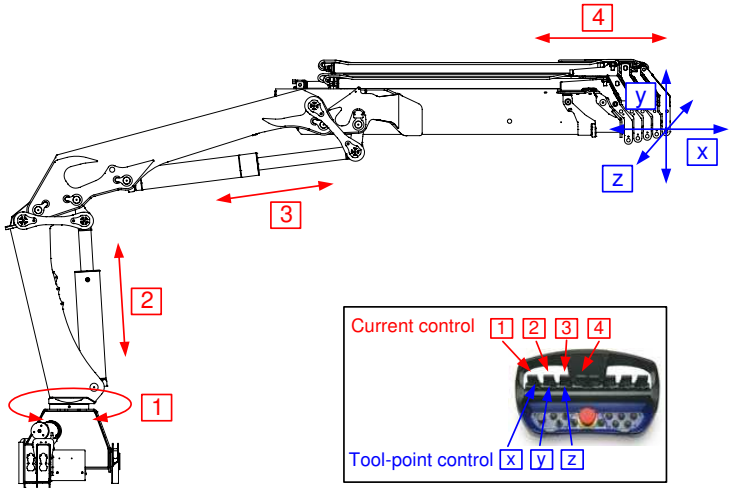

Figure 3.1: Tool point control principle.

3.2.1 Real-time Simulation

It is expedient to apply real-time simulation here, since the crane will be controlled online by an operator, and his influence on the control scheme is difficult to include otherwise.

A simulation model is therefore developed in Simulink using the 3D animation toolbox. It takes input from the operator continuously via joystick, calculates the resulting motion and displays it in the form of a 3D animation. As shown in Fig. 3.2, the model consists of a hydraulic model and a mechanical model, which together forms a virtual crane.

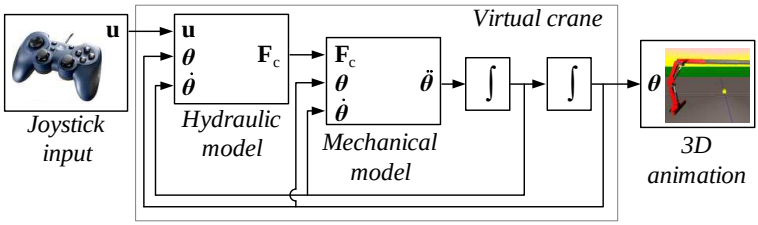

Figure 3.2: Overview of the simulation, *Paper D.*

Achieving real-time simulation performance relies on the following two Simulink concepts; rate-transition blocks and embedded Matlab blocks. Rate-transition blocks allows for part of the simulation to run faster than the rest, e.g. the computationally heavy animation update is only performed at $10Hz$. Embedded Matlab blocks contain Matlab script code that is automatically converted to C code and compiled before running the Simulink model and thus executes very fast. Using the fixed step 4th order Runge-Kutta integrator (ODE4) and a time step of $2.5ms$ yields real-time execution on a standard 2GHz laptop computer for the simulation model presented here.

In the mechanical model, the equations of motion is established in the joint space, in order to achieve the smallest possible system matrix for inversion. The mass and inertia is furthermore lumped into few bodies and the telescopic extension system is modeled as single body with variable inertia properties depending on the extension length. In total, the model includes 6 DOF; 4 hydraulically actuated and 2 passive, which models the in-plane and lateral flexibility.

The hydraulic system is modeled using the pressure build-up equations and thus takes into account the flexibility of the oil in hoses etc. Loader cranes are equipped with over-center valves (OCVs), which typically complicates simulation due to very fast dynamics. Here, these are modeled according to a simple discharge characteristic which includes the steady-state influence of the OCV, but neglects the dynamics of the OCV spool.

This model enabled investigation of the traditional tool point control approach for loader cranes by interactively testing it on the virtual crane in real-time simulation. Several issues where identified and the control scheme were further developed, as described in the following section.

3.2.2 Control Scheme

The purpose of the tool point control scheme is to make it more intuitive for the operator to control the crane and avoid potential excessive or abrupt motion, thus lowering the dynamic loading on the crane even at increased velocities.

Since the crane is redundant, the Jacobian is not square and thus cannot be directly inverted. A pseudo inverse approach is therefore used to find a set of joint velocities, that will produce the desired tool point motion. The pseudo inverse returns the minimum velocity norm in the joint space, as discussed by Beiner and Mattila (1999):

$$\dot{\mathbf{r}}_{TP} = \mathbf{J}\dot{\boldsymbol{\theta}} \tag{3.1}$$

The pseudo inverse is then

$$\dot{\boldsymbol{\theta}} = \mathbf{J}^{+}\dot{\mathbf{r}}_{TP} + (\mathbf{I} - \mathbf{J}^{+}\mathbf{J})\mathbf{z} \tag{3.2}$$

The first term is a set of joint velocities that will produce the desired tool point velocity. The second term describes a set of joint velocities which have no influence on the tool point, but can be used to control the so-called self-motion of the crane. Both of them are controlled by the operator.

The pseudo inverse is furthermore weighted in order to implement joint limit avoidance and configuration control. Joint limit avoidance is implemented according to Chan and Dubey (1993), but the weighting matrix is extended in order to include automatic optimization of the torque arm of the main lift cylinder. The configuration control thus comprise both automatic optimization of the main joint lifting capacity, but also active control by the operator allowing him/her to control the self-motion directly e.g. to avoid obstacles.

The reference velocities determined above do not account for the significant flexibility of loader cranes and a straight horizontal tool point trajectory will be difficult to achieve. A deflection compensation scheme is therefore developed, inspired by the simple approach presented by Yuan et al. (2009). Here a small upwards velocity is continuously added to the tool point reference velocity, when the crane telescopic system is extending.

Flow sharing is necessary in order to avoid both the valve- and pump flow limits, otherwise the reference joint velocities, and thus the desired tool point velocity, will not be realized. A flow sharing scheme is therefore implemented, similar to that used by Pedersen and Nielsen (2002), which scales down the reference velocity of all actuators if one reaches saturation. Hence only the tool point speed is violated, but the direction is maintained.

During the development of this control scheme, the interactive real-time simulation model proved to be indispensable. As an example, Fig. 3.3 shows the difference between a predefined operator model without any feedback and an active operator using visual feedback to adjust the input. It is clear that, when the operator capabilities are included in real-time simulation, the control performance is excellent.

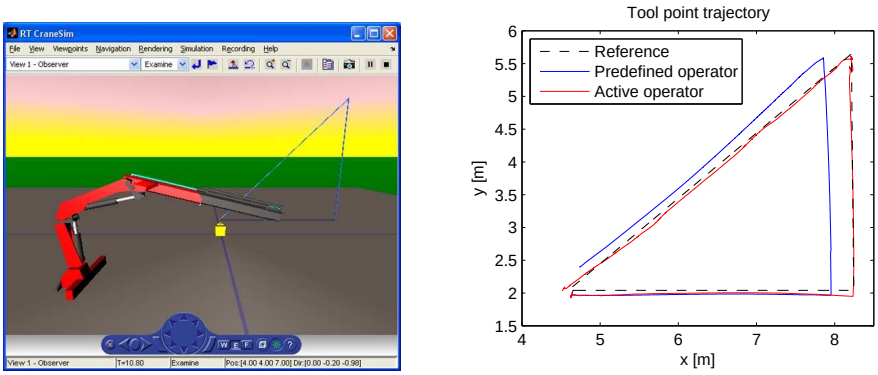

Figure 3.3: Influence of the active operator, *Paper D*.

3.3 Hardware-in-the-loop Simulation

Hardware-in-the-loop (HIL) simulation is a method for testing controller software, without using the actual machine for which the controller is intended. Here, the machine is simulated in real-time in a computer and the controller IO interface is connected to the simulation.

Previously, testing were typically performed using the real machine, however, it is time consuming and difficult to make accurate and repeatable tests this way. Recent advances in computer hardware and software, have made it possible to implement very cost-effective HIL simulation platforms for such machinery, and thus significantly improving testing capabilities.

Early HIL simulation (HILS) platforms typically considered a single component or minor isolated systems for testing controller software with limited visual output, e.g. Linjama et al. (2000). However, advances in computational power have propelled a rapid evolution of HILS platforms which now considers entire systems, such as heavy construction machinery or offshore structures and offer rich 3D animation output.

A HILS system for a hydraulic excavator with both audio and visual simulation output integrated in the operator cabin of a real excavator, was presented by Elton et al. (2009). The system included a remote hydraulic load emulator for a variable displacement pump, connected via Internet. The simulation are thus fed accurate (non-modeled) information from the pump.

Ghabcheloo and Hyvönen (2009) discusses development of a motion control system for a hydraulic wheel loader in a HILS platform called GIMsim. It consists of 5 PCs communicating via LAN to accommodate animation, dynamics, tire contact, IO including CAN and simulation control. The simulation is developed in Matlab/Simulink, compiled and transfered to an xPCtarget for hard real-time operational speed.

Recently, Trydal (2010) presented a very advanced proprietary HILS platform from National Oilwell Varco. It concerns an offshore drill-rig including the entire drilling process equipment and displays a 3D animation in a dome in order to completely immerse the operators. Instead of physical IOs, each controller are connected to a similar controller which simulates the IO functionality.

The general trend is to develop the simulation in Matlab/Simulink, use several PCs connected via LAN and use hardware IO connectivity from National Instruments, dSpace or others. Simulation input are given from real operator interfaces and results are presented using more and more realistic 3D animations. The animation software is often developed specifically for the considered system e.g. in C++ using OpenGL.

In this work, a cost effective approach to HIL simulation is demonstrated using only standard high-level engineering software. A truck and loader crane with a total of 21 DOFs is simulated with less than 10.000$ in total expenses for hardware and software.

3.3.1 Loader Crane HIL Simulator

The HIL simulator presented in this work is developed for the specific controller currently used on HMF loader cranes, however, the same approach should be applicable for similar machinery. The HIL simulator consists of a simulation PC running Matlab which is connected to the CAN network including the controller through another PC running LabView, Fig. 3.4. The two PCs communicate via LAN over the UDP/IP protocol, and are denoted *Hardware Gateway* and *Simulation PC*, respectively.

LAN communication using the UDP protocol is an efficient approach to achieve co-simulation with two different programs. Using several PCs gives a performance advantage and enables additional monitoring possibilities and remote location of hardware. It is thus possible to take advantage of the simulation features of Matlab and at the same time use the excellent hardware connectivity features of LabView - in the same simulation.

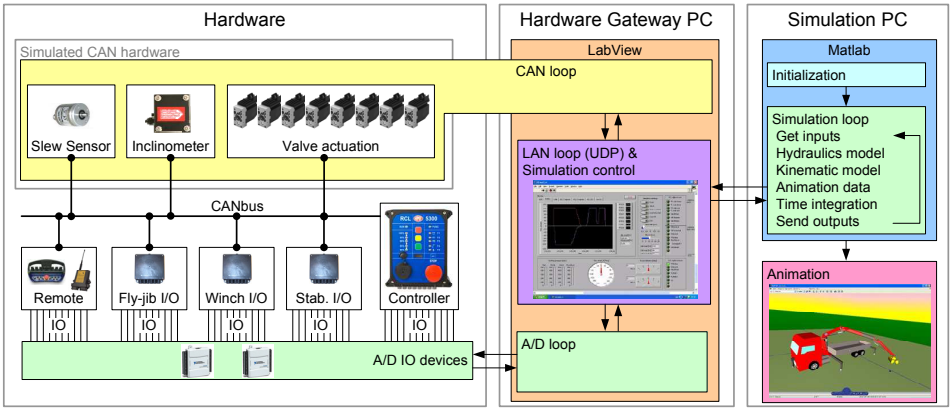

Figure 3.4: Overview of the HIL simulation, *Paper E*.

The Hardware Gateway runs the low-level communication with the controller hardware and emulates a number of CAN devices, i.e. virtual sensors and virtual hydraulic valves. As shown in Fig. 3.4, the Labview program is divided in three separate loops; a LAN loop, CAN loop and A/D loop. Each loop covers communication between the gateway and LAN network, CAN network or analog/digital hardware, respectively.

The simulation contains a full kinematic model of the truck and crane, including a number of crane accessories, and a number of virtual sensors, which generates the necessary input to the controller. The simulation is driven by the flow commands send from the controller to the virtual hydraulic valves and a number of output signals. The results of the kinematic analysis is presented as a 3D animation.

Using this HIL simulator, it has become possible to perform much more precise and repeatable testing of the current controller software, and a platform is established for development and testing of the next generation software.

3.4 Summary

This chapter presented the work carried out in this project regarding improvement of control performance of loader cranes, including the following topics:

- An approach to interactive, real-time dynamic simulation of loader cranes is established, with the aim to develop more advanced control principles.
- A tool point control scheme have been investigated and further developed in order to adapt it to current HMF loader cranes, and verify its effectiveness for this application.
- A demonstration of a cost effective approach to HIL simulation is presented with the ability to simulate all necessary IO functionality in the current controller of HMF cranes.

4

Conclusion

This work spans two distinct topics in mechanical engineering; fatigue of welded joints and control of mobile hydraulic systems. It was planned to devote more effort to implementation of the tool point control strategy in a real crane using a specific newly developed hydraulic servo valve from an undisclosed manufacturer. Unfortunately, the final development of this valve was delayed and it was not ready in due time to be part of this project.

The original plan of evaluating the fatigue performance of a crane with tool point control against one with traditional control was therefore discarded. Other topics in the project were then expanded and several contributions within each field are made.

The main contribution of this project is a set of tools enabling development of high performance lightweight structures, such as loader cranes with increased fatigue- and control performance, as compared to current standards. Due to the nature of this project, the contributions presented are all directly applicable in industrial context, e.g. in the sponsor company Højbjerg Maskinfabrik A/S.

Contributions

Regarding fatigue of welded joints, this project have contributed with:

- An evaluation of the post weld treatments; TIG dressing, burr grinding and high frequency peening under the specific conditions of loader cranes, including the aspects of practical implementation in mass production.
- A better understanding of the reliability involved in fatigue assessment of welded joints using the notch stress approach, including the effect of mild-notch joints.
- A proposal for extension of the notch stress approach to include the post weld treatments; TIG dressing, burr grinding and high frequency peening treatment in an efficient and practical manner.

Within control of mobile hydraulics, this project have contributed with:

- An approach to real-time interactive simulation of loader cranes, including the dynamics of the hydraulic and mechanical systems.

- A validation of a tool point control scheme with an operator in the loop, i.e. showing the positive effect of operator visual feedback.
- An approach to cost-effective hardware-in-the-loop simulation for loader cranes using only standard engineering software.

Recommendations for Further Work

A subject within post weld treatment of high strength steel, that has only been briefly touched upon here, and in general, is the effect of high frequency peening treatment, e.g. UIT, in the low to medium cycle fatigue area and the associated high stress ranges. There is a need for thorough investigation of the stability of the treatment in this area, due to the risk of relaxation of the compressive residual stresses introduced by the treatment.

In regards to fatigue assessment using the notch stress approach, there is a need for better understanding of the effects of mild notch joints. Since the notch stress approach is an ideal choice for optimizing the local geometry of a welded joint, including the weld shape, it will often be applied in a context where the designer works towards mild notches. The approach is thus intentionally used in the direction of the limit of applicability – which is not well defined.

The implementation of tool point control in loader cranes in industrial context opens up for a number of research topics. While much research – including this work – have demonstrated the benefits of tool point control of mobile hydraulic manipulators, very few actual implementations are found in a commercial context. Especially the task of achieving a sufficiently accurate flow control in connection with the over-center valves poses an interesting research topic.

While the developed HIL simulator possess a sufficient level of detail to test the current controller used on HMF loader cranes, it would be interesting to include the dynamics of both the truck and the crane in the simulation model. Computationally, this is a very challenging task, but it should be possible by including one or more computers dedicated to solving the dynamics and connecting these to the current setup via LAN.

Bibliography

Barsoum, Z. (2008), Residual stress analysis and fatigue assessment of welded steel structures, Ph.d. thesis, KTH, Stockholm, Sweden.

Beiner, L. (1997), 'Minimum force redundancy control of hydraulic cranes', *Mechatronics* **7**(6), 537–547.

Beiner, L. and J. Mattila (1999), 'An improved pseudoinverse solution for redundant hydraulic manipulators', *Robotica* **17**, 173–179.

Booth, G. (1983), *Improving the Fatigue Strength of Welded Joints*, TWI, Abington Publishing, UK.

Chan, T. F. and R. V. Dubey (1993), 'A weighted least-norm solution based scheme for avoiding joint limits for redundant manipulators', *Robotics and Automation* **3**, 395–402.

Dürr, A. (2007), Zur Ermüdungsfestigkeit von Schweisskonstruktionen aus höherfesten Baustählen bei Anwendung von UIT-Nachbehandlung [Fatigue Resistance of Welded High Strength Steel Structures Using UIT Post Weld Treatment], Ph.d. thesis, Universität Stuttgart, Germany.

Ebbesen, M. K. (2007), Optimal Design of Flexible Multibody Systems, Ph.d. thesis, Institute of Mechanical Engineering, Aalborg University, Denmark.

Elton, M.D., A.R. Enes and W.J. Book (2009), A virtual reality operator interface station with hydraulic hardware-in-the-loop simulation for prototyping excavator control systems, *in* 'IEEE/ASME International Conference on Advanced Intelligent Mechatronics', Singapore.

EN12999 (2010), 'FprEN12999:2010, Cranes - Loader cranes'.

Esqué, S., A. Raneda and A. Ellman (2003), 'Techniques for studying a mobile hydraulic crane in virtual reality', *Int J Fluid Power* **4**(2), 25–34.

Fricke, W. (2003), 'Fatigue analysis of welded joints: State of development', *Marine Structures* **16**, 185–200.

Fricke, W. (2008), 'Guideline for fatigue assessment by notch stress analysis for welded structures'. IIW Doc. XIII-2240r1-08.

Fricke, W. and O. Feltz (2009), 'Fatigue tests and numerical analyses of partial-load and full-load carrying fillet welds at cover plates and lap joints'. IIW Doc. XIII-2278-09.

Fukuoka, T. and K. Mochizuki (2010), 'Effect of plate thickness on fatigue strength of typical welded joints for a ship structure'. IIW Doc. XIII-2333-10.

Ghabcheloo, R. and M. Hyvönen (2009), Modeling and motion control of an articulated-frame-steering hydraulic mobile machine, *in* '17th Mediterranean Conference on Control and Automation', Thessaloniki, Greece.

Gurney, T.R. (1979), *Fatigue of Welded Structures*, Cambridge University Press, Cambridge, UK.

Haagensen, P.J. (1985), Improving the fatigue strength of welded joints, *in* A.Naess, ed., 'Fatigue Handbook - Offshore Steel Structures', Tapir, Trondheim, Norway, pp. 259–289.

Haagensen, P.J. (2007), 'Fatigue improvement techniques - advantages and limitations', *Welding in the World* **47**, 43–63.

Haagensen, P.J. and S.J. Maddox (2008), 'IIW recommendations on post weld improvement of steel and aluminium structures'. IIW Doc. XIII-2200r1-07.

Hansen, M. R. and T. O. Andersen (2005), A method for deriving the optimal operation of mobile hydraulic manipulators, *in* 'Proc 9th Scandinavian International Conference on Fluid Power, SICFP'05', Linköping, Sweden.

HMF (2010), 'www.hmf.dk'. HMF history.

Hobbacher, A. (2008), *IIW Recommendations for Fatigue Design of Welded Joints and Components*, WRC Bulletin 520, New York, USA.

Jonsson, B. and J. Samuelsson (2008), 'A new weld quality system'. IIW Doc. XIII-2235-08.

Kabus, S. and M. Haastrup (2008), Simulations of flexible loader crane with designed tool point control, Master's thesis, Institute of Mechanical Engineering, Aalborg University, Denmark.

Kirkhope, K.J., R. Bell, L. Caron, R.I. Basu and K.T. Ma (1999), 'Weld detail fatigue life improvement techniques. part 1 and 2', *Marine Structures* **12**, 447–496.

Kranz, B. and C.M. Sonsino (2009), 'Verification of the notch stress concept for the reference radii of rref=1.00 and 0.05mm'. IIW Doc. XIII-2274-09/XV-1312-09.

Krus, G. and J. O. Palmberg (1992), Vector control of a hydraulic crane, *in* 'Proc International Off-Highway and Power plant Congress and Exposition', Milwaukee, USA.

Lagerqvist, O., M. Clarin, J. Gozzi, B. Völling, D. Pak, J. Stötzl, H.P. Lieurade, B. Depale, I. Huther, S. Herion, J. Bergers, R.M. Martsch, M. Carlsson, A. Samuelsson and C. Sonander (2007), *LiftHigh - Efficient Lifting Equipment with Extra High-Strength Steel*, European Commission, Technical Steel Research, EUR22569EN, Brussels, Belgium.

Lihavainen, V.M. (2006), A Novel Approach for Assessing the Fatigue Strength of Ultrasonic Impact Treated Welded Structures, Ph.d. thesis, Lappeenranta University of Technology, Lappeenranta, Findland.

Linjama, M., T. Virvalo, J. Gustafsson, J. Lintula, V. Aaltonen and M. Kivikoski (2000), 'Hardware-in-the-loop environment for servo system controller design, tuning and testing', *Microprocessors and Microsystems* **24**, 13–21.

Maddox, S.J. (1991), *Fatigue Strength of Welded Structures, 2nd ed.*, Abington Publishing, Cambridge, UK.

Maddox, S.J. (2003), 'Key developments in the fatigue design of welded constructions', *Welding in the World* **47**, 6–40.

Mattila, J. and T. Virvalo (2000), Energy efficient motion control of a hydraulic manipulator, *in* 'Int Proc Robotics and Automation', San Francisco, USA.

Münzer, M E. (2003), Resolved Motion Control of Mobile Hydraulic Cranes, Ph.d. thesis, Insitute of Energy Technology, Aalborg University, Denmark.

Nykänen, T., G. Marguis and T. Björk (2007), 'Simplified assessment of weld quality for fatigue loaded cruciform joints'. IIW Doc. XIII-2177-07.

Ohta, A., T. Mawari and N. Suzuki (1990), 'Evaluation of effect of plate thickness on fatigue strength of butt welded joints by a test maintaining maximum stress at yield strength', *Engineering Fracture Mechanics* **37(5)**, 987–993.

Olivier, R., V.B. Köttgen and T. Seeger (1989), *Schweissverbindung I [Welded Joints I]*, FKM Forschungshefte 143, Frankfurt/M, Germany.

Olivier, R., V.B. Köttgen and T. Seeger (1994), *Schweissverbindung II [Welded Joints II]*, FKM Forschungshefte 180, Frankfurt/M, Germany.

Olivier, R. and W. Ritter (1979), *Wöhlerlinienkatalog für Schweissverbindungen aus Baustählen [SN curve catalog for welded joints in structural steels]*, DVS GmbH, Düsseldorf, Germany.

Pedersen, H. C. and B Nielsen (2002), Resolved motion control of flexible hydraulic manipulators, Master's thesis, Institute of Mechanical Engineering, Aalborg University, Denmark.

Radaj, D. (1990), *Design and Analysis of Fatigue Resistant Welded Structures*, Woodhead Publishing, Cambridge, UK.

Radaj, D., C.M. Sonsino and W. Fricke (2006), *Fatigue Assessment of Welded Joints by Local Approaches, 2nd ed.*, Woodhead Publishing, Cambridge, UK.

Radaj, D., C.M. Sonsino and W. Fricke (2009), 'Recent developments in local concepts of fatigue assessment of welded joints', *Int. J. Fatigue* **31(1)**, 2–11.

Rasmussen, L.V. (2008), Levetidsbestemmelse og analyse af typisk svejst krandetalje i højstyrkestål (danish). [Fatigue assessment and analysis of typical welded crane detail in high strength steel], Master's thesis, Institute of Mehanical Engineering, Aalborg University, Denmark.

Roy, S. (2006), Experimental and Analytical Evaluation of Enhancement in Fatigue Resistance of Welded Details Subjected to Post-Weld Ultrasonic Impact Treatment, Ph.d. thesis, Dept. of Civil and Env. Eng., Lehigh University, USA.

Samuelsson, J. (2007), *Integrated Design and Manufacturing of Welded Structures*, Norden - Nordic Innovation Centre, Oslo, Norway.

Sonsino, C.M., T. Bruder and J. Baumgartner (2009), 'Sn-curves for welded thin joints - suggested slopes and fat-values for applying the notch stress concept with various reference radii'. IIW Doc. XIII-2280-09.

Trydal, S. (2010), 'HIL simulator. Hardware In Loop Simulator med fokus på integrerte prosesser. [HIL simulator. hardware-in the loop simulator with focus on integrated processes]'. www.nodeproject.no/index.php?articleid=393.

Weich, I. (2008), Ermüdungsverhalten mechanisch nachbehandelter Schweissverbindungen in Abhängigkeit des Randschichtzustands [Edge Layer Condition and Fatigue Strength of Welds Improved by Mechanical Post Weld Treatment], Ph.d. thesis, Technischen Universität Brauschweig, Germany.

Wiedner, P., I. Weich and T. Ummenhofer (2010), 'High frequency hammer peening of LCF-stressed ultra high strength steels'. IIW Doc. XIII-2341-10.

Yuan, Q., J. Lew and D. Piyabongkarn (2009), Motion control of an aerial work platform, *in* 'Proc. American Control Conference', St. Louis, MO, USA.

Appended Papers

A

Comparison of Post Weld Treatment of High Strength Steel Welded Joints in Medium Cycle Fatigue

M.M. Pedersen, O.Ø. Mouritsen, M.R. Hansen, J.G. Andersen, J. Wenderby
Welding in the World, **54** (7/8), pp. 208-217, 2010.

Abstract. This paper presents a comparison of three post weld treatments for fatigue life improvement of welded joints. The objective is to determine the most suitable post weld treatment for implementation in mass production of certain crane components manufactured from very high strength steel. The processes investigated are; burr grinding, TIG dressing and ultrasonic impact treatment.

The focus of this investigation is on the so-called medium cycle area, i.e. 10,000-500,000 cycles and very high stress ranges. In this area of fatigue design, the use of very high strength steel becomes necessary, since the stress range can exceed the yield strength of ordinary structural steel, especially when considering positive stress ratios ($R \geq 0$).

Fatigue experiments and qualitative evaluation of the different post weld treatments leads to the selection of TIG dressing. The process of implementing TIG dressing in mass production and some inherent initial problems are discussed. The treatment of a few critical welds leads to a significant increase in fatigue performance of the entire structure and the possibility for better utilization of very high strength steel.

Introduction

It is a well known fact that welded joints have a low fatigue strength compared to the base material. This is mainly caused by local stress concentrations due to the presence of notches and high tensile residual stresses. Notches occur both because of the geometry of the joint, but also because of weld imperfections such as undercuts and slag inclusions. Tensile residual stresses arise from the contraction of the weld metal during cooling and solidification.

The fatigue strength of as-welded joints proves to be practically independent of the base material strength. Thus, when applying higher strength steels, the gap between the static and fatigue strength increases. However, in many applications, e.g. mobile machinery, there is a tendency to pursue an increase in the performance to weight ratio by applying higher strength steels. In such cases, the fatigue strength of the welded joints becomes the dominating factor and limits the benefit of the application of the high strength steel.

Improvement of the fatigue strength of welded joints by application of different post-weld treatments has therefore received much attention lately e.g. [1-5], especially treatments based on high frequency peening, e.g. UIT. These relatively new treatments consistently provide very significant improvements in fatigue strength, particularly in the high cycle regime.

Unfortunately, only little effort has been put into investigation of the medium cycle area, i.e. the upper area marked in Fig. A.1. In this area of fatigue design, there is an obvious reason for using high strength steels, since the stress range exceeds the yield strength of ordinary structural steel, assuming $R > 0$. Ordinarily this area would be classified as low cycle fatigue, and plasticity should be taken into account. When applying high strength steel, on the other hand, the elastic region extends upwards in the Wöhler diagram, and plasticity is not an issue.

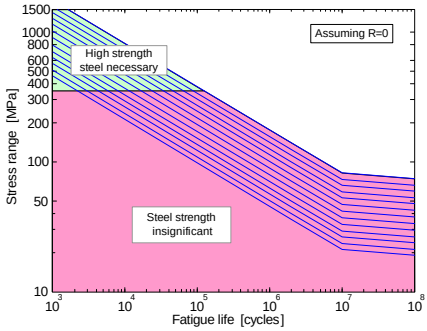

Figure A.1: Net of S-N curves according to the IIW [6].

Figure A.2: A truck mounted loader crane is primarily manufactured from S700, S900 and S1100.

Even though the fatigue strength of as-welded joints is independent of the base material strength at lower stress ranges, this is not the case for the high stress / medium cycle area. There is a need for special fatigue design guidelines in this area considering the use of high strength steel. An example is the IIW parent material curve FAT160, see Hobbacher [6], which is too conservative for high strength steel. The new crane code EN13001 [7] for instance suggests FAT315 for high strength steel parent material.

Mobile lifting equipment, e.g. loader cranes as shown in Fig. A.2, is a good example of structures designed for high stresses and medium cycle fatigue lives, e.g. 20,000 - 250,000 full load lifting cycles. The manufacturers strive to increase the lifting capacity and reduce the weight of these structures using higher and higher steel grades and thin,

locally reinforced plate structures. This tendency inevitably leads to fatigue problems, which is why post weld treatment becomes more and more interesting for these new structures, instead of upgrading/repair of existing ones.

This work investigates three different post weld treatments in the medium cycle area, under very high stress ranges, i.e. up to the yield strength of the base material. The objective is to determine the most suitable treatment in this area when also considering the practical issues of implementation in mass production of crane components.

Experimental

The fatigue investigation was carried out on simple T-joint specimens in four point bending. The high stress ranges and the required accuracy are more easily achieved in bending tests as compared to tests in tension. Furthermore, by testing in bending loading, misalignment-induced secondary bending stresses are avoided. This is essential, since the different post weld treatments cause different levels of distortion in the specimens.

Test specimens

The test specimens are produced by robotic MAG welding of Domex 700 by the Danish loader crane manufacturer HMF A/S, using a matching filler material. The plate was initially clean blasted and pre-bent 3 degrees to counteract welding distortion. The final specimen geometry is shown in Fig. A.3 and the welding parameters are listed in Tab. A.1.

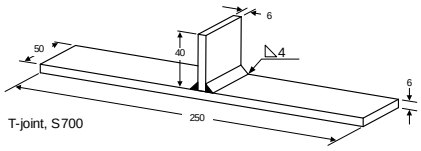

Figure A.3: Test specimen geometry.

Current	270A
Voltage	26V
Travel speed	440mm/min
Shielding gas	90% Argon, 10% CO_2
Heat input	0.8kJ/mm
t8/5 time	6sec

Table A.1: Welding parameters.

The specimen edges were ground longitudinally and the corners slightly rounded using a burr grinder. The weld quality was considered normal. The cooling rate, expressed as the time for cooling from 800° to 500° ($t_{8/5}$ time), was within the margins specified by the steel manufacturer, SSAB, namely between 5 and 25 seconds for the Domex 700 steel.

Fatigue testing

Fatigue testing was performed using a 100kN Schenk hydraulic fatigue testing machine at the Department of Mechanical Engineering at Aalborg University. The tests were performed in four point bending, at constant amplitude, using the equipment shown in Fig. A.4 and Fig. A.5. The stress ratio was kept at $R = 0.1$, and the frequency was varied from $7 - 28Hz$. The tests were performed at room temperature and no heating of the specimens occurred.

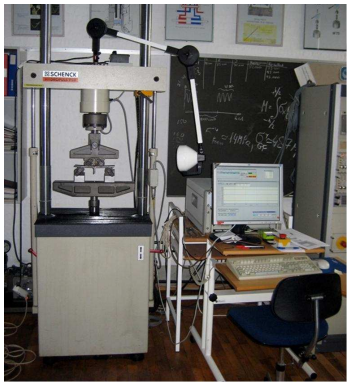

Figure A.4: Fatigue testing machine.

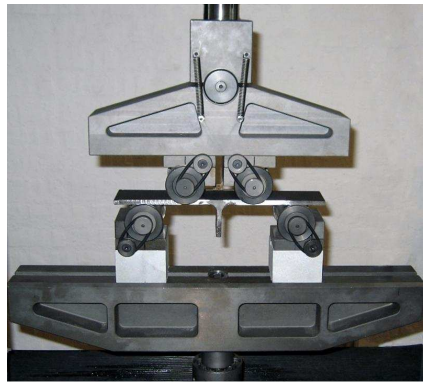

Figure A.5: Fatigue test method.

Post Weld Treatment

Three post weld treatments were selected for the investigation; burr grinding (BG), TIG dressing and ultrasonic impact treatment (UIT). The first two processes mainly aim at improving the weld toe geometry in order to reduce the stress concentration here. UIT on the other hand primarily aims at improving the residual stress state in the weld toe area.

Since the fatigue testing was carried out under very high stresses, it was anticipated that the residual stresses would not influence the fatigue life significantly due to relaxation. The majority of the improvement is therefore expected to stem directly from improvement in the weld toe geometry. Fig. A.6 shows the specimens and Fig. A.7 shows micrographs of the weld toe geometry in as-welded and post weld treated conditions.

All post weld treatments have potential drawbacks under the conditions of this investigation. Burr grinding is difficult due to the high hardness of the material. TIG dressing may lead to excessive softening of the high strength steel. The compressive residual stresses introduced by UIT may be relaxed due to the high stresses.

Evidently, the weld toe stress concentration factor will be reduced by all the post weld treatments considered. However, TIG dressing seemed to leave the weld toe with the smoothest transition between the base material and weld face. Nevertheless, the transition geometry of the TIG dressed weld toe varied significantly along the treated weld seam due to minor variations in the welding torch angle and treatment speed.

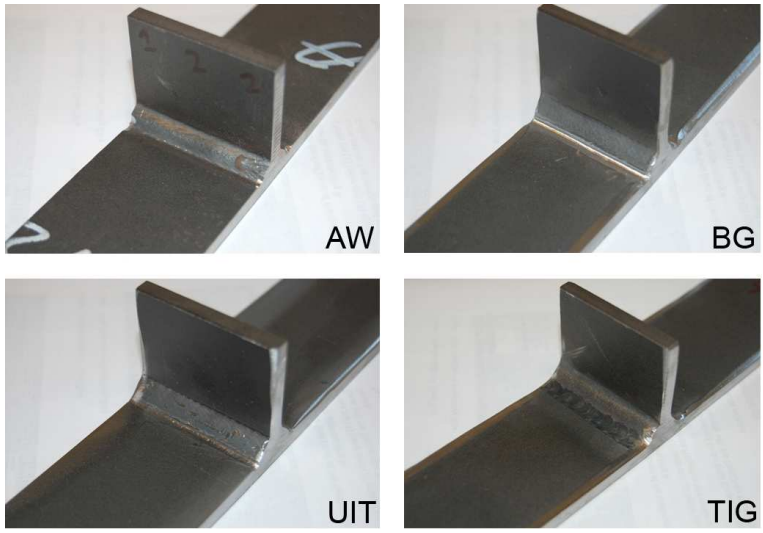

Figure A.6: As-welded and post weld treated test specimens.

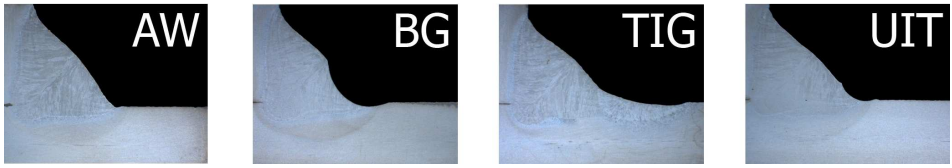

Figure A.7: Micrographs illustrating the different toe geometries obtained by post-weld treatment.

Burr grinding

The purpose of burr grinding is to remove minor weld defects in the weld toe by machining, while at the same time reducing the stress concentration factor of the weld toe. The use of a burr grinder instead of a disc grinder leaves the grinding marks parallel to the direction of loading, which prevents them from acting as crack initiation sites.

Hansen et al. [8] report significant improvements in fatigue life from a two-stage burr grinding procedure, using first a rough tungsten carbide burr followed by a second run with a finer grinder, see Fig. A.8. This procedure has therefore been adopted in this investigation, together with the general guidelines provided by the IIW, see Haagensen and Maddox [9].

A relatively small diameter burr ($\varnothing 6mm$) was used in order to limit the reduction of section of the base plate due to excessive grinding. The treatment left a shiny smooth surface in the weld toe. When inspected under microscope, there were no sign left of the original weld toe.

Figure A.8: 6mm diameter tungsten-carbide burr (top) and fine grinder (bottom).

Burr grinding in high strength steel is rather slow because of the high hardness of the steel, which also causes significant wear in the burr. The fact, that some of the base plate must be ground away in order to remove weld defects furthermore limits the use of this treatment in the very thin plates commonly used when applying high strength steel, e.g. $4 - 5mm$ plate.

High Frequency Peening (HFP) treatment

The following different types of high frequency peening treatments are described in the literature; ultrasonic impact treatment (UIT) [10], ultrasonic peening (UP) [11], high frequency impact treatment (HiFIT) [12] and ultrasonic needle peening (UNP) [13], see Fig. A.9. UIT is based on magnetostriction, UP uses a piezoelectric transducer, whereas HiFIT is pneumatically actuated. Although they are different processes, their properties and resulting improvement in fatigue strength appear to be similar.

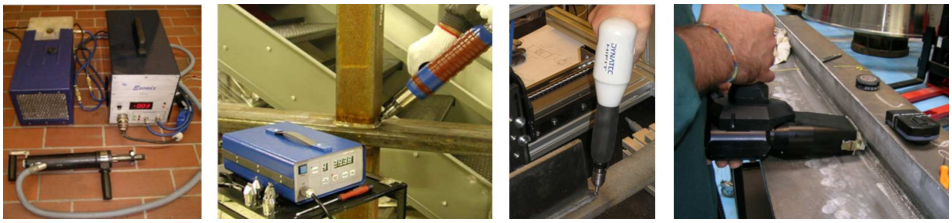

Figure A.9: Examples of four different tools for high frequency peening treatment. From left; UIT [3], UP [4], HiFIT [5] and UNP [6].

They all operate in a manner similar to ordinary hammer peening equipment, only at a considerably higher frequency, which reduces vibration and noise and is claimed to give a high improvement in fatigue strength. The tip of the tool oscillates at about $200Hz$ with a displacement of only about $40\mu m$. Usually, the tip of the tool is fitted with several hardened pins, e.g. 3-4 on a line, but many different configurations exist. The tools are usually handheld, but a robot-mounted version of the UIT device has also been developed.

According to Lihavainen [14] only a force of approximately $30N$ is necessary on the UIT tool, whereas ordinary hammer peening tools require a force of more than $200N$ against the material being treated. The application of a HFP treatment is therefore much more comfortable for the operator, which may lead to a better result.

The HFP treatments improve the fatigue strength of the welded joint in several ways by plastic deformation of the weld toe. Firstly, the tensile residual stress state present in the weld seam is relieved and beneficial compressive residual stresses are introduced. Secondly, the sharp notch in the weld toe is blunted and the treatment leaves behind a smooth trace with a radius of $2-3mm$, see Fig. A.7. Finally, the surface material is mechanically hardened, which locally increases the fatigue strength of the material in the notch.

In this investigation, UIT was applied. Fig. A.10 shows the tool used for the treatment - a single pin shaped to accommodate treatment along the length of a weld seam. The treatment produced an even, smooth trace along the weld toe, approximately $3mm$ wide and increased the weld toe radius to approximately $R2$.

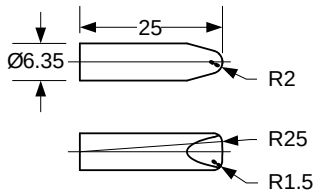

Figure A.10: Double radius pin used for ultrasonic impact treatment.

The treatment can be performed at a speed of about $700-900mm/min$ for high-quality even weld seams. Irregularities, e.g. start/stops, significantly reduce the treatment speed though and may require grinding. UIT is therefore by far the fastest treatment of the three investigated in this project, but at the same time the one that requires the largest initial investment.

TIG dressing

The objective of TIG dressing is to remove welding imperfections, such as undercuts, cold laps and inclusions by remelting the weld toe, thereby leaving the weld practically defect free. Moreover, the treatment significantly reduces the stress concentration factor of the weld toe by introducing a smooth transition.

Current	175A
Voltage	18V
Travel speed	100mm/min
Shielding gas	90% Argon, 10% CO_2
Heat input	1.3kJ/mm
t8/5 time	16sec

Table A.2: TIG dressing parameters

TIG dressing was carried out according to IIW recommendations [9] and following the steel manufacturer cooling rates. The weld seam and adjacent plate were thoroughly

cleaned by sand blasting prior to TIG dressing. Tab. A.2 lists the TIG dressing parameters. The heat input and $t_{8/5}$ time were calculated assuming an efficiency of 0.7 for the TIG process. Again, the cooling rate is well within the specifications of the steel manufacturer.

The TIG dressing treatment was carried out manually using standard TIG welding equipment without adding filler material. The TIG welding torch was aimed 1mm from the weld toe, directing most of the heat towards the base plate. As seen in Fig. A.7, there is a slight tendency towards an undercut in the TIG dressed welds; however, the very generous transition radius limits the negative effect of this undercut.

A major concern when performing TIG dressing in high strength steel is whether it will cause excessive softening of the material. In order to investigate this, hardness measurements through the TIG dressed area were made, see Fig. A.11. The investigation showed a resulting hardness drop of approximately $15 - 20\%$ in the TIG dressed area.

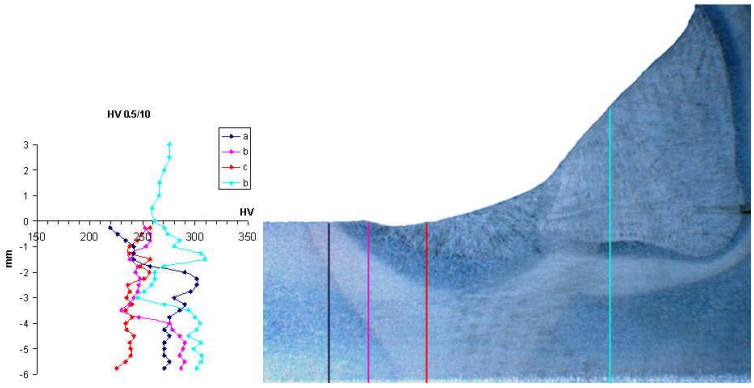

Figure A.11: Hardness profiles through the thickness of a TIG dressed weld.

In this investigation TIG dressing could be performed at approximately twice the speed of burr grinding, i.e. approximately $100 - 200 mm/min$. Observations and experience clearly indicate that the TIG dressing process is less demanding for the operator than the burr grinding process. Additionally, TIG dressing is found to be the best suited post weld treatment for handling irregularities in the weld seam, e.g. a start/stop.

Fatigue Test Results

All specimens failed from a weld toe. Fig. A.12 shows a typical example of the fracture surface. It is seen that the fatigue crack initiates in the middle of the specimen. Investigations using the notch stress approach also suggest the middle as the weakest point of the specimens.

The fatigue test results are listed in Tab. A.3 and plotted in Fig. A.13. Evidently, all three post weld treatments led to significant improvements in fatigue strength. The degree of improvement is comparable for all treatments; however, TIG dressing is the most effective

AW		BG		TIG		UIT	
$\Delta\sigma$	$N[cycles]$	$\Delta\sigma$	$N[cycles]$	$\Delta\sigma$	$N[cycles]$	$\Delta\sigma$	$N[cycles]$
619	48.246	623	144.801	675	84.527	732	48.833
525	58.992	735	44.373	709	93.788	659	72.024
454	136.462	757	39.727	631	156.266	666	73.094
660	26.231	714	72.084	548	352.235	648	166.486
702	28.558	651	74.943	524	666.989	778	27.413
527	78.961	625	76.851	712	91.578	774	15.562
696	20.159	561	172.042	638	112.553	776	35.199
411	164.733	685	102.958	598	179.863	708	45.417
561	43.719	715	100.913	616	136.497	668	83.970
515	96.224	817	25.283	725	36.907	547	244.956
441	128.156	803	25.292	656	94.745		
632	35.701			796	48.665		
401	305.201			811	44.062		
432	154.325						
683	19.303						
776	12.663						
778	15.205						

Table A.3: Fatigue test results.

treatment in the medium cycle regime. UIT on the other hand seems to be the most effective in the high cycle regime.

Contrary to what might be expected, the UIT treatment provided significant improvement, even under the highest applied stresses, i.e. up to the yield point of the base material. The compressive residual stresses introduced by the UIT treatment were expected to relax, thus not improving the fatigue strength of the specimens. However, the UIT treatment also improves the local geometry of the weld toe, which might explain the improvement in fatigue life seen in this investigation.

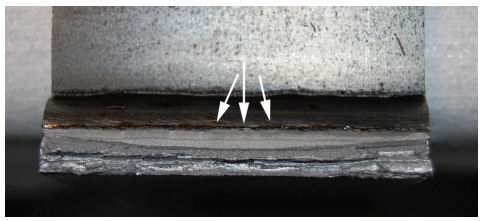

Figure A.12: Example of the fracture surface.

S-N curves were fitted to each set of results by free regression analysis. Curves representing characteristic fatigue strengths, set two standard deviations of logN below the mean curves, are included in Fig. A.13. The characteristic fatigue strengths at $2 \cdot 10^6$ cycles (FAT values in the IIW scheme [6]) obtained from these curves are summarised in Tab.

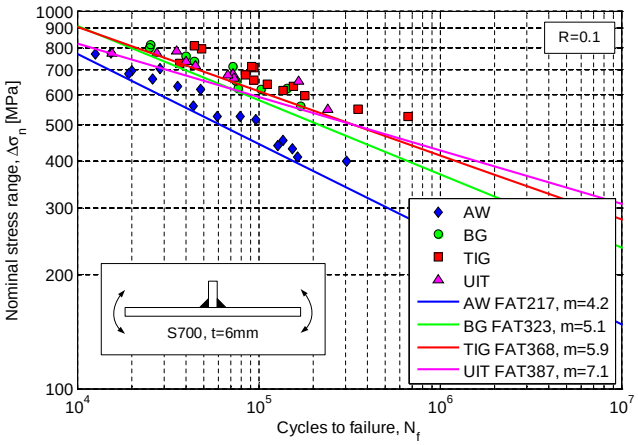

Figure A.13: Fatigue test results with characteristic fatigue strength S-N curves.

	AW	BG	UIT	TIG
Free slope	4.2	5.1	7.1	5.9
2,000,000 cycles	217	323 (+49%)	387 (+78%)	368 (+70%)
100,000 cycles	443	581 (+31%)	590 (+33%)	611 (+38%)

Table A.4: Characteristic fatigue strengths [MPa].

A.4. In addition, the fatigue strengths at 100,000 cycles, which seem more appropriate in this investigation are also given.

It is clear that the improvement in fatigue strength is greater at 2,000,000 cycles than 100,000 cycles, because the S-N curves for the improved details are shallower than that of the as-welded specimens. However, due to the limited number of test results in the high cycle regime, the FAT values at 2,000,000 are quite uncertain. At 100,000 cycles, on the other hand, the results are less scattered, the level of improvement being essentially the same for all post weld treatments.

Comparison with published results

In Fig. A.14, the results obtained in this investigation are compared with existing results extracted from the literature [4,15,16,17,19]. All results are for T-joints tested in four point bending at a stress ratio of $R = 0.1$, but with differences in steel grade, thickness, welding process etc.

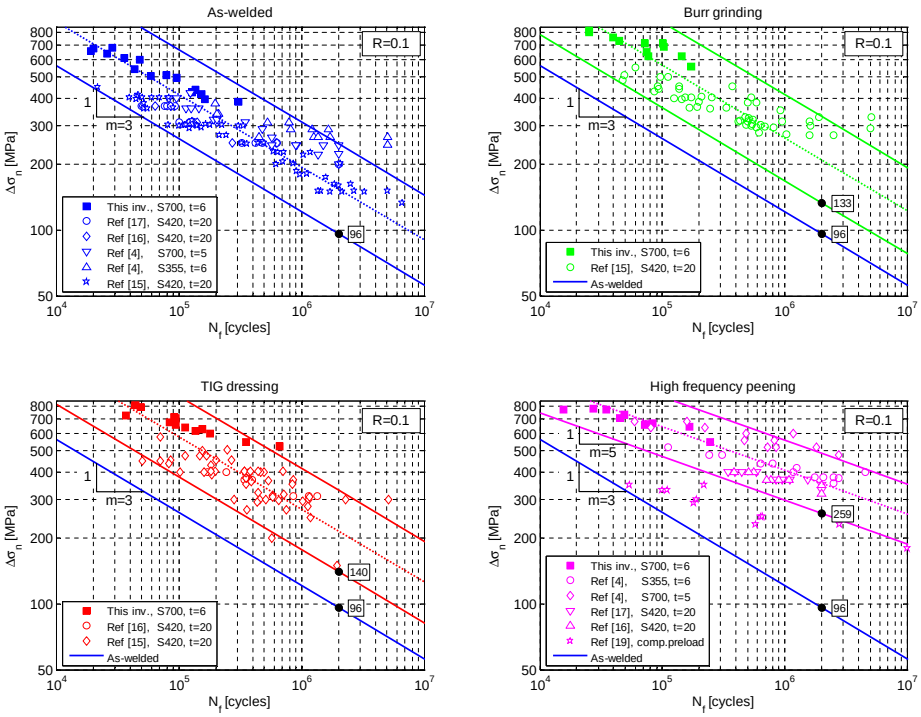

Figure A.14: Results from this investigation compared with similar results from the literature.

The scatter bands in Fig. A.14 were calculated from all results pooled together. They are not meant for design purposes, only for comparison. The curves for AW, BG and TIG series were calculated using $m = 3$, whereas the curves for the HFP series were based on $m = 5$.

The fatigue data from this investigation are seen to be consistent with the published data and provide a useful extension of each database to higher applied stresses. It will also be evident that the present results provide no support for the current recommendation [9] to limit the design curves for improved welds to the IIW design curve for plain steel, FAT160 with $m = 5$, as long as a high strength steel is used.

The HFP treated specimens of [19] was preloaded in compression 5 times at a magnitude of 85% of the yield strength, in order to study the effect of improvement of HFP after potential relaxation of the introduced compressive residual stresses. These results are therefore not included in the scatter bands in Fig. A.14. It is clear, that the degree of improvement obtained in [19] is significantly reduced because of the compressive preloading.

TIG Dressing in Mass Production

The objective of this work was to determine a suitable post weld treatment procedure for implementation in mass production of crane components. TIG dressing was chosen due to the large improvement in fatigue strength observed during tests, but also because of the availability of the equipment and the flexibility of the process.

Many crane components are made from very high strength steel and therefore have a very high static strength. The weld seams are placed in compressive zones or zones with low stresses as far as practically possible. Still, the fatigue strength of the component is governed by one or few critical welds which are highly stressed and cannot be moved or improved by means other than increasing the plate thickness or by post weld treatment. Fig. A.15 shows an example of such a critical weld.

Figure A.15: Welded crane component with illustration of highly stressed weld subjected to TIG dressing.

The designated weld seam is subjected to TIG dressing, in order to increase its fatigue strength to the level of the remainder of the component. Instructions were prepared and a short course was given for the operators and quality control personnel. A new weld quality class was adopted for specification of post weld treatment in technical drawings, similar to VB in the new Volvo CE weld quality system, described by Jonsson and Samuelsson [18].

As expected, taking the process from the laboratory to mass production caused problems. Initially, operators failed to follow instructions and a very low quality treatment was achieved. Fig. A.16 shows examples of the resulting deep undercuts and presence of slag.

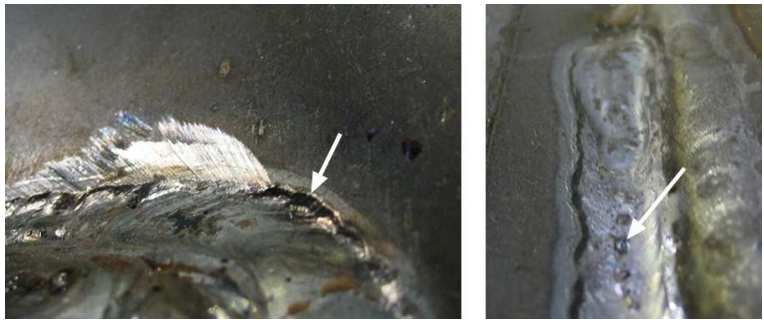

Figure A.16: Initial quality problems with TIG dressing.

The following problems were identified

- Incorrectly inclined work piece caused the weld pool to run away from the base plate.
- Mill scale on the base plate obstructed joining of base material and re-melted weld metal.
- Insufficient de-slagging and cleaning after the primary welding.
- Too high heat input and wrong welding torch angles.
- Insufficient operator experience with the TIG welding process.

Many of the initial problems could be remedied with increased focus on thorough cleaning of the work pieces. The mill scale on the base plate was removed by sand blasting prior to the primary welding. Subsequently, using a chisel and an electric rotating wire brush, the weld seam was carefully cleaned before TIG dressing. The operator was also given more time to practise and instructed to level the work piece in order to avoid undercuts, as illustrated in Fig. A.17.

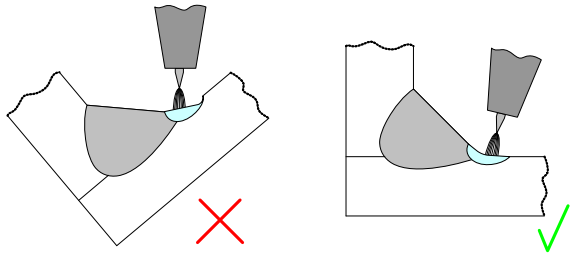

Figure A.17: Correct levelling of the work piece helps avoid undercuts.

A proper heat input was obtained by letting the operator select current and weld speed freely for the TIG dressing operation at hand, but always maintaining a weld pool of

Figure A.18: Examples of final production quality TIG dressing, free from undercutting and significant imperfections.

$6 - 7mm$ in diameter. Finally, a satisfactory and repeatable quality level was obtained, as seen in Fig. A.18.

In such cases, where only a few critically loaded welds govern the fatigue strength of the entire structure, post weld treatment can be a very economic alternative to increasing the plate thickness. For generally highly stressed components, on the other hand, post weld treatment may be too expensive compared to increased plate thicknesses.

On a typical loader crane, only a few welds are loaded to such extend that post weld treatment is necessary. In this example, only approximately $500mm$ weld seam is treated, but this small effort significantly increases the fatigue performance of the crane and allows for a very lightweight and durable design.

Conclusions

On the basis of this investigation of the benefit of selected weld toe improvement methods on the fatigue performance of S700 grade high-strength steel T-joints, the following conclusions were drawn:

- High strength steel can be used very advantageously in the medium cycle fatigue regime when used in combination with local post weld treatment.
- At a fatigue life of 100,000 cycles, the fatigue strength improvement levels obtained from the three methods investigated were almost identical, i.e. 31% for burr grinding, 33% for UIT and 38% for TIG dressing.
- The UIT process showed a consistent high level of improvement, even under stress ranges up to the yield strength of the base material.
- TIG dressing was found to be the best suited post weld treatment for implementation in mass production of crane components, because of the large improvement observed in the experiments, the availability of equipment and the flexibility of the process.
- However, practical experience highlighted the importance of correct work-piece preparation prior to the application of an improvement technique and operator training.

Acknowledgements

Mr. Thaddeus Stam and Applied Ultrasonics Europe are gratefully acknowledged for performing the ultrasonic impact treatment. The research work is funded by an Industrial PhD-grant from the Danish Agency for Science, Technology and Innovation under the Danish Ministry for Science, Technology and Innovation.

References

1 Marquis G. and Björk T. Variable Amplitude Fatigue Strength of Improved HSS Welds, IIW Doc. XIII-2224-08, 2008.

2 Lieurade H.P., Huther I., Lefebvre H. Effect of Weld Quality and Post Weld Improvement Techniques on the Fatigue Resistance of Extra High Strength Steel, IIW Doc. XIII-2184-07, 2007.

3 Lagerqvist O., Clarin M., Gozzi J., Völling B., Pak D., Stötzl J., Lieurade H.P., Depale B., Huther I., Herion S., Bergers J., Martsch R.M., Carlsson M., Samuelsson A. and Sonander C. LiftHigh - Efficient Lifting Equipment with Extra High-Strength Steel, European Commission, Technical Steel Research, EUR22569EN, Brussels, Belgium, 2007.

4 Galtier A. and Statnikov E.S. The Influence of Ultrasonic Impact Treatment on Fatigue Behaviour of Welded Joints in High-Strength Steel, Welding in the World, 48, no. 5/6, 2004.

5 Manteghi S. and Maddox S.J. Methods for Fatigue Life Improvement of Welded Joints in Medium and High Strength Steels, IIW-Doc. XIII-2006-04, 2004.

6 Hobbacher A. (editor), Recommendations for Fatigue Design of Welded Joints and Components, IIW Doc. IIW-1823-07, 2008.

7 DS/CEN/TS EN13001-3-1, Cranes - General Design - Part 3-1: Limit States and Proof of Competence of Steel Structures, 1st edition, 2005.

8 Hansen A.V., Agerskov H. and Bjørnbak-Hansen J., Improvement of Fatigue Life of Welded Structural Components by Grinding, IIW Doc. XIII-2051-05, 2005.

9 Haagensen P.J. and Maddox S.J., IIW Recommendations on Post Weld Improvement of Steel and Aluminium Structures, IIW Doc. XIII-2200r1-07, 2008.

10 Dürr A., Zur Ermüdungsfestigkeit von Schweisskonstruktionen aus höherfesten Baustählen bei Anwendung von UIT-Nachbehandlung [Fatigue Resistance of Welded High Strength Steel Structures Using UIT Post Weld Treatment], PhD thesis, Universität Stuttgart, 2007.

11 Kudryavtsev Y., Kleiman J., Lugovskoy A. and Prokopenko G., Fatigue Life Improvement of Tubular Welded Joints by Ultrasonic Peening, IIW Doc. XIII-2117-06, 2006.

12 REFRESH Project, http://outpost.stahl.bau.tu-bs.de/refresh/index.php?id=180&L=1, 02-02-2009.

13 Bousseau M. and Millot T., Fatigue Life Improvement of Welded Structures by Ultrasonic Needle Peening Compared to TIG Dressing, IIW-Doc. XIII-2125-06, 2006.

14 Lihavainen V.M., A Novel Approach for Assessing the Fatigue Strength of Ultrasonic Impact Treated Welded Structures, PhD thesis, Lappeenranta University of Technology, Finland, 2006.

15 Haagensen P.J. IIW's Round Robin and Design Recommendations for Improvement Methods, Proceedings of the IIW 50th Annual Assembly Conference, San Francisco, Welding Research Council Inc., New York, USA, 1997.

16 Statnikov E.S., Muktepavel V.O. and Blomqvist A. Comparison of Ultrasonic Impact Treatment (UIT) and Other Fatigue Life Improvement Methods, Welding in the World 46, pp. 28- 39, 2002.

17 Trufiakov V.I., Statnikov E.S., Mikheev P.P. and Kuzmenko A.Z. The Efficiency of Ultrasonic Impact Treatment for Improving the Fatigue Strength, IIW Doc. XIII-1745-98, 1998.

18 Jonsson B. and Samuelsson J., A New Weld Quality System, IIW Doc. XIII-2235-08, 2008.

19 Lopez-Martinez L. and Haagensen P.J. Life Extenion of Class F and Class F2 Details Using Ultrasonic PeeningIIW Doc. XIII-2143-07, 2007.

B

Re-analysis of Fatigue Data for Welded Joints Using the Notch Stress Approach

M.M. Pedersen, O.Ø. Mouritsen, M.R. Hansen, J.G. Andersen, J. Wenderby
International Journal of Fatigue, **32**, pp.1620-1626, 2010.

Abstract. Experimental fatigue data for welded joints have been collected and subjected to re-analysis using the notch stress approach according to IIW recommendations. This leads to an overview regarding the reliability of the approach, based on a large number of results (767 specimens). Evidently, there are some limitations in the approach regarding mild notch joints, such as butt joints, which can be assessed non-conservatively. In order to alleviate this problem, an increased minimum notch factor of $K_w > 2.0$ is suggested instead of the current recommendation of $K_w > 1.6$. The data for most fillet welded joints agree quite well with the FAT225 curve; however a reduction to FAT200 is suggested in order to achieve approximately the same safety as observed in the nominal stress approach.

Introduction

The notch stress approach for fatigue assessment of welded joints correlates the stress range in a fictitious rounding in the weld toe or root to the fatigue life using a single S-N curve. The notch stress is typically obtained using finite element models with the reference radius of $1mm$ in order to avoid the stress singularities in sharp notches.

The approach has received much attention lately, due to the increasing available computational power. The approach is very flexible in the sense that all types of welded joints can be assessed using a single S-N curve. It does, however, require more modelling and analysis work than e.g. the nominal or structural stress approaches.

Radaj et al. [1] presents a thorough review of the history of the approach. Fricke [2] gives practical guidelines for the notch modelling and stress analysis and Sonsino [3] proposes S-N curves to be used under different conditions. The approach is included in the IIW fatigue design recommendations by Hobbacher [4].

In this paper, we consider the notch stress approach according to the IIW [2]. The approach is based on the work by Radaj [5] and modified by Seeger and co-workers, see Olivier et al. [6,7]. The reference radius of $R1$ is determined as a mean value and the fatigue strength (FAT225) is derived from experiments.

While many recent publications on fatigue experiments also discuss the results in terms of notch stresses [8-11], the amount of published experimental evidence of the reliability of the approach is very limited.

This investigation therefore presents a systematic re-analysis of fatigue data extracted from the literature and converted to the notch stress system. This provides an overview of the reliability of the approach and a basis for discussion of the observed limitations.

Extraction of Fatigue Data

Constant amplitude fatigue testing results have been extracted from the literature [12-35]. Tab. B.1 presents an overview of the different test series, for which data have been extracted. All data are plotted in Fig. B.1.

The data have been limited to small scale specimens from recent investigations. Only investigations with positive stress ratios are considered and only papers with thorough description of specimen geometry. The only difference in the data considered here is the specimen geometry, since this is the only parameter considered in the notch stress approach.

Only specimens failing from the weld toe is considered and only welded specimens of comparable quality in as-welded condition. The steel grades vary from S235 to S1100, specimen thickness varies from $5-25mm$ and stress ratios vary from 0 to 0.5+. Run-outs are included as well, but the main focus of this study is on the finite life region.

In many cases, the fatigue data were listed in the references; otherwise software assisted extraction from the SN diagrams has been performed. The presentation of fatigue data in Fig. B.1 is divided according to specimen type, in the nominal stress system. Only the four most popular specimen types are considered; T-joints, double sided transversal attachments (non-load carrying cruciform joints), butt joints and double sided longitudinal attachments.

The relatively large scatter in the results is explained by different thickness, weld quality, misalignment, stress ratio and so forth. The large scatter is considered positive in this investigation, since a more general overview can be achieved. Fig. B.2 shows all specimens.

All data agree quite well with the FAT classes suggested by the IIW, and only very few data points fall below the design S-N curves. It is clear that the T-joints show much better results than suggested by the FAT80 curve. This is expected though, since they are tested in bending, considering the positive effect of the steep stress gradient and little to none negative effect from misalignment.

	ID	Ref	$S_y[MPa]$	$t[mm]$	K_t	R	Loading	Process
T-joints	Haa1	[12]	420	20	2.80	0.1	bending	SAW
	Bud1	[16]	550-690	16	2.64	0.0-0.5	bending	SAW
	Sta1	[13]	420	20	2.91	0.1	bending	SAW
	Gal1	[23]	700	5	1.99	0.1	bending	?
	Gal2	[23]	355	6	2.03	0.1	bending	?
	Ped1	[25]	700	6	2.03	0.1	bending	MAG
	Tru1	[31]	420	20	2.73	0.1	bending	?
Transversal attachments	Lif1	[17]	700-900-1100	8	2.35	0.2	tension	MAG
	Fos1	[18]	355-460-690	12	2.49	0.1-0.5	tension	MAG
	Fos2	[18]	355-460-690	12	2.57	0.1	tension	MAG
	Fos3	[18]	690	25	2.69	0.1	tension	MAG
	Son1	[26]	1100	8	2.20	0.0	tension	MAG
	Man1	[15]	355-700	12.5	2.72	0.1	tension	MMA
	Oht2	[30]	570	20	3.01	0.0-0.5	tension	MMA
	Muc1	[32]	460	13	2.51	0.1	tension	MAG
	Hut2	[34]	235-355	8	2.32	0.5	tension	?
	Kud1	[35]	260	20	3.10	0.0	tension	?
Butt joints	Lif2	[17]	700-900	8	1.60	0.2	tension	MAG
	Wan2	[20]	235-390-700	8	1.60	0.0-0.1	tension	?
	Hut3	[34]	235-355	8	1.60	0.5	tension	?
	Dic1	[21]	318	24	2.05	0.0	tension	MMA
	Oht1	[27]	284-579	20	1.95	0.0-0.5	tension	SAW
	Nak1	[28]	431	20	1.95	0.0-Sy	tension	MMA
Longitudinal attachments	Lif3	[17]	690-900-1100	8	3.42	0.2	tension	MAG
	Lif4	[17]	690-900-1100	8	3.85	0.2	tension	MAG
	Haa2	[19]	355-700	8	3.73	0.1	tension	?
	Hut1	[22]	700	8	3.73	0.1-0.5	tension	?
	Wan1	[20]	235-390-700	8	2.69	0.0-0.1	tension	?
	Mad1	[24]	355	13	3.32	0.1	tension	MMA
	Lop1	[14]	355-590	12	3.82	0.0	tension	MAG
	Dim1	[33]	333	12.7	3.62	0.1	tension	MAG
	Mor1	[29]	417	12	4.01	0.0	tension	MAG

Table B.1: Extracted experimental fatigue data series. K_t is determined according to the IIW recommendations for fatigue assessment using the notch stress approach [2]

Conversion to the Notch Stress System

Using the notch stress approach, the stress concentration factor (SCF) of an arbitrary welded joint can be determined using finite element analysis. Radaj et al. [1] explain how the geometric SCF K_t corresponds to the fatigue effective SCF K_f, due to the fictitious rounding of the notch.

$$K_f = K_t(R_{ref} = 1mm). \tag{B.1}$$

The notch approach thereby uses an idealized geometry, which makes the above statement true. Conversion of the extracted fatigue data in the nominal stress system $\Delta\sigma_n$ to the notch stress system $\Delta\sigma_k$ for a given specimen can thus be accomplished as follows.

$$\Delta\sigma_k = K_f \cdot \Delta\sigma_n. \tag{B.2}$$

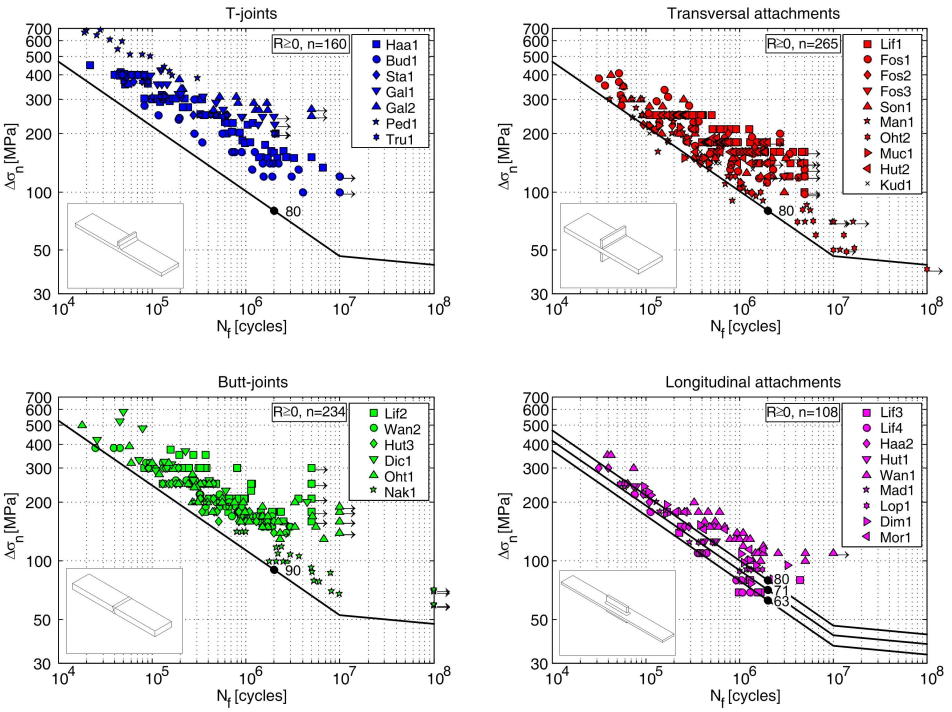

Figure B.1: Extracted fatigue data in the nominal stress system.

The stress concentration factors of all specimens are therefore determined using complete FE models, according to IIW recommendations [2,4]. Here, the procedure is exemplified using the specimens from Lagerqvist et al. [17], (Lif1). The FE analysis was performed using mesh refinement in the area around the weld toe, as shown in Fig. B.3.

A reference radius of 1mm was used and flank angles of 45° for fillet welds and 30° for butt welds, as recommended in [4]. A tensile nominal stress of 1MPa was applied to the specimen, such that the maximum principal stress observed in the notch corresponds to the SCF, see Fig. B.4. The principal stress hypothesis is used for all notch stress analysis.

No misalignment is considered directly in the FE analysis for the determination of the SCFs. However, the SCF for the butt joints is multiplied by a stress magnification factor km, since these specimens are very prone to misalignment. Hobbacher [4] suggests $k_m = 1.10$ for butt joints made in flat position in shop. This value has been applied here.

Extracted Fatigue Data in the Notch Stress System

The converted fatigue data are plotted in Fig. B.5. The immediate conclusion is that the results agree quite well with the FAT225 curve for all fillet welded joints, but not so

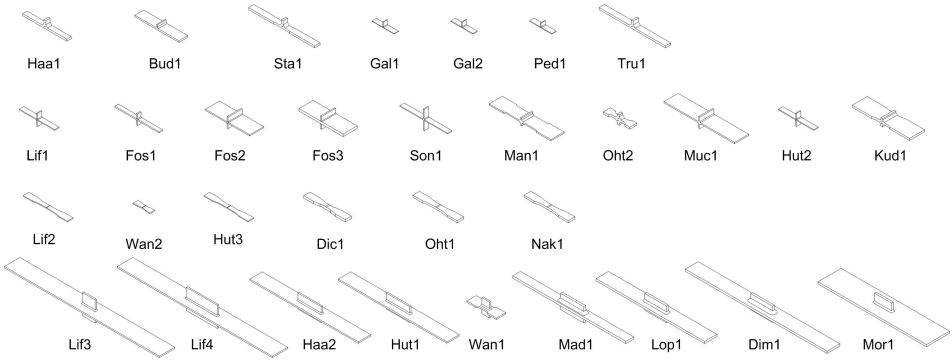

Figure B.2: Specimen geometry and associated ID.

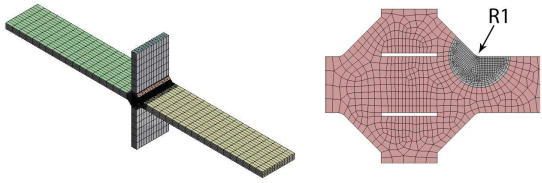

Figure B.3: Lif1-specimen: element size in the notch is $0.1mm$. Only the weld toe is considered here.

well for the butt joints. As expected, the results for the T-joints are somewhat above the FAT225 curve, which can be explained by them being tested in bending.

For the double sided transversal and longitudinal attachments, the results agree reasonably well with the FAT225 curve, however, some data points fall below the curve. The reason for this is unclear, but the few specimens falling below the FAT225 curve is assumed to suffer from some unfortunate conditions, e.g. misalignment or poor local weld toe profile. It is noted, that the FAT225 curve is derived for 'welds with relatively good quality toe profiles', according to Fricke [2, p.13].

The results for many of the butt joints, on the other hand, lie significantly below the FAT225 curve. This is expected to be due to the relatively mild notch present in butt joints with little overfill. The stress concentration factor determined for these joints were calculated to $1.6 - 2.0$, whereas the stress concentration factor for the fillet welded joints were in the range of $2.0 - 4.0$. The problem is especially pronounced for thin butt joints, e.g. in 8mm plate, which has a stress concentration factor of approximately 1.6.

It is well known that some low-SCF joints, such as butt joints, can be assessed in a non-conservative manner using the notch stress approach. Fricke [2] therefore suggests a correction for mild notches, i.e. assuming a notch factor $K_w = \sigma_k/\sigma_{hs}$ of at least 1.6,

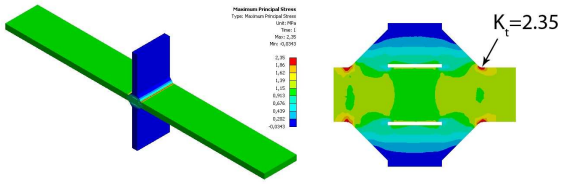

Figure B.4: The SCF of the specimen is determined by applying a nominal stress of 1MPa to the FE model.

where σ_{hs} is the structural hot spot stress. However, in this investigation, the notch factor was above 1.6 for all butt joints, and this correction was thus not applied.

Fatigue assessment of butt joints by the notch stress approach is investigated further in the following section.

Notch Stress Assessment of Butt Joints

In order to obtain a more reliable basis for evaluating the notch stress approach for butt joints, additional test results from many investigations of butt joints were extracted from the S-N curve catalogue by Olivier and Ritter [36]. Only fully penetrated butt joints (I, V and X joints) and only toe-failures are considered. Extreme values are ignored, i.e. only series with a probability of occurrence in the interval $10 - 90\%$ are considered here. Series outside of this interval are presumably affected by severe weld defects on the one side or a significant crack-initiation period on the other side. Run-outs are excluded as well.

In Fig. B.6 the fatigue data for the butt joints are compared in the nominal (left) and notch stress system (right). The fatigue data is converted using the formula for K_t in Fig. B.7 (left) and $k_m = 1.10$ for misalignment. It is seen that the fatigue strength of all butt joints are approximately identical in the nominal stress system, regardless of the different specimen thickness. In the notch stress system, however, the thin joints are assessed non-conservatively because of the very low SCF determined for these joints ($K_t < 2.0$).

Sonsino et al. [37] also reports problems with fatigue assessment using the notch stress approach considering thin/flexible welded joints, e.g. butt joints. They observed shallower slopes for these particular joints and therefore suggest the use of $m = 5$ while maintaining the FAT225 value. As it is seen in Fig. B.6 (right), this approach seems promising in the high cycle area, but too conservative in the medium-to-low cycle area.

In Fig. B.7 (left), it is seen how the stress concentration factor decreases rapidly for thin butt joints. The stress concentration factor determined using FEM is compared to a formula by Anthes et al. [38], which shows a similar tendency. Accordingly, the notch stress approach will estimate very high fatigue strength for thin butt joints.

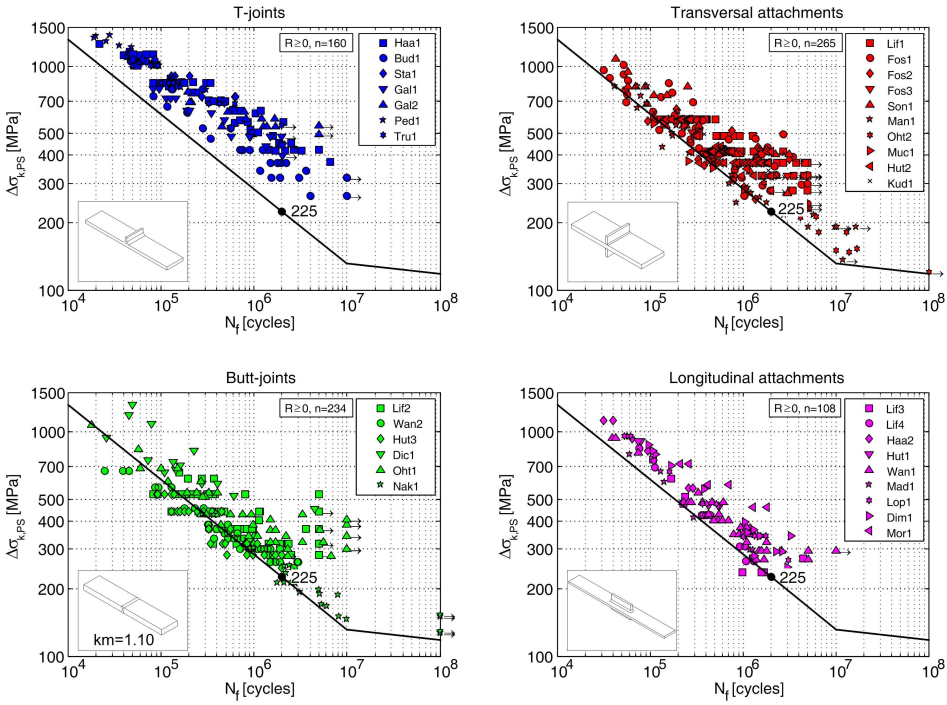

Figure B.5: Fatigue data converted to the notch stress system.

The fatigue capacity of all butt joint specimens from this investigation and [36] are plotted as a function of the thickness in Fig. B.7 (right). The fatigue capacity is plotted instead of e.g. the characteristic fatigue strength, in order to avoid uncertainties due to statistical treatment. The fatigue capacity is calculated assuming $m = 3.0$. For the notch stress assessment, misalignment is considered using $k_m = 1.10$.

It is seen, that the fatigue capacity estimated by the notch stress approach can become very non-conservative especially for thin butt joints. The experimental data in Fig. B.7 (right) does not show a significantly higher fatigue capacity for thin joints. There do not seem to be any clear thickness dependency at all in this range. Or at least, there do not seem to be any support for the tendency suggested by the notch stress approach for thin butt joints.

Fig. B.7 furthermore shows the effects of a minimum notch factor K_w limit of 1.6 and 2.0, respectively. It is seen, that the current recommendation of $K_w = 1.6$ only affects butt joints thinner than approximately $7mm$ and has relatively little effect. If the minimum notch factor is increased to $K_w = 2.0$ on the other hand, a much more conservative result is obtained for thin butt joints and other low SCF joints.

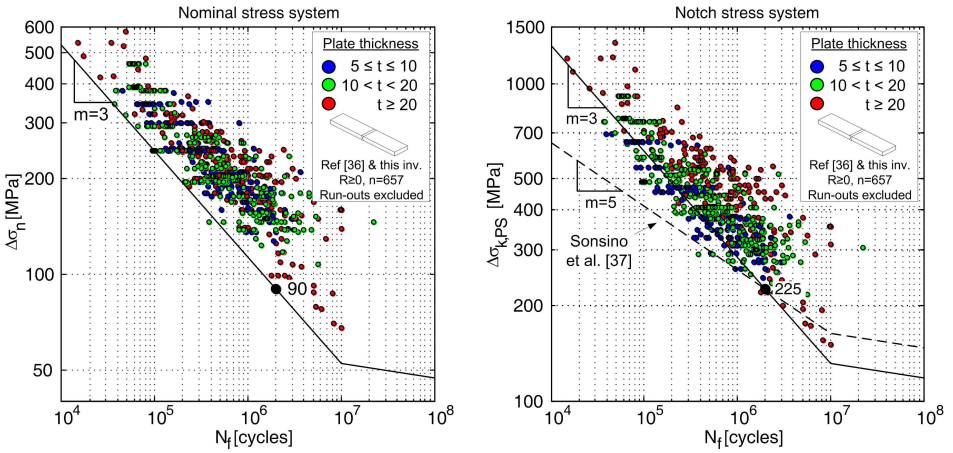

Figure B.6: In the nominal stress system (left) the fatigue strength seems independent of thickness. In the notch stress system (right), on the other hand, the low SCF of thin specimens cause them to be assessed non-conservatively.

In most standards and e.g. the IIW recommendations [4], the thickness effect is only considered for welded joints in plate thicker than $25mm$. However, recent work e.g. Gustafsson [39], reports higher fatigue strength in plates thinner than $25mm$. He reports a significant improvement in the fatigue strength for longitudinal attachments down to $3mm$.

Ohta et al. [40] have studied the thickness effect of butt joints. They report that the fatigue strength of butt joints in 9 and $40mm$ plate was similar when testing by cycling down from the yield strength ($\sigma_{max} = \sigma_y$). On the other hand, if tested at $R = 0$, the 9mm specimens showed significantly higher fatigue strength. They suggest that thinner butt joints have an apparent higher fatigue strength (when tested at low R-ratios), than thick butt joints. This is only indirectly due to the thickness, but is because butt joints in thicker plates better hold a high level of tensile residual stresses.

Conclusively, it seems that the fatigue strength for thin butt joints estimated by the notch stress approach is too optimistic and there is a need for guidance in order to alleviate this problem, e.g. by requiring an increased minimum notch factor of $K_w = 2.0$ or alternatively use a shallower slope of $m = 5$, as suggested by Sonsino et al. [37].

Further Observations

In the following, a minimum notch factor of $K_w = 2.0$ is assumed for thin butt joints. By considering the fatigue data in the notch stress system, the difference in the geometry of the specimens can be disregarded to some extend. At least the effect of different stress concentration factors of the specimens can be disregarded; however, some specimens hold

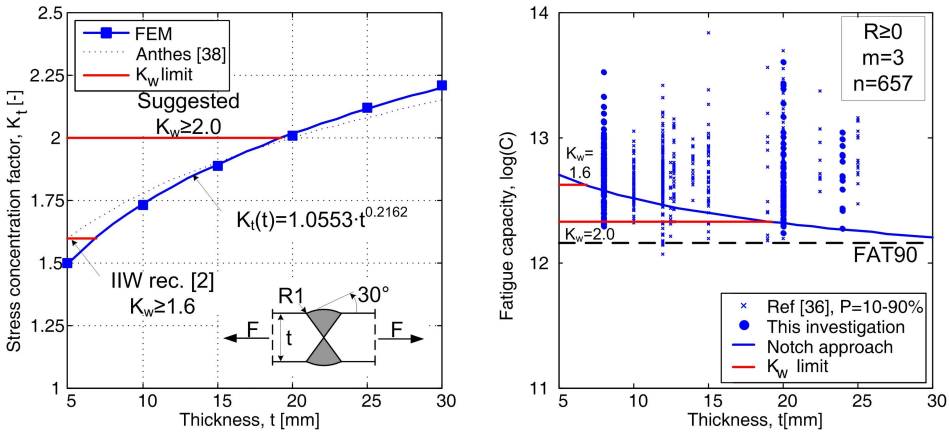

Figure B.7: The thickness has a large influence on the stress concentration factor of the idealized butt joint and thus the estimated fatigue strength. However, this estimation does not correspond well with experimental data.

tensile residual stresses better than others and this effect cannot be disregarded. Still, observations can be made based on a larger amount of fatigue data than usual.

It is clear from Fig. B.8, that the cutting off by the parent material curve FAT160·K_w, $m = 5$ seems unnecessary. However, high strength steel must be applied for high stress ranges and the specimen edge roughness must be sufficiently fine. Sperle [41] showed that the fatigue strength even for thermally cut edges in high strength steel can be significantly higher, than the current IIW recommendation for parent material.

If excluding run-outs and using a slope of $m = 3.0$, the mean fatigue strength ($P_s = 50\%$) is FAT305. Assuming a log-normal distribution, the standard deviation of $\log(C)$ is 0.28, which yields a design curve ($P_s = 97.7\%$) of FAT199 (mean - 2 standard deviations).

Comparing the plots of Fig. B.1 and Fig. B.5, it seems that the nominal stress approach is more conservative than the notch stress approach, since less data points fall below the respective S-N curves. The reason for this is not clear, however, it seems that if the FAT225 curve is reduced to FAT200, it gives approximately the same safety as observed in the nominal stress system, see Fig. B.8.

Conclusions

The following conclusions are drawn based on re-analysis of a large amount of recent fatigue data in the notch stress system using the principal stress hypothesis.

1. For most fillet-welded joints, the experimental fatigue data agrees reasonably well with the current IIW guidance, i.e. using FAT225 S-N curve, except for few data points.

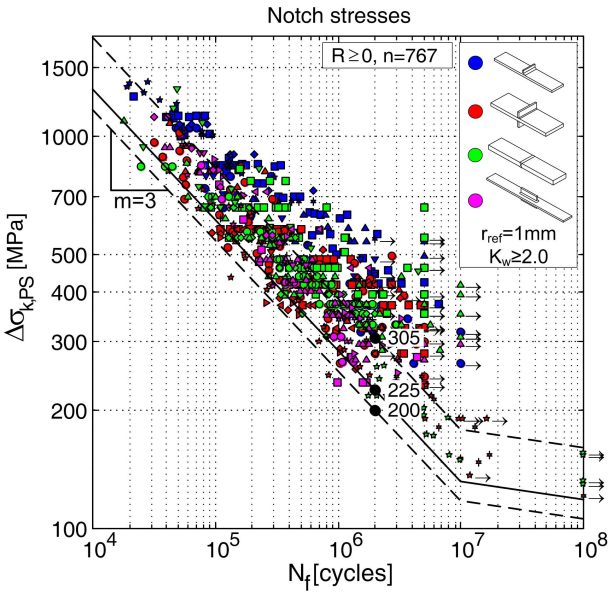

Figure B.8: Fatigue data in notch stresses for all series pooled together.

2. FAT200 is proposed instead though, as it seems to give the same safety as observed in the nominal stress system.
3. The current IIW recommendations can cause non-conservative assessment for thin butt joints. Increasing the minimum notch factor from $K_w = 1.6$ to 2.0 is therefore proposed to alleviate this.
4. The parent material limit of FAT160·K_w seems unnecessary if high strength steel is applied.

Acknowledgements

The research work is funded by an Industrial PhD-grant from the Danish Agency for Science, Technology and Innovation under the Danish Ministry for Science, Technology and Innovation. IIW commission XIII members are gratefully acknowledged for their comments and suggestions for this work.

References

1 D. Radaj, C.M. Sonsino, W. Fricke, Fatigue Assessment of Welded Joints by Local Approaches, second ed., Woodhead Publishing Ltd., Cambridge, 2006.

2 W. Fricke, Guideline for Fatigue Assessment by Notch Stress Analysis for Welded Structures, IIW Doc. XIII-2240r1-08/XV-1289r1-08, 2008.

3 C.M. Sonsino, Suggested Allowable Equivalent Stresses for Fatigue Design of Welded Joints According to the Notch Stress Concept with the Reference Radii rref=1.00 and 0.05mm, IIW Doc. XIII-2216-08/XV1285-08, 2008.

4 A. Hobbacher, Recommendations for Fatigue Design of Welded Joints and Components, IIW Doc. IIW-1823-07, 2008.

5 D. Radaj, Design and Analysis of Fatigue Resistant Welded Structures, Woodhead Publishing Ltd., Cambridge, 1990.

6 R. Olivier, V.B. Köttgen, T. Seeger, Schweissverbindung I, FKM Forschungshefte 143, Frankfurt/M, 1989.

7 R. Olivier, V.B. Köttgen, T. Seeger, Schweissverbindung II, FKM Forschungshefte 180, Frankfurt/M, 1994.

8 W. Fricke, A. Kahl, Local Stress Analysis and Fatigue Assessment of Bracket Toes Based on Measured Weld Profile, IIW-Doc. XIII-2166-07/XV-1253-07, 2007.

9 Z. Barsoum, Residual Stress Analysis and Fatigue Assessment of Welded Steel Structures, Doctoral Thesis, KTH, Stockholm, 2008.

10 B. Kranz, C.M. Sonsino, Verification of the Notch Stress Concept for the Reference Radii of rref=1.00 and 0.05mm, IIW-Doc. XIII-2274-09/XV-1312-09, 2009.

11 W. Fricke, H. Paetzold, Full-scale Fatigue Tests of Ship Structures to Validate the SN-approaches for Fatigue Strength Assessment, IIW-Doc. XIII-2279-09/XV-1321-09, 2009.

12 P.J. Haagensen, IIW's Round Robin and Design Recommendations for Improvement Methods, Proc. IIW 50th Annual Assembly Conference, San Francisco, Welding Research Council Inc., New York, 1997.

13 E.S. Statnikov, V.O. Muktepavel, A. Blomqvist, Comparison of Ultrasonic Impact Treatment (UIT) and Other Fatigue Life Improvement Methods, Welding in the World 46, pp.28-39, 2002.

14 L. Lopez Martinez, A. Blom, Influence of Life Improvement Methods on Different Steel Grades under Fatigue Loading, Fatigue Design 1995. Proc. VTT Symposium 157, Helsinki, 5-8. Sept., 1995.

15 S. Manteghi, S.J. Maddox, Methods for Fatigue Life Improvement of Welded Joints in Medium and High Strength Steels, IIW-Doc. XIII-2006-04, 2004.

16 S. Budano, M. Kuppers, H. Kaufmann, A.M. Meisozo, C. Davis, Application of High Strength Steel Plates to Welded Deck Components for Ships and Bridges Subjected to Medium/High Service Loads, EUR22571EN, European Commission, Brussels, 2007.

17 O. Lagerqvist, M. Clarin, J. Gozzi, B. Völling, D. Pak, J. Stötzl, H.P. Lieurade, B. Depale, I. Huther, S. Herion, J. Bergers, R.M. Martsch, M. Carlsson, A. Samuelsson, C. Sonander, LiftHigh - Efficient Lifting Equipment with Extra High-Strength Steel, European Commission, EUR22569EN, Brussels, 2007.

18 U. Kuhlmann, A. Dürr, J. Bergmann, R. Thumser, Effizienter Stahlbau aus höherfesten Stählen unter Ermüdungsbeanspruchung, Forschungsvorhaben P620, FOSTA, Verlag und Vertriebsgesellschaft GmbH, Düsseldorf, 2006.

19 P.J. Haagensen, Ø. Alnes, Progress Report on IIW WG2 Round Robin Fatigue Testing Program on 700MPa and 350MPa YS Steels, IIW Doc. XIII-2081-05, 2005.

20 T. Wang, D. Wang, L. Huo, Y. Zhang, Discussion on Fatigue Design of Welded Joints Enhanced by Ultrasonic Peening Treatment (UPT), International Journal of Fatigue, 31, pp. 644-650, 2009.

21 T. Dickerson, C. Moura Branco, Weld Improvement Methods for Low Cycle Fatigue Applications, EUR17823, European Commission, Brussels, 1997.

22 I. Huther, Y. Suchier, H.P. Lieurade, Fatigue Behaviour of Longitudinal Non-load Carrying Joints Improved by Burr Grinding, TIG dressing, IIW Doc. XIII-2108-06, 2006.

23 A. Galtier, E.S. Statnikov, The Influence of Ultrasonic Impact Treatment on Fatigue Behaviour of Welded Joints in High-Strength Steel, Welding in the World, 48 (5/6), 2004.

24 S.J. Maddox, Improving the Fatigue Strength of Toe Ground Welds at the End of Longitudinal Stiffeners, IIW-Doc. XIII-2156-07, 2007.

25 M.M. Pedersen, O.Ø. Mouritsen, M.R. Hansen, J.G. Andersen, J. Wenderby, Comparison of Post Weld Treatment of High Strength Steel Welded Joints in Medium Cycle Fatigue, IIW Doc. XIII-2272-09, 2009.

26 C. Sonander, Ermüdung von geschweissten Kreuzstössen aus Weldox 1100, Stahlbau, 69 (4), 2000.

27 A. Ohta, N. Suzuki, Y. Maeda, Shift of S N Curves with Stress Ratio, Welding in the World, 47 (1/2), 2003.

28 Nakamura, Nishijima and A. Ohta, A Method for Obtaining Conservative S- N Data for Weld Structures, Journal of Testing and Evaluation, JTEVA, 16 (3), pp.280-285, 1988.

29 T. Mori, T. Inomata, Influence of Grinding on Fatigue Strength of Out of Plane Gusset Welded Joint, IIW Doc. XIII-1970-03, 2003.

30 A. Ohta, Y. Maeda, N. Suzuki, Residual Stress Effect on Fatigue Strength of Non-Load-Carrying Cruciform Welded Joints of SM570Q Steel for Welded Structures, IIW Doc. XIII-1921-02, 2002.

31 V.I. Trufiakov, E.S. Statnikov, P.P. Mikheev, A.Z. Kuzmenko, The Efficiency of Ultrasonic Impact Treatment for Improving the Fatigue Strength, IIW Doc. XIII-1745-98, 1998.

32 A. Muck, Ertüchtigung von ermüdungsbeanspruchten SchweiSSverbindungen durch Anwendung von Ultrasonic Impact Treatment (UIT), Diplomarbeit, Universität Stuttgart, 2005.

33 S.D. Dimitrakis, F.V. Lawrence, Improving the Fatigue Performance of Fillet Weld Terminations, Fatigue Fract Engng Mater Struct 24, 429-438, 2001.

34 I. Huther, V. Minard, Y. Royer, H.P. Lieurade, Burr Grinding Effect on the Fatigue Strength as Regard to Initial Weld Quality, IIW Doc. XIII-2038-04, 2004.

35 Y. Kudryavtsev, J. Kleiman, A. Lugovskoy, L. Lobanov, V. Knysh, O. Voitenko, G. Prokopenko, Rehabilitation and Repair of Welded Elements and Structures by Ultrasonic Peening, Welding in the World, 51 (7/8), 2007.

36 R. Olivier, W. Ritter, Wöhlerlinienkatalog für Schweissverbindungen aus Baustählen, DVS GmbH, Düsseldorf, 1979.

37 C.M. Sonsino, T. Bruder, J. Baumgartner, SN-curves for Welded Thin Joints - Suggested Slopes and FAT-values for Applying the Notch Stress Concept with Various Reference Radii, IIW-Doc. XIII-2280-09, 2009.

38 R.J. Anthes, V.B. Köttgen, T. Seeger, Kerbformzahlen von Stumpfstössen und Doppel-T-Stössen Schweissen und Schneiden, 45 (12), pp.685-688, 1993.

39 M. Gustaffsson, A Study on Thickness Effect on Fatigue in Thin Welded High Strength Steel Joints, Steel Research International, 77 (12), 2006.

40 A. Ohta, T. Mawari, N. Suzuki, Evaluation of Effect of Plate Thickness on Fatigue Strength of Butt Welded Joints by a Test Maintaining Maximum Stress at Yield Strength, Engineering Fracture Mechanics, 37 (5), pp.987-993, 1990.

41 J.O. Sperle, Influence of Parent Metal Strength on the Fatigue Strength of Parent Material with Machined and Thermally Cut Edges, IIW-Doc. XIII-2174-07, 2007.

C

Experience with the Notch Stress Approach for Fatigue Assessment of Welded Joints

M.M. Pedersen, O.Ø. Mouritsen, M.R. Hansen, J.G. Andersen
Proceedings of the Swedish Conference on Light Weight Optimized Welded Structures, Borlänge, Sweden, pp. 122-133, March 24-25, 2010.

Abstract. In this paper, fatigue assessment using the notch stress approach is discussed based on re-analysis of many fatigue test results and experience from practical application. Three topics are treated; evaluation of the fatigue strength for as-welded details (FAT225) in the notch stress system, problems regarding assessment of mild-SCF details and a novel proposal for extension of the notch stress approach for use with post-weld treated details.

Introduction

The notch stress approach has received much attention lately due to the increasing available computational power and the need for assessing more increasingly complex geometries. The approach is very flexible in the sense that both the toe and the root of all types of welded joints can be assessed using a single S-N curve.

Radaj et al. [1] presents a thorough review of the history of the approach. Fricke [2] gives practical guidelines for the notch modelling and stress analysis and Sonsino [3] proposes S-N curves to be used under different conditions. The approach is included in the IIW fatigue design recommendations by Hobbacher [4].

The notch stress approach correlates the stress range in a fictitious rounding in the weld toe or root to the fatigue life using a single S-N curve. The notch stress is typically obtained using finite element models with the reference radius of 1mm in order to avoid the stress singularities in sharp notches. The approach is schematically illustrated in Fig. C.1. In this paper, notch stresses are calculated using the first principal stress (denoted by index PS in diagrams).

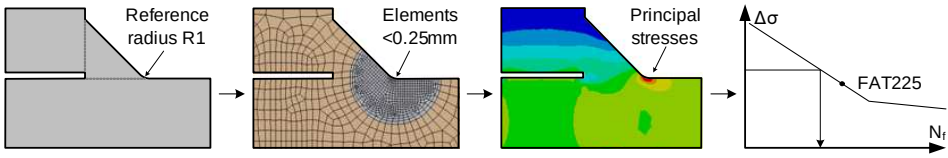

Figure C.1: Schematic principles of fatigue assessment using the notch stress approach.

The approach is based on the work by Radaj [5] and modified by Seeger and co-workers, see Olivier et al. [6,7]. Here, the reference radius of R1 is determined as a mean value and the design fatigue strength (FAT225) is derived from experiments.

Fatigue strength in the notch stress system

The IIW recommends the use of FAT225 when considering the fatigue strength of welded steel joints using the notch stress approach. This value was derived based on the results of a large experimental investigation of different T- and Y-joints [6,7] and further re-analysis of the results assembled by Olivier and Ritter [8]. Kranz and Sonsino [9] explain the assumptions that led to the derivation of the FAT225 fatigue class.

Pedersen et al. [10] carried out a re-analysis using the notch stress approach, and found the FAT225 to be slightly non-conservative, as shown in Fig. 2. The re-analysis was carried out to evaluate the notch stress approach according to the IIW and provide further experimental evidence to the approach.

The fatigue data was extracted from recent publications and converted to the notch stress system by scaling the nominal stress range with the stress concentration factor determined by FE analysis. Only tests carried out in the as-welded condition and under positive stress ratio ($R \geq 0$) were considered. The steel grade varied from S235-S1100 and the thickness was $5 - 25mm$.

Four different specimen types were considered; T-joints, double-sided transversal attachments, butt joints and double-sided longitudinal stiffeners. The T-joints are assessed very conservatively because they are tested in bending. In the nominal stress system, the fatigue data agree quite well with the FAT classes suggested by the IIW [4], therefore, the quality of the specimens is considered to be representative of normal quality.

If excluding run-outs and using a slope of $m = 3.0$, the mean fatigue strength ($P_S = 50\%$) is FAT305. The standard deviation of $log(C)$ is 0.28, and thus the design curve can be calculated ($P_S = 97.7\%$) to FAT199 (mean - 2 standard deviations). It was therefore suggested to reduce the fatigue strength from FAT225 to FAT200 to achieve approximately the same safety as observed in the nominal stress system.

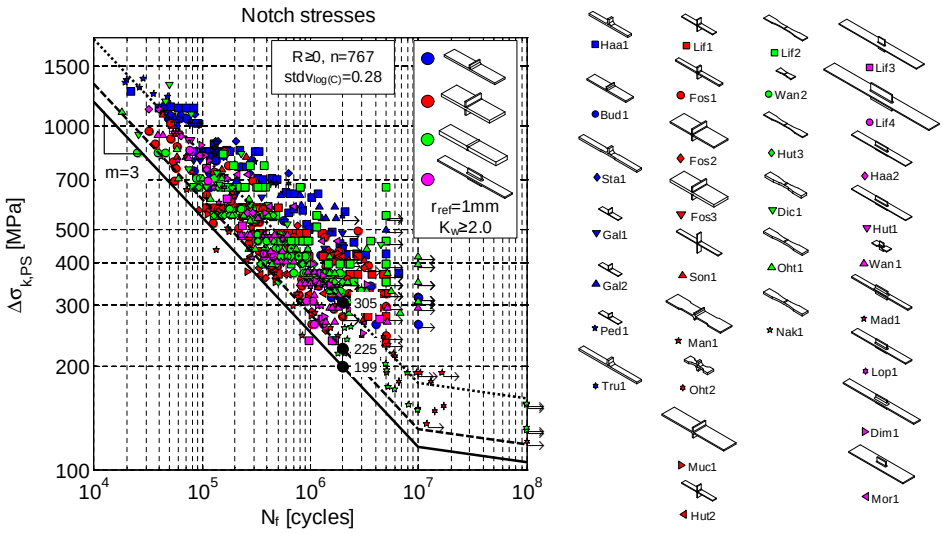

Figure C.2: FAT225 seems to be too optimistic and the reduced FAT200 is therefore proposed in order to achieve approximately the same safety as in the nominal stress system [10].

Mild SCF joints

It is well known that the notch stress approach can lead to non-conservative assessment of mild SCF joints, e.g. thin butt joints, thus there is a need for further insight into the problem. The subject is discussed in terms of thin butt joints and a mild SCF crane detail.

Butt Joints

For butt joints, the IIW suggests the idealized geometry shown in Fig. C.3 for notch stress analysis. The problem with this geometry is that the resulting SCF will be very, low especially for thin joints, e.g. $K_t \approx 1.6$ for $8mm$ thickness.

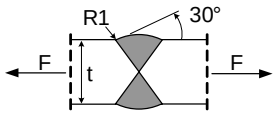

Figure C.3: Idealized geometry for notch stress assessment of butt joints.

In Fig. C.4 fatigue test data for many butt joints are compared in the nominal (left) and notch stress system (right). The fatigue data is converted using the formula $K_t(t) = 1.055\cdot$

$t^{0.216}$ derived in [10] and $k_m = 1.10$ to consider a stress increase due to misalignment, as suggested by Hobbacher [4].

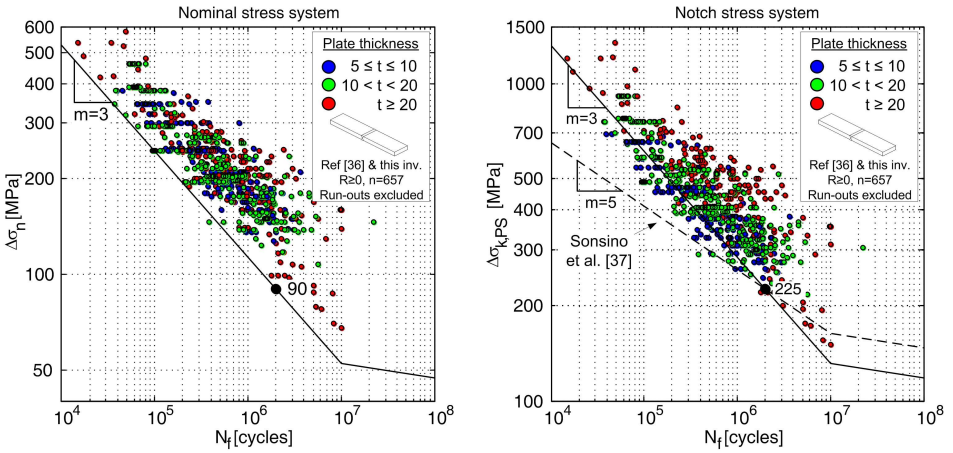

Figure C.4: Thin butt joints can be assessed non-conservatively by the notch stress approach [10].

It is seen that the fatigue strength of all butt joints are approximately identical in the nominal stress system, regardless of the different specimen thickness. In the notch stress system, however, many thin joints are assessed non-conservatively because of the very low SCF determined for these joints. A remedial action was therefore suggested, i.e. requiring a minimum notch factor of $K_w \geq 2.0$, instead of the current $K_w \geq 1.6$ given by the IIW [2].

Sonsino et al. [11] also reports problems with fatigue assessment using the notch stress approach considering thin/flexible welded joints, e.g. butt joints. They observed shallower slopes for these particular joints and therefore suggest the use of a shallower slope, $m = 5.0$, while maintaining the FAT225 value. As it is seen in Fig. C.4 (right), this approach seems promising in the high cycle area, but too conservative in the medium-to-low cycle area.

Crane Detail

Another type of mild SCF joint where the notch stress approach can lead to non-conservative results is the crane detail shown in Fig. C.5. The fatigue critical location is the weld toe in front of the termination of the weld seam around the reinforcement plate. This type of reinforcement is often used in high strength steel structures, where a concentrated load is distributed into the main plate, e.g. in a revolute joint, since the bearing load will otherwise be too high. There are many examples of complicated geometries used in order to 1) reduce the stress concentration factor by softening/tapering out the reinforcement and 2) move the fatigue critical location to an area with reduced loading, e.g. near the centreline of beams.

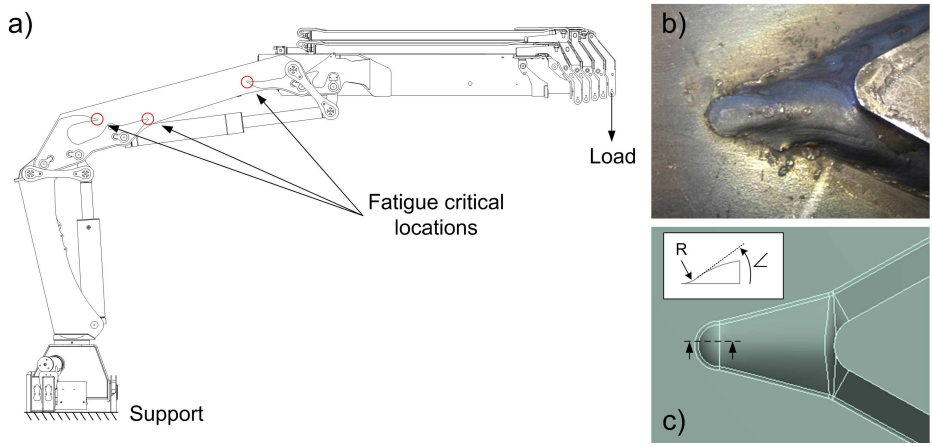

Figure C.5: a) Crane with reinforcement detail, b) actual weld, c) idealized weld.

Rasmussen [12] investigated the considered detail experimentally and numerically, Tab. C.1 and Fig. C.6. This detail is a good example of a weld, where the geometry of the weld itself has a significant influence on the fatigue strength and therefore has to be taken into account, e.g. by using the notch stress approach.

The welded specimens were manufactured by the Danish crane manufacturer HMF A/S using $5mm$ thick S700 and normal quality MAG welding. Fatigue testing were carried out at Aalborg University at a stress ratio of $R = 0.1$ and with special attention to the medium cycle area.

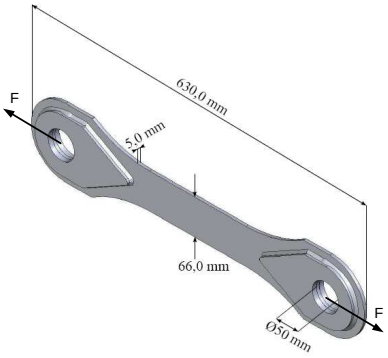

Figure C.6: Specimen geometry [12].

$\Delta F[kN]$	$\Delta\sigma_n[MPa]$	$N_f[cycles]$
168	509	18.414
168	509	12.966
88	267	183.228
86	261	131.935
115	348	48.740
63	191	306.932
164	497	12.805
164	497	11.148
87	264	346.114
115	348	64.980
64	194	242.445

Table C.1: Fatigue testing results [12].

For such a detail, the question arises, how to idealize the local weld geometry? Assuming a reference radius of $R1$ seems logic, but what about the remainder of the weld, especially the flank angle?

The results are presented in Fig. C.7 in the notch stress system using two different modelling techniques - real flank angle (15°) and assumed flank angle (45°). Using the real flank (15°), the SCF is determined to $K_t = 1.72$ and using the assumed 45° flank angle, the SCF is $K_t = 2.53$. It is clear from Fig. C.7, that the results fit the FAT225 curve best, if the assumed 45° flank angle is applied. It is however a quick-and-dirty solution for achieving conservative results using the notch stress approach for this particular detail.

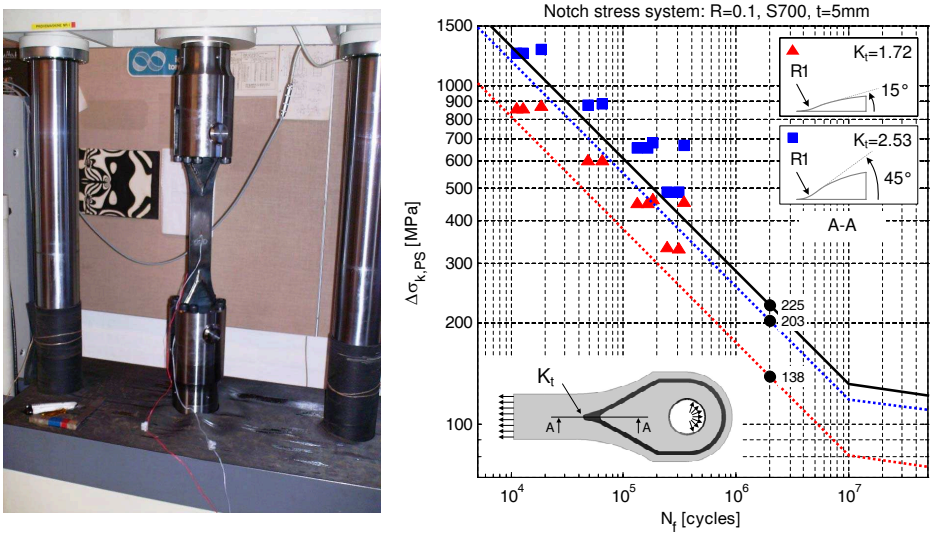

Figure C.7: Fatigue testing results for crane detail, incl. design curves ($P_S = 97.7\%$) for two different modelling techniques compared with the FAT225 curve.

The example shows how important the idealization of the weld geometry is to the final result of the fatigue assessment using the notch approach. It is clear, that experience with the approach is needed, and it is highly recommended to compare results with other (local) approaches.

Extension to post weld treatment

Using the notch stress approach for fatigue assessment of post weld treated details is a subject still under debate. The IIW recommendations by Fricke [2] suggest using a model of the real toe radius $+1mm$ and evaluate the principal stress range here against the FAT200 SN curve. However, it is also stated, that this approach is only valid for relatively sharp notches, i.e. with a toe radius of $R1 - 3mm$, and that the approach has not been verified.

Fig. C.8 shows examples of increased weld toe radii due to different post weld treatments. Typically, when performing post weld treatment, a large toe radius is desired and e.g. grinding and TIG dressing will generally leave a radius larger than $R3$.

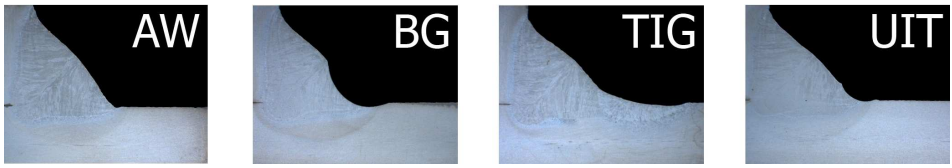

Figure C.8: Typical toe profiles for post-weld treated welds compared to as welded condition [23].

Fig. C.9 shows the results of measurements of weld toe profiles published in the literature. It is clear, that the toe radius will vary a lot in production and will be difficult to estimate in a design situation. The question therefore arises, which 'real' radius to use - the mean, or some lower value? Since the value of the toe radius typically follows a Gaussian distribution, the minimum value is not well defined.

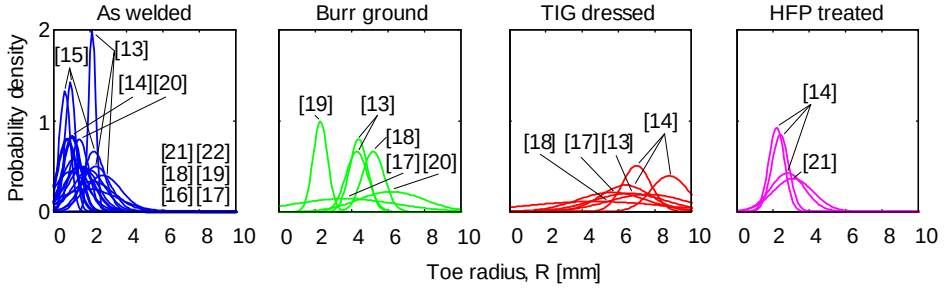

Figure C.9: Measurements of toe radius for as welded and post weld treated welds toes [13-22].

For welds in the as-welded condition, the average toe radius is approximately $R1 - R1.5$, depending on the quality level. For burr ground welds, the average is in the order of $R4$, depending on the chosen burr and the skill of the operator. The radius of TIG dressed welds varies the most - from $R0$ to $R12+$. This radius depends heavily on the skill of the operator and position of the weld relative to gravity. The average is approximately $R6$. Welds treated by high frequency peening (HFP) also achieves varying radii, but not as random as TIG - here the average is around $R2.5$.

Conclusively, if the approach suggested by IIW [2], should be applied with the average radius, it will only be applicable for HFP post weld treatment, since BG and TIG typically results in radii larger than $R3$.

Weich [24] recently proposed an approach for assessing HFP treated welded joints using the notch stress approach. The idea is to consider an effective stress ratio and hereby apply an improvement factor of up to $f(R'_{eff}) = 1.6$ for effective stress ratios of $R'_{eff} < -1$. The effective stress ratio is based on a superposition of the local stresses and compressive residual stresses introduced by the treatment. This approach is presumably

quite accurate, but difficult to apply in a design situation, because the level of compressive residual stresses introduced by the treatment will be unknown.

A New Approach

An alternative procedure for assessing post weld treated joints using the notch stress approach is investigated in the following. The basic idea is to maintain the reference radius at $R1$ and use a higher FAT class for fatigue assessment of post weld treated joints. This is chosen such that an engineer can easily assess whether post weld treatment is necessary and sufficient, using the same FE model as used for assessing the joint in as-welded state. This approach seems very practical, but also has the obvious drawback, that the computed notch stress becomes even more of a model-number, than in the as-welded case, because the model geometry differs more from the actual geometry.

The higher FAT classes are derived based on a large collection of experimental results for post weld treated details. Only burr grinding, TIG dressing and high frequency peening (HFP), e.g. UIT, are considered and only fillet welded joints. Post weld treated butt joints are considered unsuitable for assessment using the notch stress approach, since the notch stress concentration may be completely removed, as in the case of disc grinding.

Most test results considered are for high strength steel, S355-S1100, except some in the series denoted Hut2, Kud1 and Wan1 which also considers mild steel. Only fatigue tests carried out under positive stress ratios are considered and only publications with thorough description of the specimen geometry.

By considering the fatigue data for post weld treatment in the notch stress system, the difference in the geometry of the test specimens can be disregarded to some extend. At least the effect of different stress concentration factors of the specimens can be disregarded. However, some specimens can contain higher levels of tensile residual stresses than others and this effect cannot be disregarded. Still, suggestions for design curves can be given based on a larger volume of fatigue data than usual.

Traditional statistical treatment of the experimental results yields poor results because of very large scatter in the data. This is due to different testing conditions, quality of the post weld treatment, thickness etc. The suggested FAT classes are therefore not directly calculated but simply given based on practical estimation.

T-joints					Transversal attachments					Longitudinal attachments				
ID	Ref	Sy	t	Kt	ID	Ref	Sy	t	Kt	ID	Ref	Sy	t	Kt
Haa1	[25]	420	20	2.80	Lif1	[30]	700-1100	8	2.35	Lif3	[30]	690-1100	8	3.42
Bud1	[26]	550-690	16	2.64	Fos1	[14]	355-690	12	2.49	Lif4	[30]	690-1100	8	3.85
Sta1	[27]	420	20	2.91	Fos2	[14]	355-690	12	2.57	Haa2	[34]	355-700	8	3.73
Gal1	[28]	700	5	1.99	Fos3	[14]	690	25	2.69	Hut1	[18]	700	8	3.73
Gal2	[28]	355	6	2.03	Son1	[31]	1100	8	2.20	Wan1	[35]	235-700	8	2.69
Ped1	[23]	700	6	2.03	Man1	[32]	355-700	12.5	2.72	Wei2	[36]	690	16	2.40
Tru1	[29]	420	20	2.73	Hut2	[19]	235-355	8	2.32	Mad1	[37]	355	13	3.32
					Kud1	[33]	260	20	3.10	Lop1	[38]	355-590	12	3.82
										Dah1	[39]	355-590	12	3.82
										Mor1	[20]	417	12	4.01

Table C.2: Extracted fatigue data series. K_t is determined according to [2].

Burr Grinding and TIG Dressing

Grinding reduces the stress concentration factor of welded joints and removes included defects in the ground area. The experimental data suggests parallel shifting of the S-N curve upwards and FAT300 is suggested, as shown in Fig. C.10. This corresponds to an increase of approximately a factor of 1.3 on the fatigue strength. This is the same factor as suggested by the IIW [40] for mild steel joints in the nominal stress system.

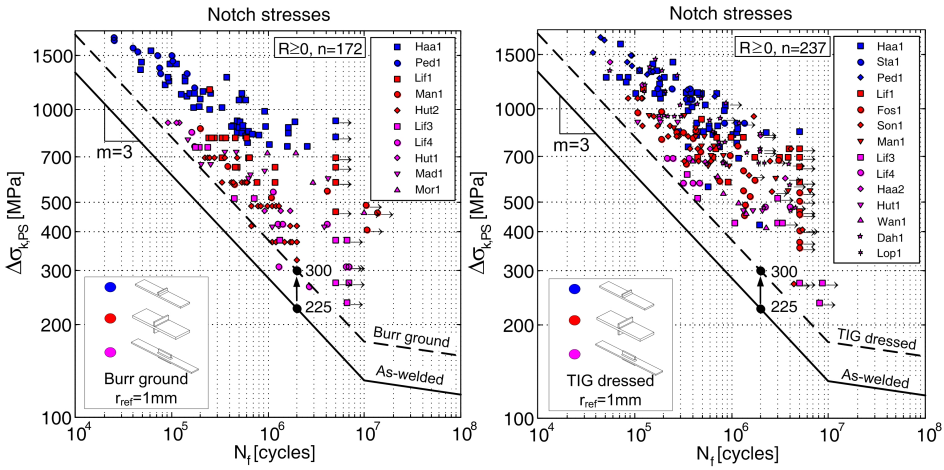

Figure C.10: Fatigue data for burr grinding (left) and TIG dressing (right) compared to the as-welded design curve in the notch stress system.

TIG dressing improves the welded joint in much the same way as grinding, i.e. the stress concentration is reduced and defects are removed. The experimental data also supports the use of the same S-N curve for both ground and TIG dressed welded joints, i.e. FAT300.

High Frequency Peening (HFP) Treatment

The following different types of high frequency peening treatments are described in the literature; ultrasonic impact treatment (UIT) [14], ultrasonic peening (UP) [29], high frequency impact treatment (HiFIT) [36] and ultrasonic needle peening (UNP) [41]. UIT is based on magnetostriction, UP uses a piezoelectric transducer, whereas HiFIT is pneumatically actuated.

Although they are different processes, their properties and resulting improvement in fatigue strength appear to be similar. Here, the treatments are considered equal and denoted HFP treatments.

The HFP treatments improve the fatigue strength of the welded joint in several ways by plastic deformation of the weld toe. Firstly, the tensile residual stress state present in the weld seam is relieved and beneficial compressive residual stresses are introduced. Secondly, the sharp notch in the weld toe is blunted and the treatment leaves behind

a smooth trace with a radius of $2-3mm$, see Fig. C.8. Finally, the surface material is mechanically hardened, which locally increases the fatigue strength of the material in the notch [42].

Since peening treatments improve the fatigue strength of welded joints primarily based on the introduction of compressive residual stresses, a flatter S-N curve is expected. As evident from Fig. C.11, a rotated S-N curve using FAT360 with the slope of $m = 5.0$, fits the experimental data well.

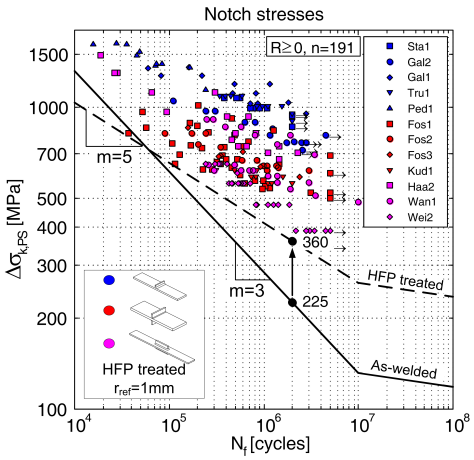

Figure C.11: Fatigue data for HFP treatment compared to the as-welded design curves in the notch stress system.

Due to the flatter slope, the HFP design curve is lower than the as-welded design curve for $N < 50,000$. However, it is clear that the lack of further experimental data, especially in the low cycle area, limits the reliability of the suggested design curve here. It is not likely, that the HFP treatment decreases the fatigue strength in the low cycle area; therefore, the as-welded design curve could be applied here.

Conclusions

The following conclusions are drawn based on re-analysis of fatigue data and practical experience with the notch stress approach.

1. For fatigue assessment using the notch stress approach, it is proposed to reduce the fatigue strength to FAT200 for as-welded normal quality, based on a large amount of experimental data.
2. For mild SCF joints, it is suggested to use a minimum notch factor of $K_w \geq 2.0$ instead of the current $K_w \geq 1.6$. Alternatively, conservative results can be achieved by modelling the flank angle steeper than the real flank angle.

3. For fatigue assessment of post-weld treated details, an approach is suggested where the stress analysis is carried out identically to as-welded details, i.e. the reference radius of $R1$ is maintained, but the FAT class is increased.
   (a) For both burr ground and TIG dressed details, a FAT class of FAT300 using $m = 3.0$ is suggested.
   (b) For HFP treated details, e.g. UIT, FAT360 is suggested with a flatter slope of $m = 5.0$.

Acknowledgements

The research work is funded by HMF A/S and an industrial PhD-grant from the Danish Ministry for Science, Technology and Innovation.

References

1 Radaj D., Sonsino C.M., Fricke W., Fatigue Assessment of Welded Joints by Local Approaches, 2nd ed., Woodhead Publishing Ltd., Cambridge, 2006.

2 Fricke W., Guideline for Fatigue Assessment by Notch Stress Analysis for Welded Structures, IIW Doc. XIII-2240r1-08/XV-1289r1-08, 2008.

3 Sonsino C.M., Suggested Allowable Equivalent Stresses for Fatigue Design of Welded Joints According to the Notch Stress Concept with the Reference Radii rref=1.00 and 0.05mm, IIW Doc. XIII-2216-08/XV1285-08, 2008.

4 Hobbacher A., Recommendations for Fatigue Design of Welded Joints and Components, IIW Doc. IIW-1823-07, 2008.

5 Radaj D., Design and Analysis of Fatigue Resistant Welded Structures, Woodhead Publishing Ltd., Cambridge, 1990.

6 Olivier R., Köttgen V.B., Seeger T., Schweissverbindung I, FKM Forschungshefte 143, Frankfurt/M, 1989.

7 Olivier R., Köttgen V.B., Seeger T., Schweissverbindung II, FKM Forschungshefte 180, Frankfurt/M, 1994.

8 Olivier R., Ritter W., Wöhlerlinienkatalog für Schweissverbindungen aus Baustählen, DVS GmbH, Düsseldorf, 1979.

9 Kranz B., Sonsino C.M., Verification of the Notch Stress Concept for the Reference Radii of Rref = 1.00 and 0.05mm, IIW Doc. XIII-2274-09, 2009.

10 Pedersen M.M., Mouritsen O.Ø., Hansen M.R., Andersen J.G., Wenderby J., Re-analysis of Fatigue Data for Welded Joints Using the Notch Stress Approach, accepted for publication in International Journal of Fatigue, 2010.

11 Sonsino C.M., Bruder T., Baumgartner J., SN-curves for Welded Thin Joints - Suggested Slopes and FAT-values for Applying the Notch Stress Concept with Various Reference Radii, IIW-Doc. XIII-2280-09, 2009.

12 Rasmussen L.V., Levetidsbestemmelse og analyse af typisk svejst krandetalje i højstyrkestål (Danish), M.Sc. thesis, Inst. of Mechanical Engineering, Aalborg University, 2008.

13 Lieurade H.P., Huther I., Lefebvre F., Effect of Weld Quality and Post Weld Improvement Techniques on the Fatigue Resistance of Extra High Strength Steels, IIW Doc. XIII-2184-07, 2007.

14 Kuhlmann U., Dürr A., Bergmann J., Thumser R., Effizienter Stahlbau aus höherfesten Stählen unter Ermüdungsbeanspruchung, Forschungsvorhaben P620, FOSTA, Verlag und Vertriebsgesellschaft GmbH, Düsseldorf, 2006.

15 Jonsson B.J., Barsoum Z., Ghavi Bazou A., Influence From Weld Position on Fillet Weld Quality, IIW Doc. XIII-2273-09, 2009.

16 Barsoum Z., Residual Stress Analysis and Fatigue Assessment of Welded Steel Structures, Ph.D. Thesis, KTH, Stockholm, 2008.

17 Moura Branco C., Gomes E.C., Development of Fatigue Design Curves for Weld Improved Joints, Fatigue Design 1995. Proceedings VTT Symposium 157, Helsinki, 5-8th Sept.1995.

18 Huther I., Suchier Y., Lieurade H.P., Fatigue Behaviour of Longitudinal Non-load Carrying Joints Improved by Burr Grinding, TIG dressing, IIW Doc. XIII-2108-06, 2006.

19 Huther I., Minard V., Royer Y., Lieurade H.P., Burr Grinding Effect on the Fatigue Strength as Regard to Initial Weld Quality, IIW Doc. XIII-2038-04, 2004.

20 Mori T., Inomata T., Influence of Grinding Method on Fatigue Strength of Out-of-Plane Gusset Welded Joints, IIW Doc XIII-1970-03, 2003.

21 Tominaga T., Matsuoka K., Sato Y., Suzuki T., Fatigue Improvement of Weld Repaired Crane Runway Girder by Ultrasonic Impact Treatment, IIW Doc. XIII-2170-07, 2007.

22 Lee C-H., Chang K-H., Jang G-C, C-Y. Lee, Effect of Weld Geometry on the Fatigue Life of Non-load-Carrying Fillet Welded Cruciform Joint, Engineering Failure Analysis, 16, pp.849-855, 2009.

23 Pedersen M.M., Mouritsen O.Ø., Hansen M.R., Andersen J.G., Wenderby J., Comparison of Post Weld Treatment of High Strength Steel Welded Joints in Medium Cycle Fatigue, IIW Doc. XIII-2272-09, 2009.

24 Weich I., Edge Layer Condition and Fatigue Strength of Welds Improved by Mechanical Post Weld Treatment, IIW Doc. XIII-2265-09, 2009.

25 Haagensen P.J., IIW's Round Robin and Design Recommendations for Improvement Methods, Proc. IIW 50th Annual Assembly Conference, San Francisco, Welding Research Council Inc., New York, 1997.

26 Budano S., Kuppers M., Kaufmann H., Meisozo A.M., Davis C., Application of High Strength Steel Plates to Welded Deck Components for Ships and Bridges Subjected to Medium/High Service Loads, EUR22571EN, European Commission, Brussels, 2007.

27 Statnikov E.S., Muktepavel V.O., Blomqvist A., Comparison of Ultrasonic Impact Treatment (UIT) and Other Fatigue Life Improvement Methods, Welding in the World 46, pp.28-39, 2002.

28 Galtier A., Statnikov E.S., The Influence of Ultrasonic Impact Treatment on Fatigue Behaviour of Welded Joints in High-Strength Steel, Welding in the World, 48 (5/6), 2004.

29 Trufiakov V.I., Statnikov E.S., Mikheev P.P., Kuzmenko A.Z., The Efficiency of Ultrasonic Impact Treatment for Improving the Fatigue Strength, IIW Doc. XIII-1745-98, 1998.

30 Lagerqvist O., Clarin M., Gozzi J., Völling B., Pak D., Stötzl J., Lieurade H.P., Depale B., Huther I., Herion S., Bergers J., Martsch R.M., Carlsson M., Samuelsson A., Sonander C., LiftHigh - Efficient Lifting Equipment with Extra High-Strength Steel, European Commission, EUR22569EN, Brussels, 2007.

31 Sonander C., Ermüdung von geschweissten Kreuzstössen aus Weldox 1100, Stahlbau, 69 (4), 2000.

32 Manteghi S., Maddox S.J., Methods for Fatigue Life Improvement of Welded Joints in Medium and High Strength Steels, IIW-Doc. XIII-2006-04, 2004.

33 Kudryavtsev Y., Kleiman J., Lugovskoy A., Lobanov L., Knysh V., Voitenko O., Prokopenko G., Rehabilitation and Repair of Welded Elements and Structures by Ultrasonic Peening, Welding in the World, 51 (7/8), 2007.

34 Haagensen P.J., Alnes Ø., Progress Report on IIW WG2 Round Robin Fatigue Testing Program on 700MPa and 350MPa YS Steels, IIW Doc. XIII-2081-05, 2005.

35 Wang T., Wang D., Huo L., Zhang Y., Discussion on Fatigue Design of Welded Joints Enhanced by Ultrasonic Peening Treatment (UPT), International Journal of Fatigue, 31, pp. 644-650, 2009.

36 Weich I., Ermüdungsverhalten mechanisch nachbehandelter SchweiSSverbindungen in Abhängigkeit des Randschichtzustands, Ph.D. Thesis, Technischen Universität Brauschweig, 2008.

37 Maddox S.J., Improving the Fatigue Strength of Toe Ground Welds at the End of Longitudinal Stiffeners, IIW-Doc. XIII-2156-07, 2007.

38 Lopez Martinez L., Blom A., Influence of Life Improvement Methods on Different Steel Grades under Fatigue Loading, Fatigue Design 1995. Proc. VTT Symposium 157, Helsinki, 5-8. Sept., 1995.

39 Dahle T., Design Fatigue Strength of TIG-dressed Welded Joints in High-Strength Steels Subjected to Spectrum Loading, ABB Corporate Research, S-721, 78, Sweden, 1998.

40 Haagensen P.J., Maddox S.J., IIW Recommendations on Post Weld Improvement of Steel and Aluminium Structures, IIW Doc. XIII-2200-07, 2007.

41 Bousseau M. and Millot T., Fatigue Life Improvement of Welded Structures by Ultrasonic Needle Peening Compared to TIG Dressing, IIW-Doc. XIII-2125-06, 2006.

42 Ummenhofer T., Weich I., Fatigue Design Concepts for Welds Improved by High Frequency Hammer Peening Methods, Proceedings of the Fatigue Design 2007 conference, CETIM 21-23. November, 2007.

D

Developing a Tool Point Control Scheme for a Hydraulic Crane Using Interactive Real-time Dynamic Simulation

M.M. Pedersen, M.R. Hansen, M. Ballebye
Modelling, Identification and Control **31**, Vol. 4, pp. 133-143, 2010.

Abstract. This paper describes the implementation of an interactive real-time dynamic simulation model of a hydraulic crane. The user input to the model is given continuously via joystick and output is presented continuously in a 3D animation. Using this simulation model, a tool point control scheme is developed for the specific crane, considering the saturation phenomena of the system and practical implementation.

Introduction

Current mobile hydraulic manipulators, such as loader cranes, forestry machines and aerial lifts are typically controlled by electro-hydraulic actuation via joystick or remote control. One axis on the joystick commands one hydraulic cylinder. In order to move the tool point (end effector) in a controlled way, it is normally necessary to use several DOF of the manipulator simultaneously. This is often a highly nonlinear task, which only experienced operators can do accurately. Therefore one of the main advantages of automated or semi-automated tool point control is the reduced skill level required or, alternatively, the increased productivity.

Tool point control of mobile hydraulic manipulators has been subjected to research for several years. Such control is different from control of typical industrial robots, due to the non-ideal behavior of mobile hydraulic directional control valves, complex dynamics of the hydraulic and mechanical system, continuous online control by an operator, significant structural flexibility, vehicle mounting flexibility, highly varying loads and eigenfrequencies. Furthermore, there are several saturation phenomena associated with the hydraulic actuation.

Thus, for practical implementation of tool point control in mobile hydraulic manipulators, there are many issues to be addressed. Model based development and testing is preferred, since practical testing of such machinery is unsafe and costly in the initial design stages.

Krus and Palmberg (1998) presented a simple vector control strategy for a 2 DOF hydraulic crane in the early nineties. Mattila and Virvalo (2000) describe a more advanced control scheme for a similar crane; where an online model is used to reduce the pressure levels and thus the energy consumption. Beiner (1997) solves the redundancy in a 3 DOF hydraulic crane using the minimum norm of the actuator forces. Recently, Yuan et al. (2009) presented a motion control for a 4 DOF non-redundant aerial lift including vibration suppression and static deflection compensation. An interactive real time simulation was achieved by Esque et al. (2003) for a simplified 2 DOF crane.

Adapting robot control principles in motion control of mobile hydraulic manipulators has been a key area of research at Aalborg University for several years, see Pedersen and Nielsen (2002), Münzer (2003), Hansen and Andersen (2005), Ebbesen (2007) and Kabus and Hastrup (2008) where the Kuhn-Tucker optimality criteria, are applied continuously in directly calculating optimal actuator velocities, while simultaneously minimizing power consumption.

Typically, a tool point control scheme for such systems is based on velocity control of the manipulator, and the premise, that the operator closes the loop regarding the tool point position. In order to verify this concept, an interactive real-time simulation model is developed, with actual operator-in-the-loop capabilities.

Recent advances in computational power has made it possible to make interactive dynamic simulations run in real-time on an ordinary laptop computer for limited systems. Here, the implementation of such a simulation model is presented in 3D for a 4 DOF crane including simple flexibility.

This paper describes the development of a tool point control scheme for commercial loader cranes, considering the practical implementation. This means that the costs of sensors and control valves must be kept at a minimum. The developed tool point control scheme is purely feed forward, based on a pseudo inverse approach for handling the redundancy. Flow sharing, deflection compensation, configuration control and joint limit avoidance is also implemented.

Considered system

An HMF 2020K4 mobile loader crane is used as case study, Figure D.1. The crane consists of the following 5 bodies; base, column, main boom, jib and extension boom system. The base is considered stationary and neglected from the dynamic analysis.

The crane has 4 controlled joints; slew, main, jib, and extension. The first 3 are revolute joints and the 4th is prismatic. Each joint is actuated by one or more hydraulic cylinders. The slew joint connects through a rack-and-pinion. Both the main and jib joints connects through a linkage system. The extension joint consists of beam segments sliding within

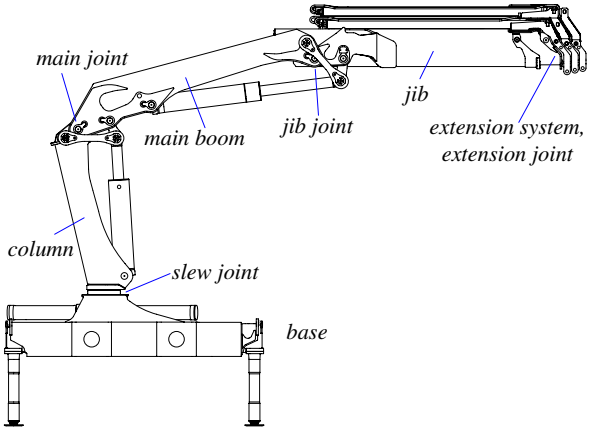

Figure D.1: HMF 2020K4 loader crane.

each other. It is actuated by 4 cylinders coupled in parallel and the sequence is controlled hydraulically.

For the simulation task at hand, the crane is modelled in 3 subsystems; a control system model, a hydraulic model and a mechanical model.

The control model establishes the reference input for the hydraulic model based on user input via an ordinary PC joystick. The hydraulic model then determines the actuator forces based on the states of both the mechanical system and hydraulic system and the current reference input. The actuator forces are then used as input in the mechanical model, which solves the forward dynamics of the system and returns the joint accelerations for integration, see Figure D.2.

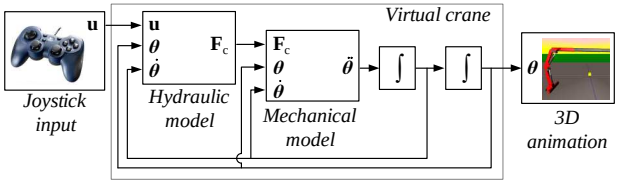

Figure D.2: Overview of the simulation model.

The modelling is as detailed as possible without violating the demand for real time simulation.

This paper is organized as follows; chapter 3 and 4 present the mechanical and hydraulic models. Chapter 5 discusses the implementation of these, and chapter 6 presents the developed tool point control algorithm. Results are presented in chapter 7.

Mechanical model

A simplified 6 DOF model of the crane is considered in order to limit the computational effort. All flexibility is lumped in a passive universal joint within the jib body, modelled by rotational springs around the vertical and lateral axes, see Figure D.3 and D.4.

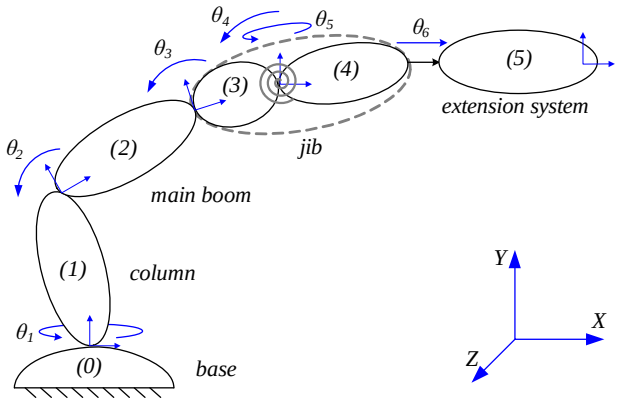

Figure D.3: Mechanical model.

The dynamics of the mechanical system is implemented using the joint coordinate formulation and non-centroidal coordinate systems, as described by Nikravesh (1990 and 1991).

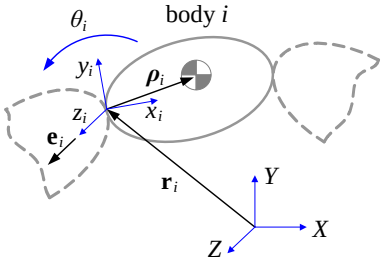

Figure D.4: Joint and body definitions.

The body-fixed coordinate system is located in the joint connecting the given body to the previous in the chain by the vector **r**. The vector **e** describes the axis of the joint.

Equations of motion

Each body is defined by its mass m, inertia matrix $\mathbf{J}$ and location of centre of mass $\boldsymbol{\rho}$. The equations of motion is given by

$$\mathbf{M}_i \dot{\mathbf{v}}_i = \mathbf{g}_i. \tag{D.1}$$

Here, the ith mass matrix and force vector are

$$\mathbf{M}_i = \begin{bmatrix} m\mathbf{I} & -m\tilde{\boldsymbol{\rho}} \\ m\tilde{\boldsymbol{\rho}} & \mathbf{J} \end{bmatrix}_i \; and \; \mathbf{g}_i = \begin{bmatrix} \mathbf{f} & -m\tilde{\boldsymbol{\omega}}\tilde{\boldsymbol{\omega}}\boldsymbol{\rho} \\ \mathbf{n} & -\tilde{\boldsymbol{\omega}}\mathbf{J}\boldsymbol{\omega} \end{bmatrix}_i, \tag{D.2}$$

where $\mathbf{f}$ and $\mathbf{n}$ are the forces and moments, respectively, acting on the body. The vector of Cartesian velocities $\mathbf{v}$ is defined as

$$\mathbf{v} = \begin{bmatrix} \mathbf{v}_1 & \mathbf{v}_2 & \mathbf{v}_3 & \mathbf{v}_4 & \mathbf{v}_5 \end{bmatrix}^T \; and \; \mathbf{v}_i = \begin{bmatrix} \dot{\mathbf{r}}_i \\ \boldsymbol{\omega}_i \end{bmatrix}. \tag{D.3}$$

For a system of constrained bodies, the equations of motion are combined with the constraints, yielding

$$\mathbf{M}\dot{\mathbf{v}} - \mathbf{D}^T\boldsymbol{\lambda} = \mathbf{g}. \tag{D.4}$$

Here, $\mathbf{D}$ and $\boldsymbol{\lambda}$ are the Jacobian of the constraints and a vector of Lagrange multipliers.

This equation system can be solved for the accelerations and Lagrange multipliers by inverting a system matrix of size 54x54 (6x number of bodies + 24 constraints). However, in order to increase computational efficiency, the system is reduced to a minimum set using velocity transformations.

Reduction to a minimum set

The vector of joint velocities is defined as

$$\dot{\boldsymbol{\theta}} = \begin{bmatrix} \dot{\theta}_1 & \dot{\theta}_2 & \dot{\theta}_3 & \dot{\theta}_4 & \dot{\theta}_5 & \dot{\theta}_6 \end{bmatrix}^T. \tag{D.5}$$

Transformation between the Cartesian and joint space is handled by the transformation matrix $\mathbf{B}$ as follows

$$\mathbf{v} = \mathbf{B}\dot{\boldsymbol{\theta}}. \tag{D.6}$$

Accelerations are then transformed by

$$\dot{\mathbf{v}} = \mathbf{B}\ddot{\boldsymbol{\theta}} + \dot{\mathbf{B}}\dot{\boldsymbol{\theta}}. \tag{D.7}$$

It can be shown that the $\mathbf{B}$ matrix is orthogonal to the constraint Jacobian $\mathbf{D}$, such that

$$\mathbf{DB} = \mathbf{0}. \tag{D.8}$$

Thus, by inserting eq. (D.7) into eq. (D.1) and pre-multiplying with $\mathbf{B}^T$ we get

$$\mathbf{B}^T\mathbf{M}\mathbf{B}\ddot{\boldsymbol{\theta}} = \mathbf{B}^T(\mathbf{g} - \mathbf{M}\dot{\mathbf{B}}\dot{\boldsymbol{\theta}}). \tag{D.9}$$

Using the inertia matrix and force vector in joint space, $\overline{\mathbf{M}}$ and $\overline{\mathbf{f}}$, then leads to the following short notation

$$\overline{\mathbf{M}}\ddot{\boldsymbol{\theta}} = \overline{\mathbf{f}}, \tag{D.10}$$

where

$$\begin{aligned} \overline{\mathbf{M}} &= \mathbf{B}^T\mathbf{M}\mathbf{B} \\ \overline{\mathbf{f}} &= \mathbf{B}^T(\mathbf{g} - \mathbf{M}\dot{\mathbf{B}}\dot{\boldsymbol{\theta}}). \end{aligned} \tag{D.11}$$

Here, the constraints will be implicitly enforced and the constraint Jacobian as well as the Lagrange multipliers need not be determined. The system matrix, which needs to be inverted in this formulation, is only 6x6, corresponding to the number of DOFs.

Velocity transformation

The velocity transformation matrix $\mathbf{B}$ and its time derivative can be established from joint specific block matrices. For the ith body and the jth revolute ($\mathbf{R}$) or prismatic joints ($\mathbf{P}$), these are

$$\mathbf{R}_{ij} = \begin{bmatrix} -\tilde{\mathbf{d}}_{ij}\mathbf{e}_j \\ \mathbf{e}_j \end{bmatrix} \; and \; \mathbf{P}_{ij} = \begin{bmatrix} \mathbf{e}_j \\ \mathbf{0} \end{bmatrix}. \tag{D.12}$$

The distance vectors $\mathbf{d}_{ij} = \mathbf{r}_i - \mathbf{r}_j$ are illustrated in Figure D.5, where it should be noted that $\mathbf{d}_{ii} = \mathbf{0}$. Combining the block matrices of two revolute joints yields a Universal joint ($\mathbf{U}$).

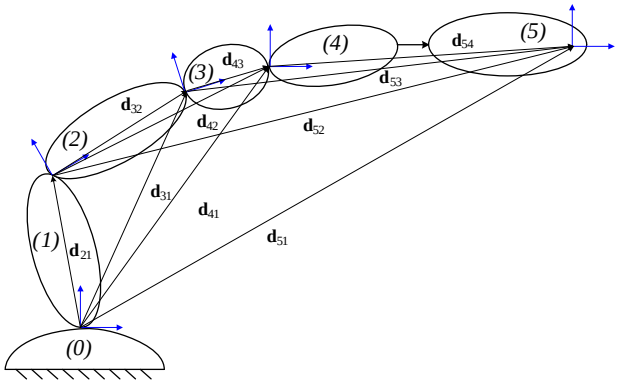

Figure D.5: Distance vectors.

The $\mathbf{B}$ matrix is thus built by inserting block matrices in the following way, such that $\mathbf{R}_{ij}$ relates the joint velocity contribution of joint j to the Cartesian velocity of body i.

$$\mathbf{B} = \begin{bmatrix} \mathbf{R}_{11} & \mathbf{0} & \mathbf{0} & \mathbf{0} & \mathbf{0} \\ \mathbf{R}_{21} & \mathbf{R}_{22} & \mathbf{0} & \mathbf{0} & \mathbf{0} \\ \mathbf{R}_{31} & \mathbf{R}_{32} & \mathbf{R}_{33} & \mathbf{0} & \mathbf{0} \\ \mathbf{R}_{41} & \mathbf{R}_{42} & \mathbf{R}_{43} & \mathbf{U}_{44} & \mathbf{0} \\ \mathbf{R}_{51} & \mathbf{R}_{52} & \mathbf{R}_{53} & \mathbf{U}_{54} & \mathbf{P}_{55} \end{bmatrix} \tag{D.13}$$

The derivative matrix $\dot{\mathbf{B}}$ is built in the same manner as eq. (D.13), but using the derivative block matrices

$$\dot{\mathbf{R}}_{ij} = \begin{bmatrix} -(\dot{\tilde{\mathbf{d}}}_{ij} + \tilde{\mathbf{d}}_{ij}\boldsymbol{\omega}_j)\mathbf{e}_j \\ \tilde{\boldsymbol{\omega}}_j\mathbf{e}_j \end{bmatrix} \; and \; \dot{\mathbf{P}}_{ij} = \begin{bmatrix} \tilde{\boldsymbol{\omega}}_j\mathbf{e}_j \\ \mathbf{0} \end{bmatrix} \tag{D.14}$$

where $\dot{\mathbf{d}}_{ij} = \dot{\mathbf{r}}_i - \dot{\mathbf{r}}_j$.

Flexibility

Mobile manipulators are typically highly weight optimized and therefore, the influence of the structural flexibility cannot be ignored. The influence of flexibility is investigated by Linjama and Virvalo (1999) and Mikkola (1997). The flexibility significantly influences

the eigenfrequency of the structure and thus needs to be included in the mechanical model.

Here, structural flexibility is included in the mechanical model, by dividing the jib-body in two and connecting the halves by a universal joint equipped with rotational springs, as shown in Figure D.3. This enables the crane model to flex both in its working plane and in the horizontal plane.

The applied spring torques $\mathbf{T}_s$ are calculated by

$$\mathbf{T}_s = (K_{s,i} \cdot \delta\theta_i - K_{d,i} \cdot \dot{\theta}_i)\mathbf{e}_i. \tag{D.15}$$

The spring constant K_s of the rotational springs are determined by physical experiments, such that the deflection of the model resembles the deflection of the real crane. Damping is included in order to stabilize the model and the damping coefficient K_d is also determined to match experiments.

This simple flexibility model lowers the eigenfrequency and gives a deviation in the tool point position, and is considered sufficient for the purpose of this model.

Extension system modelling

The extension system is modelled as a single body with variable geometry and inertia properties. The dynamics of the relative motion between segments is thus ignored. This is justified, since this motion is highly damped due to friction and its dynamics has only negligible influence.

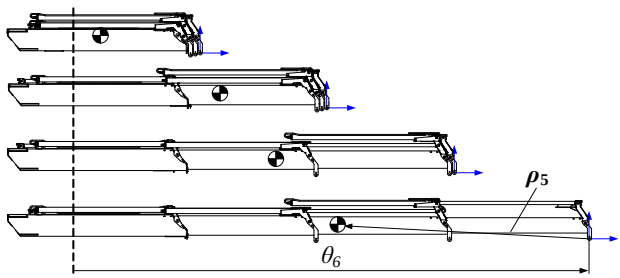

Figure D.6: Variable location of extension system Centre of Mass (COM).

An expression for the position of the centre of mass is obtained by determining it for different values of θ_6 using CAD and fitting a curve through the results, as shown in Figure D.6.

$$\boldsymbol{\rho}_5 = \begin{bmatrix} \rho_x(\theta_6) & \rho_y & \rho_z \end{bmatrix} \tag{D.16}$$

The same approach has been applied for the inertia matrix, which is approximately constant, except for the $J_{yy} \approx J_{zz}$ terms, which vary notably with θ_6,

$$\mathbf{J}_5 = \begin{bmatrix} J_{xx} & J_{xy} & J_{xz} \\ J_{yx} & J_{yy}(\theta_6) & J_{yz} \\ J_{zx} & J_{zy} & J_{zz}(\theta_6) \end{bmatrix} \tag{D.17}$$

The results of the fitting procedure are shown in Figure D.7.

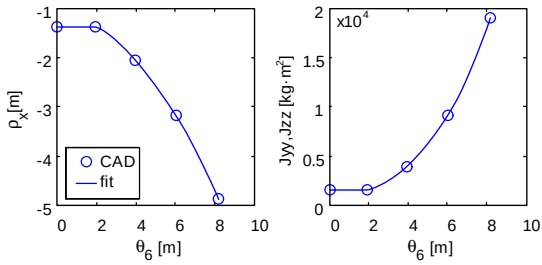

Figure D.7: Fitted location of COM and moments of inertia for the extension system.

Hydraulic model

The hydraulic system is modelled with the highest possible detail level without compromising real time simulation. Pressure losses in hoses and fittings are largely ignored and the dynamics of the directional control valves is modelled as a first order system.

All cylinders on the crane are mounted with over-center valves (OCVs) due to practical and legislative reasons. OVCs serve a number of purposes, including leak tight load holding, shock absorbtion, cavitation protection during lowering and load holding at pipe/hose bursts. Their influence on the system is significant, and their effect is included in a simple and efficient manner.

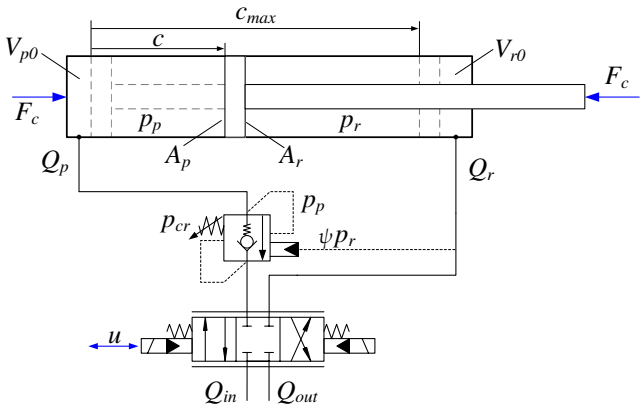

Figure D.8: Simplified hydraulic circuit; cylinder, over-center valve and directional control valve.

The system in Figure D.8 illustrates the main lift cylinder, which has only one OCV controlling the lowering motion. All other joints have double acting OCVs mounted, since the gravity load for these joints act in both directions.

The dynamics of the hydraulic fluid is introduced via the pressure gradient equation for a volume of Newtonian fluid, Merrit (1967)

$$\dot{p} = \frac{\beta}{V}(Q - \dot{V}), \tag{D.18}$$

where β is the effective bulk modulus of the fluid, Q is the flow into the volume V and $\dot{V}$ is the time derivative of the volume expansion. From this, the piston and rod side pressure gradients of the cylinders are calculated

$$\dot{p}_{p,i} = \frac{\beta}{V_{p0,i} + c_i \cdot A_{p,i}}(Q_{p,i} - \dot{c}_i \cdot A_{p,i}) \quad and \tag{D.19}$$

$$\dot{p}_{r,i} = \frac{\beta}{V_{r0,i} + (c_{max,i} - c_i)A_{r,i}}(Q_{r,i} + \dot{c}_i \cdot A_{r,i}). \tag{D.20}$$

These are then integrated to get the pressures on both sides of the piston.

$$p_{p,i} = \int \dot{p}_{p,i} dt \quad and \quad p_{r,i} = \int \dot{p}_{r,i} dt \tag{D.21}$$

The flow into the circuit Q_{in} is determined from the valve rated flow and the control signal u_i and saturates at maximum valve flow $Q_{v,max}$

$$Q_{in,i} = \begin{cases} u_i \cdot Q_{v,max,i} & for\ Q_{in,i} < Q_{v,max,i} \\ Q_{v,max,i} & for\ Q_{in,i} \geq Q_{v,max,i} \end{cases} \tag{D.22}$$

The flow out of the circuit is governed by the OCV.

$$Q_{out,i} = -Q_{OCV,i} \tag{D.23}$$

Finally, the cylinder force can be determined from the pressure and area differences and friction.

$$F_{c,i} = p_{p,i} \cdot A_{p,i} - p_{r,i} \cdot A_{r,i} - F_{\mu,i} \tag{D.24}$$

Nielsen (2005) obtained good results using the following simple cylinder friction model, which has also been implemented here. The *tanh* is continous and crosses through the origin, thus ignoring stick-slip effects.

$$F_{\mu,i} = \tanh(\frac{\dot{c}_i}{\dot{c}_\eta}) \cdot |p_{p,i} \cdot A_{p,i} - p_{r,i} \cdot A_{r,i}| \cdot (1 - \eta) \tag{D.25}$$

A mechanical efficiency of $\eta = 0.92$ is assumed and the normalization velocity $\dot{c}_\eta$ is set at 0.02m/s.

Over-center valves

The OCV model determines the flow out of the cylinders in most cases. The dynamics of the over-center valves is disregarded, and the following static approximation is applied.

$$p_{cr,i} = p_{p,i} + \psi_i \cdot p_{r,i} \tag{D.26}$$

The crack pressure p_{cr} must be balanced by the pressures in the cylinder chambers (affected by the pilot ratio ψ, typically ≈ 4 for this application) for the over-center valve to open. Assuming flow out of the piston side chamber, we have

$$Q_{OCV,i} = K_{OCV,i}\sqrt{p_{p,i} - p_t} \tag{D.27}$$

The flow out of an OCV is determined by the orifice equation, assuming a linear discharge characteristic, as shown in Figure D.9. The tank pressure p_t is assumed to be zero.

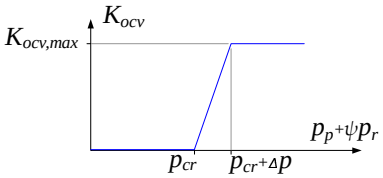

Figure D.9: Assumed OCV discharge characteristic.

The maximum value of the flow coefficient $K_{OCV,max}$ can be calculated from the OCV manufacturer datasheets. The pressure increment Δp at which the OCV is fully opened, is set to 25bar. The OCV flow coefficient is given as

$$K_{OCV,i} = \frac{K_{OCV,max,i}}{\Delta p}(p_{p,i} + \psi_i \cdot p_{r,i}) - \frac{K_{OCV,max,i}}{\Delta p}p_{cr,i}. \tag{D.28}$$

Connecting the mechanical and hydraulic models

In the hydraulic model, the crane state is expressed by cylinder stroke and velocity, i.e. actuator coordinates. The mechanical model, however, returns joint coordinates. Thus a transformation is necessary from the joint space to the actuator space.

$$\dot{\mathbf{c}} = \mathbf{A}\dot{\boldsymbol{\theta}} \tag{D.29}$$

$\mathbf{A}$ is the Jacobian matrix of the joint to actuator transformation, i.e. the instantaneous effective torque arms of the actuators, given by

$$\mathbf{A} = \begin{bmatrix} a_1 & 0 & 0 & 0 \\ 0 & a_2(\theta_2) & 0 & 0 \\ 0 & 0 & a_3(\theta_3) & 0 \\ 0 & 0 & 0 & a_4 \end{bmatrix} \tag{D.30}$$

Here, $a_1 = 0.105m$ is the constant radius of the rack and pinion slew mechanism, a_2 and a_3 vary significantly due to the linkage systems, see Figures D.10 and D.11. For the linear extension joint, $a_4 = 1$.

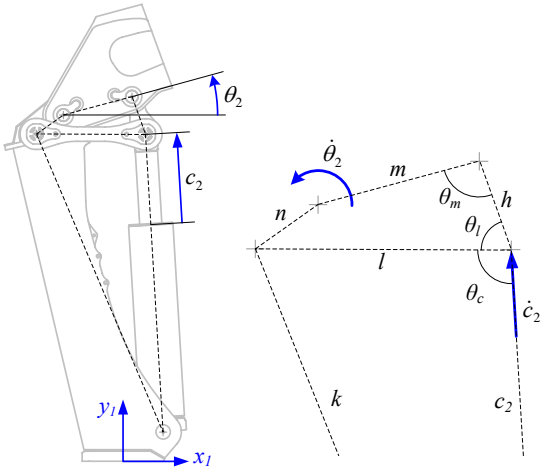

Figure D.10: Cylinder coupling through linkage system.

Given the constant lengths k, l, m, n and h and the angle θ_2, its possible to determine the angles $\theta_l, \theta_m, \theta_c$ and the cylinder stroke c_2. The instantaneous effective relationship between the cylinder velocity and joint velocity is then given by

$$\dot{c}_2 = a_2(\theta_2) \cdot \dot{\theta}_2 \tag{D.31}$$

where

$$a_2(\theta_2) = \frac{m \cdot \sin\theta_m \sin\theta_c}{\sin\theta_l} \tag{D.32}$$

The same holds for the jib joint. In order to reduce the computational burden, curve fits are used to determine a_2 and a_3 as a function of θ_2 and θ_3, as shown in Figure D.11.

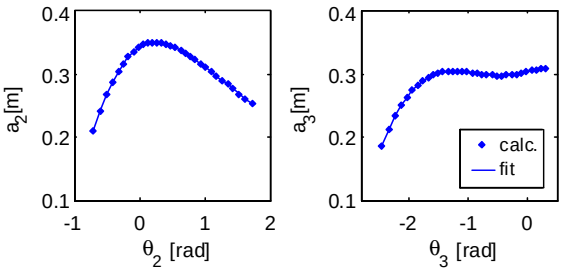

Figure D.11: Effective torque arms of cylinder 2 and 3.

The **A** matrix furthermore gives the relationship between the cylinder forces and joint torques

$$\mathbf{T}_c = \mathbf{A}\mathbf{F}_c \tag{D.33}$$

It is clear, that the maximum lifting capacity of joint 2 (main) and 3 (jib) will be where the effective torque arms have their maximum. The typical pressure layout of such a crane is that the jib joint is set to be stronger than the main joint. Therefore, for general maximum lifting capacity, the torque arm of the main joint should be maximized. The torque arm of the jib joint is approximately constant for $\theta_3 > -\pi/2$.

Model implementation

The simulation model is implemented in Simulink using the 3D animation toolbox and blocks of Embedded Matlab, Figure D.12. The Embedded Matlab blocks execute very fast, since their content is automatically pre-compiled in the background prior to execution of the Simulink model.

Using the fixed step Runge-Kutta integrator (ODE4), real time performance is achieved with a time step of 2.5ms on a standard 2GHz laptop computer.

The Simulink 3D animation toolbox includes a source block for joystick input. This is used as interactive reference input to the model, and resembles the input device typically used for controlling the real crane.

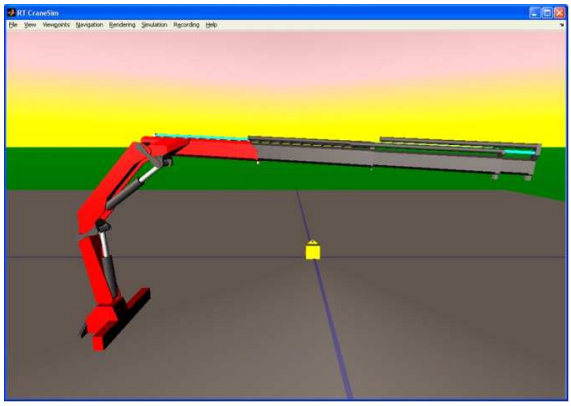

Figure D.12: Example of the 3D animation.

The 3D animation sink block featured in the same toolbox is easily applied together with CAD files for the given crane. The CAD files are converted to VRML format, and a VR-world hierarchy files is written, defining the relationship between the CAD parts.

The interactive real time model provides a better feeling with the control system during development, which can otherwise be difficult to obtain, using non-real time models with preset trajectories. It provides an excellent target for developing and testing new control strategies.

Tool point control

A feedforward control scheme is implemented, where the operator controls the velocity, i.e. direction and speed, of the tool point (hook) of the crane online. The operator will then 'close the loop' and ensure sufficient positional accuracy.

The purpose of creating the simulation model was to aid in the development of a new tool point control scheme for loader cranes. Thus a control block is inserted to transform the joystick input to a suitable reference signal for the virtual crane.

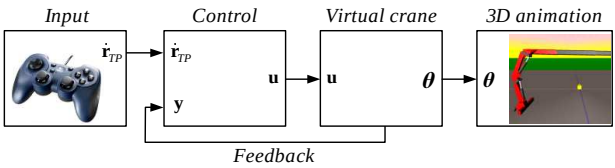

Figure D.13: Overview of the simulation.

The tool point control block must take the Cartesian velocity reference input $\dot{\mathbf{r}}_{TP}$ and, based on some feedback, return the valve flow reference $\mathbf{u}$ to the virtual crane, as shown in Figure D.13.

Joint controller

Low cost, low resolution sensors are used for the practical implementation in order to keep it commercially viable. A pure feed forward velocity controller is chosen, in order not to rely too much on the sensors for accurate feedback in a closed loop control scheme.

The Jacobian matrix of the Cartesian to joint transformation is easily established considering that each column represents the associated joint's velocity contribution to the tool point velocity.

$$\dot{\mathbf{r}}_{TP} = \mathbf{J}\dot{\boldsymbol{\theta}} \tag{D.34}$$

where

$$\mathbf{J}(\boldsymbol{\theta}) = \begin{bmatrix} \tilde{\mathbf{e}}_1\mathbf{d}_{51} & \tilde{\mathbf{e}}_2\mathbf{d}_{52} & \tilde{\mathbf{e}}_3\mathbf{d}_{53} & \mathbf{e}_6 \end{bmatrix} \tag{D.35}$$

Due to the redundancy, the Jacobian is not square, and the Moore-Penrose pseudo-inverse is used

$$\dot{\boldsymbol{\theta}} = \mathbf{J}^{+}\dot{\mathbf{r}}_{TP} \tag{D.36}$$

This corresponds to finding the minimum velocity norm in the joint space, Beiner and Mattila (1999). The requested cylinder velocity is then calculated by eq. (D.29) which is subsequently used for calculating the flow set-point.

Joint limit avoidance

Joint limits are avoided by the weighted least norm (WLN) approach, Chan and Dubey (1993), using the weighted pseudo inverse, which penalizes the motion of joints close to their limits

$$\mathbf{J}_W^{+} = \mathbf{W}^{-1}\mathbf{J}^T(\mathbf{J}\mathbf{W}^{-1}\mathbf{J}^T)^{-1} \tag{D.37}$$

Here a $\mathbf{W}$ is a symmetric positive definite weighing matrix

$$\mathbf{W} = \begin{bmatrix} w_1 & 0 & 0 & 0 \\ 0 & w_2 & 0 & 0 \\ 0 & 0 & w_3 & 0 \\ 0 & 0 & 0 & w_4 \end{bmatrix}. \tag{D.38}$$

The elements of $\mathbf{W}$ is given as the partial derivative of a performance criterion, e.g.

$$H(\boldsymbol{\theta}) = \sum_{i=1}^{4} \frac{1}{4} \frac{(\theta_{max,i} - \theta_{min,i})^2}{(\theta_{max,i} - \theta_i)(\theta_i - \theta_{min,i})}. \tag{D.39}$$

The value of H increases exponentially when a joint approaches its limit. The partial derivative of H is then used as weights in $\mathbf{W}$.

$$\frac{\partial H}{\partial \theta_i} = \frac{(\theta_{max,i} - \theta_{min,i})^2 (2\theta_i - \theta_{max,i} - \theta_{min,i})}{4(\theta_{max,i} - \theta_i)^2 (\theta_i - \theta_{min,i})^2}. \tag{D.40}$$

$$w_i = \begin{cases} 1 + |\frac{\partial H}{\partial \theta_i}| & for \;\; \Delta|\frac{\partial H}{\partial \theta_i}| \geq 0 \\ 1 & for \;\; \Delta|\frac{\partial H}{\partial \theta_i}| < 0. \end{cases} \tag{D.41}$$

The ith weight will go towards infinity, when the ith joint approaches its limit, thus effectively stopping the joint motion. On the other hand when moving away from a limit, the joint is not penalized. Here, $\Delta|\frac{\partial H}{\partial \theta_i}|$ is the rate of change of the partial derivative. It can be shown, that the weights are continuous, also when $\Delta|\frac{\partial H}{\partial \theta_i}|$ changes sign, Chan and Dubey (1993).

Configuration control

Experience shows that it is feasible to maximize the effective joint torque arm of the main joint, i.e. a_2 in Figure D.11. This can be achieved by modifying the associated weight w_2 by adding the following penalization, i.e. when moving away from the maximum.

$$w_2 = \begin{cases} K_a|\frac{da_2}{d\theta_2}| & for \;\; \dot{\theta}_2 \cdot |\frac{da_2}{d\theta_2}| < 0 \\ 0 & for \;\; \dot{\theta}_2 \cdot |\frac{da_2}{d\theta_2}| \geq 0. \end{cases} \tag{D.42}$$

In some cases it might also be necessary for the operator to control the configuration of the crane, as shown in Figure D.14. This will override the above maximization of the main joint torque arm and can be used to avoid obstacles or fine-tuning the lifting capacity.

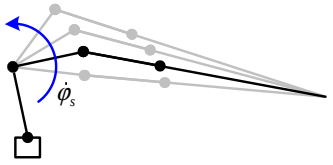

Figure D.14: Configuration control (self motion).

For a redundant system, a set of joint velocities that do not cause any tool point motion can be determined according to so-called self-motion, see e.g. Chan and Dubey (1993) or Beiner and Mattila (1999). This is typically used in some sort of optimization, e.g. in the gradient projection method, but here it is controlled directly by the operator.

$$\dot{\boldsymbol{\theta}}_s = (\mathbf{I} - \mathbf{J}^+\mathbf{J})\mathbf{z}. \tag{D.43}$$

The first term is the null space projection matrix of the Jacobian and $\mathbf{z}$ is an arbitrary vector in the null space. Then $\dot{\boldsymbol{\theta}}_s$ can be added to eq. (D.36) without interfering with the tool point motion. Since there is only on degree of redundancy, choosing

$$\mathbf{z} = \begin{bmatrix} 0 & \dot{\varphi}_s & 0 & 0 \end{bmatrix}, \tag{D.44}$$

and taking $\dot{\varphi}_s$ as input from joystick, the operator can control the configuration online. This is possible, even while simultaneously controlling the tool point motion.

Deflection compensation

The total deflection of the tool point is due to; 1) structural flexibility, 2) deformation of sliding pads between segments in the extension system, 3) mechanical slack between segments and 4) compression of hydraulic fluid in cylinders.

In a practical implementation, the joint angles of the main and jib joints would be measured using inclinometers, i.e. relative to horizontal. This means that these joint angles would be measured in the deflected state.

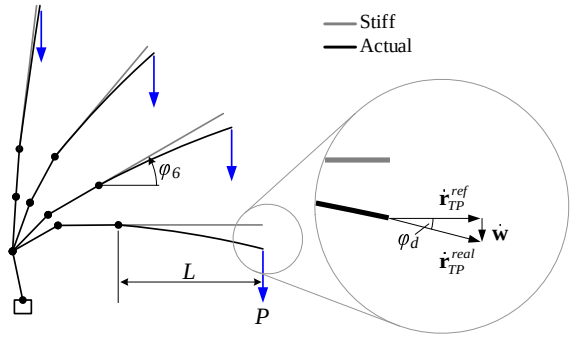

Figure D.15: Tool point velocity deviation due to deflection.

Thus, only the deflection of the extension system needs to be compensated for actively. In practise, only the in-plane vertical deflection is significant, i.e. up to $\approx 0.5m$. The deflection is especially problematic for horizontal straight-line tool point motion.

Figure D.15 illustrates how the real tool point velocity deviates from the reference due to the deflection, which can be expressed as

$$\dot{\mathbf{r}}_{TP}^{real} = \dot{\mathbf{r}}_{TP}^{ref} + \dot{\mathbf{w}}. \tag{D.45}$$

In order for the real tool point velocity to match the reference, the reference must be compensated as

$$\dot{\mathbf{r}}_{TP}^{comp} = \dot{\mathbf{r}}_{TP}^{ref} - \dot{\mathbf{w}}. \tag{D.46}$$

Determining $\dot{\mathbf{w}}$ is difficult in practise, since the deflection contribution caused by 2), 3) and 4) is difficult to isolate and quantify. Hence, a simplified approach is used here;

$$\dot{\mathbf{w}} = \begin{bmatrix} 0 \\ -K_c \sin(\varphi_d)\dot{\theta}_6 \\ 0 \end{bmatrix}. \tag{D.47}$$

Only the vertical deflection is considered and the total deflection velocity is assumed to be proportional to the telescope extension velocity $\dot{\theta}_6$. The deflection angle of an inclined cantilever beam with a load P at the free end can estimated as follows

$$\varphi_d = \frac{\cos(\varphi_6) P L^2}{2EI} \tag{D.48}$$

where $\varphi_6 = \theta_2 + \theta_3$ is the inclination angle of the extension system relative to horizontal. Thus, only the scaling factor K_c in eq. (D.47) needs to be determined from experiments.

Practically, this deflection compensator adds a small upwards velocity to the tool point reference velocity, when extending, which cancels out due to the deflection.

Flow setpoint calculation

The requested cylinder velocities are calculated using eq. (D.29) and the flow request Q_{req} is determined by the piston or rod side area, depending on the direction of the requested cylinder velocity

$$Q_{req,i} = \begin{cases} A_{p,i} \cdot \dot{c}_i & for \;\; \dot{c}_i \geq 0 \\ A_{r,i} \cdot \dot{c}_i & for \;\; \dot{c}_i < 0 \end{cases} \tag{D.49}$$

Two saturation phenomena need to be included; firstly the valve flow limit and secondly the pump flow limit. The set flow is different from the requested flow if any of the two limits are exceeded in order to maintain the tool point velocity and only violate the speed.

The requested set point signal $u_{req,i}$ is determined from the requested flow normalized by the maximum valve flow

$$u_{req,i} = \frac{Q_{req,i}}{Q_{v,max,i}} \tag{D.50}$$

Flow sharing

The requested flow is limited to the valve flow limit, typically 40-100 l/min. If one valve limit is exceeded, all requested flows are scaled down by k_v.

$$\mathbf{u}_{req} = \begin{bmatrix} u_1 & u_2 & u_3 & u_4 \end{bmatrix} \tag{D.51}$$

$$k_v = \frac{1}{\max(|\mathbf{u}_{req}|)} \tag{D.52}$$

$$\mathbf{u}_{req,v} = \begin{cases} \mathbf{u}_{req} & for \;\; k_v > 1 \\ k_v \mathbf{u}_{req} & for \;\; k_v < 1 \end{cases} \tag{D.53}$$

The total requested flow is determined by summation

$$Q_{tot} = \begin{cases} \sum |Q_{req,i}| & for \;\; k_v > 1 \\ \sum |k_v \cdot Q_{req,i}| & for \;\; k_v < 1 \end{cases} \tag{D.54}$$

Flow sharing is applied again if the total requested flow Q_{tot} exceeds the maximum pump flow Q_{pump}:

$$k_p = \frac{Q_{pump}}{Q_{tot}} \tag{D.55}$$

$$\mathbf{u} = \begin{cases} k_p \mathbf{u}_{req,v} & for \;\; Q_{tot} \geq Q_{pump} \\ \mathbf{u}_{req,v} & for \;\; Q_{tot} < Q_{pump} \end{cases} \tag{D.56}$$

It is then ensured, that neither the valve flow limit nor the pump flow limit are exceeded.

Results

Figure D.16 shows the overall control scheme developed. All motion is directly proportional to the input given by the operator, i.e. no closed loop control has been applied, in order to leave the operator in complete control.

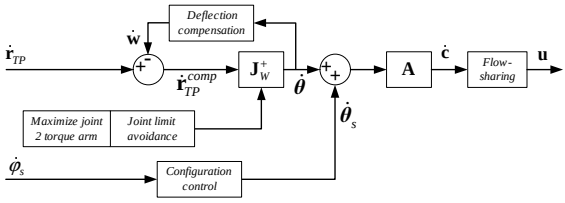

Figure D.16: Overview of the control scheme.

The following working cycle is established, in order to illustrate the advantages of real-time versus non-real-time simulation, see Figure D.17.

Traditionally, in a non-real-time simulation, the operator will be modelled, e.g. as a set of predefined trajectories which should follow a reference. This is exemplified as the "predefined operator". Using the simple feedforward joint controller, the tool point speed will generally be slightly lower than the reference, which accumulates to a position error. This is due to pressure build-up time in the hydraulics and acceleration of the mechanics.

In real-time simulation, an actual operator controls the crane tool point (hook) such that it follows the same trajectory. This is shown as the "active operator". In this case, the operator uses visual feedback to close the loop and adjust the input through the joystick, until he/she finds that the reference position is sufficiently achieved. Since the direction of the tool point is always maintained, and only the speed is violated, it is not noticed by the operator.

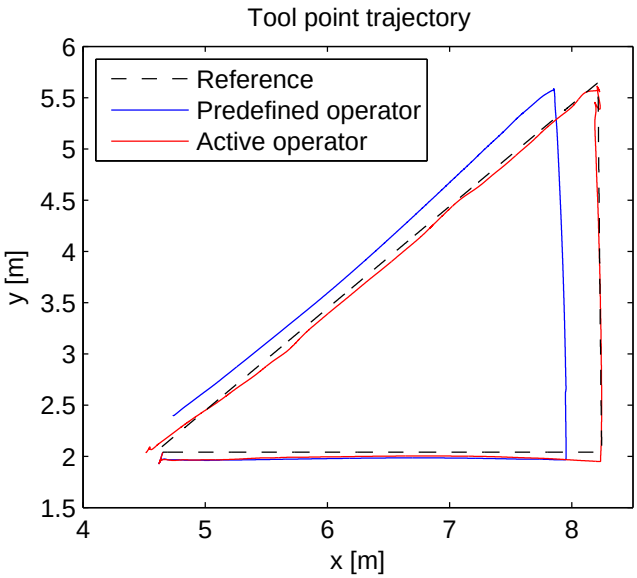

Figure D.17: Reference and actual tool point position.

Conclusions

Under normal evaluation conditions (i.e. using a predefined operator), such a control scheme would probably be deemed unacceptable. However, when the operator capabilities are included in real-time simulation, the controller performance is excellent.

Tool point control of a hydraulic loader crane seems very advantageous for many tasks, however, the operator needs the ability to control the crane traditionally as well, e.g. when folding the crane, or operating close to obstacles. Furthermore, some kind of configuration control will be needed in order to avoid obstacles in the workspace.

Interactive real-time dynamic simulation is a powerful tool for developing control strategies. It provides valuable insight into the practical application of a given control scheme. Future works could include more detailed modelling of the operator as part of a simulation. However, the only authentic way to include operator abilities is to let him/her be part of the loop.

Acknowledgements

This research work is funded by HMF A/S and an Industrial PhD-grant from the Danish Ministry for Science, Technology and Innovation.

References

Beiner L. (1997), Minimum force redundancy control of hydraulic cranes. Mechatronics **7**(6), pp.537-547.

Beiner L. and Mattila J. (1999), An improved pseudoinverse solution for redundant hydraulic manipulators. Robotica, **17**, pp.173-179, 1999.

Chan T.F. and Dubey R.V. (1993), A weighted least-norm solution based scheme for avoiding joint limits for redundant manipulators. Robotics and Automation, **3**, pp. 395-402, 1993.

Ebbesen M.K. (2007), Optimal Design of Flexible Multibody Systems. PhD Thesis, Aalborg University, Denmark, 2007.

Esqué S., Raneda A., and Ellman A. (2003), Techniques for studying a mobile hydraulic crane in virtual reality. Int J Fluid Power, **4**(2) pp.25–34, 2003.

Hansen M.R. and Andersen T.O. (2005), A method for deriving the optimal operation of mobile hydraulic manipulators. In *Proc. 9th Scandinavian International Conference on Fluid Power, SICFP'05*. Linköping, Sweden, 2005.

Kabus S. and Haastrup, M. (2008), Simulations of Flexible Loader Crane with Designed Tool Point Control. Masters Thesis, Aalborg University, Denmark, 2008.

Krus G. and Palmberg J.O. (1998), Vector control of a hydraulic crane. In *Proc International Off-Highway and Power plant Congress and Exposition*. Milwaukee, USA, 1992.

Linjama M. and Virvalo T. (1999), State-space model for control design of multi-link flexible hydraulic cranes. In *6th International Conference on Fluid Power*. Tampere, Finland, 1999.

Mattila J. and Virvalo T. (2000), Energy efficient motion control of a hydraulic manipulator. In *Int Proc Robotics and Automation*. San Francisco, USA, 2000.

Merrit H.E. (1967), *Hydraulic Control Systems*. John Wiley and Sons, Inc. New York, USA, 1967.

Mikkola A.M. (1997), Studies of Fatigue Damage in a Hydraulic Driven Boom System Using Virtual Prototype Simulations. PhD Thesis, Lappeenranta University of Technology, Finland, 1997.

Münzer M.E. (2003), *Resolved Motion Control of Mobile Hydraulic Cranes*. PhD Thesis, Aalborg University, Denmark, 2003.

Nielsen B.K. (2005), *Controller Development for a Separate Meter-in Separate Meter-out Fluid Power Valve for Mobile Applications*. PhD Thesis, Aalborg University, Denmark, 2005.

Nikravesh P.E. (1990), Systematic reduction of multibody equations of motion to a minimal set. *Int J Nonlinear Mechanics*, **25**(2/3) pp.143-151, 1990.

Nikravesh P.E. (1991), *Computational Methods in Multi-body Systems*. Notes, COMETT, DTH, Lyngby, Denmark, 1991.

Pedersen H.C. and Nielsen B. (2002), *Resolved Motion Control of Flexible Hydraulic Manipulators*. Master Thesis, Aalborg University, Denmark, 2002.

Yuan Q., Lew J., and Piyabongkarn D. (2009), Motion control of an aerial work platform.In *Proc. American Control Conference*. St. Louis, MO, USA, 2009.

E

A Cost-effective Approach to Hardware-in-the-loop Simulation

M.M. Pedersen, M.R. Hansen, M. Ballebye
Submitted to the 9th International Conference: Mechatronics 2011, September 21–24, Warsaw, Poland, 2011.

Abstract. This paper presents an approach for developing cost effective hardware-in-the-loop (HIL) simulation platforms for the use in controller software test and development. The approach is aimed at the many smaller manufacturers of e.g. mobile hydraulic machinery, which often do not have very advanced testing facilities at their disposal. A case study is presented where a HIL simulation platform is developed for the controller of a truck mounted loader crane. The total expenses in hardware and software is less than 10.000$.

Introduction

The safety demands for machinery are ever increasing, as described in e.g. the new Machinery Directive (2006) or EN13849 (2006). More and more electronic safety and control systems are therefore implemented in order to avoid potential danger, both from conventional use, but also from foreseeable misuse.

As an example from the loader crane industry, the new revision of EN12999 (2010) requires the stability of the truck to be monitored and secured via the crane safety system, in order to avoid overturning of the truck. In the case of using the loader crane for personal lifts, the safety requirements are further increased due to the obvious risk to the person(s) being lifted.

The safety system for an advanced loader crane as shown in Fig. E.1 may include in the order of 50 IOs and up to some 20 CAN modules connected to a main controller. The trend is towards more distributed IO systems communicating via CANbus networks, but also using sensors with integrated CANbus interface.

The complexity of the controller software increases in the same rate as the safety demands, and is further increased by a high level of product configurability. It thus becomes

increasingly difficult to perform end-to-end tests for such systems, using a breakout board with switches, diodes and potentiometers.

In other industries with complex safety systems, e.g. the automotive, aerospace or offshore industries, hardware-in-the-loop simulation have long been the standard platform for testing controller software. In the crane industry and other similar industries, controller software testing have typically been performed using the real machine, though this is neither safe nor efficient.

It is possible, however, to implement very cost-effective HIL simulation platforms for such machinery, and thus significantly improving testing capabilities.

Figure E.1: Truck with loader crane used for personal lift.

Earlier HIL simulation (HILS) platforms typically considered a single component or minor isolated systems for testing controller software with limited visual output. However, advances in computational power have propelled a rapid evolution of HILS platforms which now considers entire systems, such as heavy construction machinery or offshore structures and offer rich 3D animation output.

A HILS system for a hydraulic excavator with both audio and visual simulation output integrated in the operator cabin of a real excavator, was presented by Elton et al. (2009). The system included a remote hydraulic load emulator for a variable displacement pump, connected via Internet. The simulation are thus feed accurate (non-modeled) information from the pump.

Ghabcheloo and Hyvonen (2009) discusses development of a motion control system for a hydraulic wheel loader in a HILS platform called GIMsim. It consists of 5 PCs communicating via LAN to accommodate animation, dynamics, tire contact, IO + CAN

and simulation control. The simulation is developed in Matlab/Simulink, compiled and transfered to an xPCtarget for hard real-time operational speed.

Recently, Trydal (2010) presented a very advanced proprietary HILS platform from National Oilwell Varco. It concerns an offshore drill-rig including the entire drilling process equipment and displays a 3D animation in a dome in order to completely immerse the operators. Instead of physical IOs, each controller are connected to a similar controller which simulates the IO functionality.

The general trend is to develop the simulation in Matlab/Simulink, use several PCs connected via LAN and use hardware IO connectivity from dSpace, National Instruments or others. Simulation input are given from real operator interfaces and results are presented using more and more realistic 3D animation. The animation software is generally developed specifically for the considered system using OpenGL.

In this paper, a cost effective approach to HIL simulation is demonstrated for a non time-critical application using only standard high-level engineering software. It should thus be possible for it to be implemented and maintained by engineers, without in-depth software development background.

Considered System

We consider a truck with an advanced folding loader crane attached to it, Fig. E.1. The crane is equipped with a so-called flyjib, and has 6 degrees of freedom; slew, main boom, jib boom, telescope extension, fly-jib, and fly-jib telescope extension. In the tool point, a variety of accessories can be mounted, such as a rotator and grab or a personal lift basket. The crane is furthermore equipped with a winch mounted in a revolving console for parking during transport.

The crane is mounted with a stabilizer system containing 4 extensible booms each with a stabilizer leg, and an additional fixed front stabilizer leg. In total we have 19 hydraulically actuated DOFs controlled by 12 directional valves and several shift valves. The truck furthermore has two passive DOFs, enabling inclination around the roll and pitch axes in order to simulate stability issues (i.e. overturning of the truck). Fig. E.2 shows the DOFs included in the simulation.

The safety and control system, Fig. E.3, of such a crane primarily covers a number of capacity limitation, stability monitoring and collision avoidance features, but also several secondary safety features, such as smart speed reduction and selective stopping of load-increasing motion. All safety features are supported by visual and audible warning signals.

The electronic hardware consists of a CAN network with a main controller, 3 I/O modules (flyjib, winch and stabilizers), a radio remote control, a slew sensor, 2 dual axis inclinometers, and up to 12 electro-hydraulically actuated directional control valves. Inputs and outputs are thus distributed to the corresponding function via the CAN network.

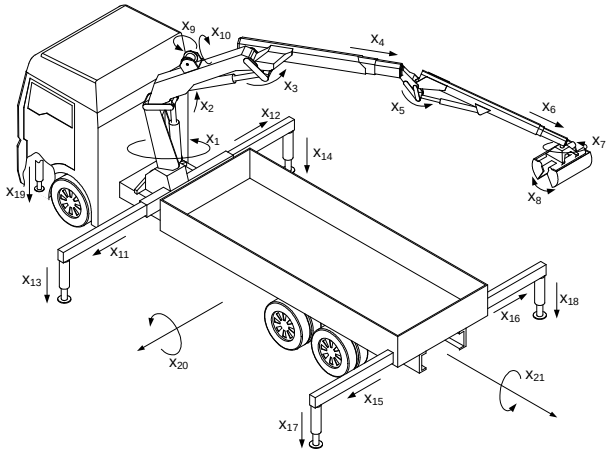

Figure E.2: Degrees of freedom in the simulation model.

The critical components are redundant, e.g. pressure transducers and inclinometers. Also the I/O modules and controller consist of two separate processors, each of which monitors the operation of the other, in order to achieve a high level of safety.

All IOs are monitored to comply with defined limits according to their use. Operating status and error reports are communicated via 12 LED indicators and a 3x7 segment display. The operator interface is typically a radio based remote control with up to 8 analog input channels, 12-20 buttons and a LCD display.

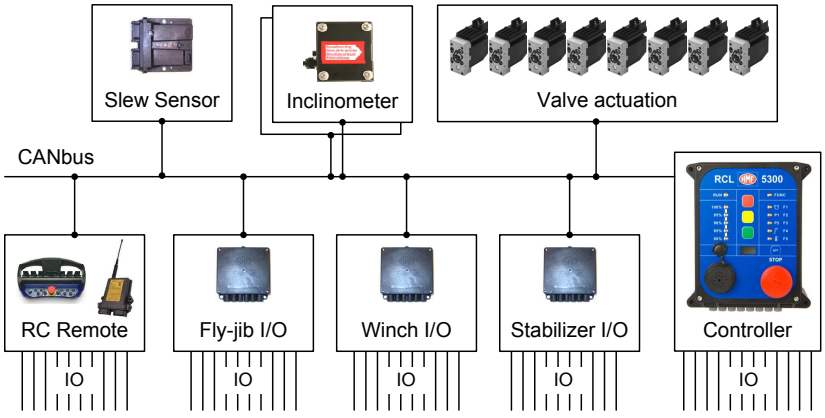

Figure E.3: Electronic crane safety and control system.

HIL Simulation

The developed HIL simulator consists of three subsections; 1) a simulation PC, 2) a hardware-gateway PC and 3) the real controller hardware, as shown in Fig. E.4.

The simulation is developed in Matlab using the Simulink 3D animation toolbox (which doesn't actually require Simulink) for visualization. The Matlab and Simulink programming environments are well known for their simple syntax and high productivity.

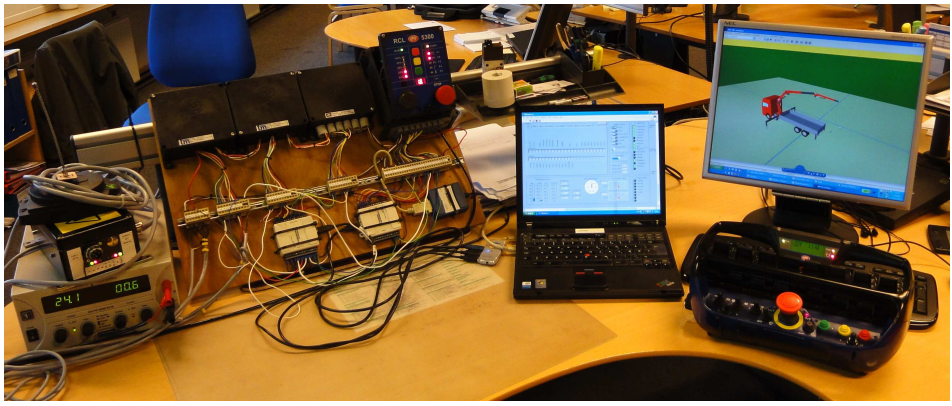

Figure E.4: Physical setup, from left: 1) controller hardware, 2) Gateway PC, 3) Simulation PC and operator interface.

The hardware-gateway is developed in LabView using low-cost USB I/O and CAN devices from National Instruments for low level communication with the controller hardware. The link between the simulation running in Matlab and the hardware controlled by LabView is achieved over the local area network (LAN), using the IP/UDP protocol.

Co-simulation via LAN/UDP

LAN communication using the UDP protocol is an effective approach to achieve co-simulation with two different programs, e.g. Matlab and LabView or others. The programs can run on either two different PCs connected by LAN, or on a single PC sending data to itself - between programs. Using several PCs gives a performance advantage though and enables additional monitoring possibilities and distributed location of equipment.

The UDP protocol is typically used for streaming media over the Internet and other applications where it is preferable to drop packets rather than wait for them. In many applications, this is not a problem, if the same data are transmitted repeatedly. Sending data with UDP requires specification of the receiver IP address and port number, receiving requires only specification of the local port number and the size of the packet in bytes.

In this case study, the UDP protocol is used to communicate between the simulation running in Matlab on the Simulation PC and the Hardware Gateway PC running LabView, see Fig. E.5. An UDP packet are sent both ways at every time-step in the simulation, all necessary data are collected and transfered in these packets.

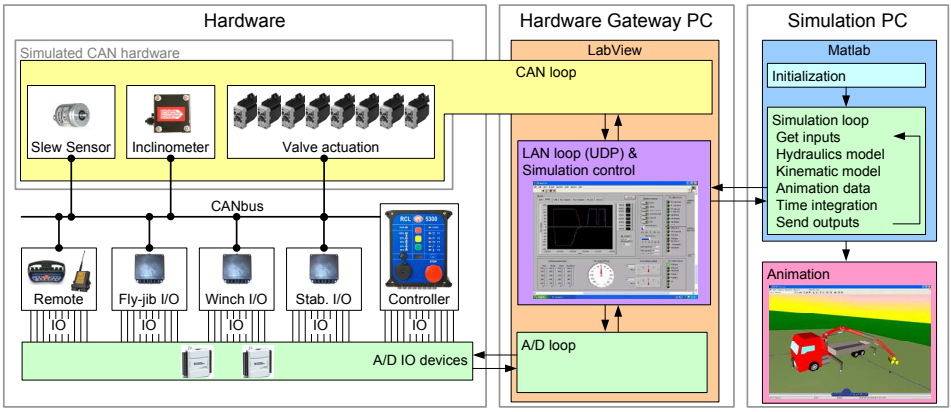

Figure E.5: Overview of the HIL simulation.

The simulation model is thereby updated with the valve flow command sent from the controller to the virtual valves, and the state of all outputs from the controller and modules, e.g. to activate shift valves or perform engine control. In the other direction, the controller hardware is updated with the state of the virtual sensors in the simulation, e.g. hydraulic pressure, truck inclination, slew angle and estimated flow from the simulated valves, etc.

Hardware Gateway

Using a separate PC with LabView to facilitate communication between the controller hardware and the simulation has several advantages. Firstly, the price is low compared to dedicated systems. Secondly, the system is very flexible and scalable. The gateway PC can furthermore be used to control and monitor values in the HIL simulation while it runs. Additional filtering or noise can also be added to the signals here.

As shown in Fig. E.6 and E.5 the Labview program is divided in three separate loops; a LAN loop, CAN loop and A/D loop. Each loop covers communication between the gateway and LAN network, CAN network or analog/digital hardware. Separate loops in LabView runs in parallel for efficient execution and at different rates of 200Hz, 50Hz and 20Hz respectively. The hardware gateway additionally simulates a number of CAN devices, i.e. sensors and valve actuation.

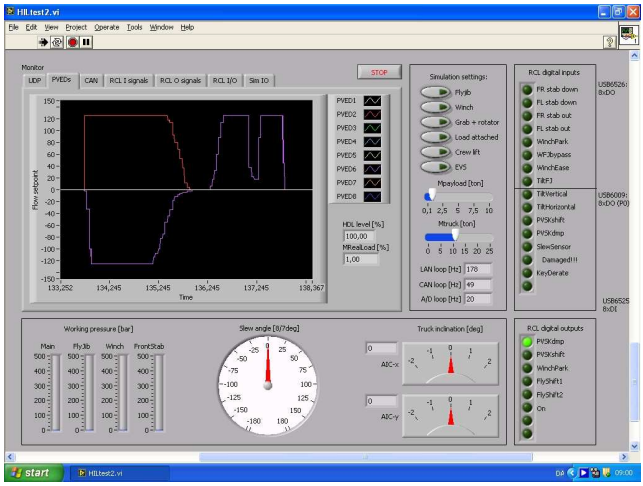

Figure E.6: Screenshot from the Hardware Gateway (LabView).

Simulating CANopen Devices

The communication profile of most CAN devices such as sensors and valves is relatively simple and these can therefore be simulated quite easily. For a thorough overview of CAN and CANopen, see Pfeiffer et al. (2003). A first approach is to let LabView send CAN frames corresponding to the the necessary transmit PDO(s) of the devices to the controller.

If needed, it is also possible to implement a limited object dictionary and SDO server in the LabView program containing the entries the controller (or other devices, e.g. a service terminal) will inquire on. Typically, to simulate e.g. a generic CAN I/O module, it will only be necessary to include in the order of 10 entries in the object dictionary.

The SDO protocol is straightforward for the expedited transfers (up to 4bytes), however if segmented or block transfers are required, this will take some more work, see CiA 301 (2002).

For the application at hand, strict real-time performance is not critical. Most of the CAN devices sample at 10-20Hz only and a small delay in the response of the simulation is acceptable.

Simulation Model

Since the simulation model must run in real time (or close to) in order to communicate with the controller, it is essential to limit the computational burden to what can be achieved with the available hardware.

Most dynamics of the system is omitted, which is acceptable since the controller mainly considers steady state values of the input. This is necessary in order to achieve near real-time performance in Matlab.

Referring to Fig. E.5, the simulation is initiated by loading the crane parameters, such geometric and inertial properties, joint states and limits, hydraulic system properties, etc.. The main simulation loop is then started which is executed as fast as possible (around 200Hz) and updates all simulation parameters and controls the animation.

All required data is retrieved from the UDP packet; flow command to the valves, state of the outputs on the controller and modules, and necessary simulation control parameters which are set in the Hardware Gateway PC, i.e. mass of payload, mass of truck, crane setup, accessories mounted, etc.

Based on the flow commands and output states, the reference velocity of all DOFs are then calculated. Since several outputs controls shift valves, in order to use the directional control valves for multiple functions, the state of these leads to different modes of operation; i.e. crane mode, stabilizer mode, winch mode, etc.

Then a complete kinematic analysis is performed in order to determine position, orientation and velocity of all parts and the resulting tool point motion. The kinematic parameters are needed in order to drive the animation.

A simple kinetic analysis is also conducted, which determines the needed parameters; crane lifting moment, truck inclination due to crane load, hydraulic pressures in the main cylinder, flyjib cylinder and winch. Additionally, the ground projection of the total Center of Mass (COM), are calculated and displayed in the animation, in order to visualize the stability margin.

The only dynamics included is for a suspended payload, which is modeled as a 2 DOF pendulum. This gives the user the impression of operating a dynamic system and thus experience the consequences of abrupt motion.

The state of all virtual sensors are then determined. These include digital sensors, monitoring whether e.g. stabilizers are fully deployed, the jib is above horizontal, the extension system is fully retracted, etc. Several analog sensors are also simulated, e.g. pressure transducers for measuring pressure in selected cylinders, crane slew angle, truck inclination and directional control estimated valve flow, etc.

Time integration of the calculated velocities for all DOF is then performed using the trapezoidal rule and the animation is updated. All the simulated devices are modeled as ideal, i.e. they respond instantaneously and with with perfect precision. In the Hardware Gateway, however, noise is added to selected signals, in order to test the controller filtering capabilities.

The necessary values are then assembled in a UDP packet and feed back to the controller via the Hardware gateway, and the simulation loop starts over.

3D Animation

Using the Simulink 3D Animation Toolbox, a Virtual Reality (VR) world can be manipulated from Matlab by translating, rotating or scaling the 3D parts at each time-step, to make it appear that the crane is moving. The VR world is defined using the VRML markup language, i.e. the relation between the parts and the surroundings.

Fig. E.7 shows a screenshot from the implemented 3D animation. Some CAD programs can export parts to VRML format, otherwise, simple geometries, e.g. boxes and cylinders, can be directly defined in the VRML language.

Using the Simulink 3D Animation Toolbox makes it simple to create an advanced 3D environment for simulation output. Its flexible and scalable and based on a simple markup language, unlike the typical custom-made OpenGL applications used for HILS animation. Output from the animation can either be displayed directly or recorded for later use.

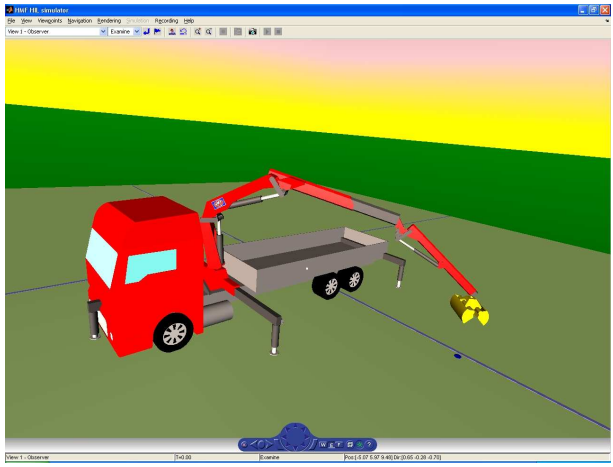

Figure E.7: Screenshot from the 3D animation.

Conclusion

The HIL simulator described in this paper have proven to posses the necessary level of detail to test all the features of the controller concerned. Indeed, its possible to create much more precise testing conditions, compared to using the real machine or a board with switches and potentiometers.

Especially when testing dangerous conditions, such as truck overturning or faults in the control system, simulation is preferred, since it is both expensive and time consuming to perform such test using the real machine.

Table E.1 gives an estimate of the total costs of the HILS platform, excluding the development of the software, which took approximately three months.

Matlab	2800 $
3D animation toolbox	1400 $
LabView	1700 $
IO modules	1000 $
2 PCs	3000 $
Total	9900 $

Table E.1: Approximate HILS platform costs.

The HIL simulator currently only comprise ad-hoc testing capability, however, it could be extended to included fully automated end-to-end testing of the controller, which will lead to additional savings on the testing expenses.

As a replacement for ad-hoc testing of controller software using the real machine or a breakout board, HIL simulation is a very effective tool. With the additional control over the testing conditions and increased monitoring possibilities, it is possible to create more repeatable and precise testing conditions. The effort required and risk of testing controller software can thus be significantly reduced.

Using only standard engineering software, such as Matlab and LabView, it is should be possible for the engineers who possess the domain knowledge to implement and maintain the HILS system, without requiring assistance from software developers.

It's difficult to determine the payback period on the investment of such HIL simulator, but a qualified estimate is 1-2 years. This is due to saved engineer-hours for testing, when comparing to testing using the real machine.

Acknowledgments

This work is funded by an Industrial PhD grant from the Danish Ministry of Science, Technology and Innovation and HMF A/S.

References

M.D. Elton, A.R. Enes and W.J. Book A Virtual Reality Operator Interface Station with Hydraulic Hardware-in- the-Loop Simulation for Prototyping Excavator Control Systems. IEEE/ASME International Conference on Advanced Intelligent Mechatronics, Singapore, July 14-17, 2009.

R. Ghabcheloo and M. Hyvnen Modeling and motion control of an articulated-frame-steering hydraulic mobile machine. 17th Mediterranean Conference on Control and Automation, Thessaloniki, Greece, June 24-26, 2009.

S. Trydal HIL Simulator. Hardware In Loop Simulator med fokus paa integrerte prosesser. (Norwegian) NODE seminar, Grimstad, Norway, 29 September, 2010. http://www.nodeproject.no/index.php?articleid=393 (09-11-2010)

EU Machinery Directive, 2006/42/EG European Union, Brussels, 2006.

EN ISO 13849-1:2006 Safety of machinery - Safety-related parts of control systems - Part 1: General principles for design. CEN, Brussels, 2006.

FprEN12999:2010 (Final Draft) Cranes - Loader cranes. CEN, Brussels, 2010.

O. Pfeiffer, A. Ayre and C. Keydel Embedded Networking with CAN and CANopen Copperhill Media, MA, USA, 2003.

CAN in Automation (CiA), e.V. CANopen, Application Layer and Communication Profile. CiA 301, 2002.